Durability of Nano-Modified Fly Ash Concrete to External Sulfate Attack under Different Environmental Conditions

By

Md. Mahbubur Rahman

A Thesis submitted to the Faculty of Graduate Studies of

The University of Manitoba

in partial fulfillment of the requirements of the degree of

Master of Science

Department of Civil Engineering

Faculty of Engineering

University of Manitoba

Winnipeg

Abstract

There are still research gaps regarding the effects of key parameters such as water-to-cementitious materials ratio (w/cm), type of binder and pore structure characteristics on the response of concrete to special forms of sulfate attack: physical salt attack (PSA) and thaumasite sulfate attack (TSA). Hence, this study aims at developing an innovative type of concrete: nano-modified fly ash concrete, incorporating various dosages of nano-silica (NS) or nano-alumina (NA) and fly ash, and explores its efficiency in resisting various forms of sulfate attack.

PSA on concrete is a distress caused by the crystallization of salts in pores near drying faces or evaporative zones, which leads to progressive scaling and flaking of the concrete surface. Although numerous concrete structures are at risk of PSA during service, there is currently no standard test method in North America for PSA of cement-based materials. Therefore, an accelerated laboratory test was developed in this research to assess the resistance of nano-modified fly ash concrete to PSA. The effects of w/cm, fly ash and two types of nanoparticles (NS and NA) addition on the resistance of concrete to PSA were investigated. The assessment criteria were based on physical properties (visual appearance, mass loss and interconnectivity of pores) and the alteration of microstructure by microscopy and mineralogical analyses. The results demonstrated that the proposed procedure can successfully assess the performance of concrete under PSA within a relatively short time interval. Hence, it can be used in the prequalification stage to facilitate decision making on concrete mixtures proposed for exposures conductive to PSA. Also, adverse effects of nanoparticles addition (excessive pore size refinement with NS and ettringite formation with NA) and higher w/cm (0.5) on the resistance of concrete to PSA were captured.

Conventional sulfate attack is associated with significant expansion and cracking of concrete, while TSA transforms concrete into a non-cohesive mass without any binding capacity. Hence, to evaluate the resistance of nano-modified fly ash binders (made with GU cement, GUL cement [GU cement blended with limestone filler] and portland-limestone cement [PLC: interground limestone with clinker]) to these forms of sulfate attack, tests were generally performed based on CSA A3004-C8 (Procedure A [immersion in sulfate solution at 23°C] and B [immersion in sulfate solution at 5°C]) procedures. The mixture design variables were the type of binder, dosage of fly ash, and incorporation of NS and NA. The assessment criteria were based on the physical properties, microscopy, thermal and mineralogical analyses. The overall performance of PLC binders in both exposures was better than the other types of binders. In addition, higher dosages of fly ash were effective at mitigating/reducing the damage to conventional and thaumasite sulfate attack. Results showed that NS addition with any dosage of fly ash inhibited the ingress of sulfate solution and thus the formation of sulfate-reaction products in the cementitious matrix at both test temperatures. Conversely, NA accelerated the rate of expansion and deterioration of specimens.

Acknowledgements

Among the numerous good things that have happened to me in my life, there is none in which I feel more blessed than the reward of Almighty Allah in getting admission with Research and Teaching Assistantship with a view to pursuing my graduate study at the University of Manitoba under the supervision of Dr. Mohamed T. Bassuoni, P.Eng., Assistant Professor, Department of Civil Engineering, University of Manitoba. My most sincere gratitude, therefore, goes to my supervisor Dr. Mohamed T. Bassuoni, for his unremitting guidance and cordial support in all stages of this research accomplishment. I do also deeply convey my sincere thanks to him for his encouragement and help to organize my ideas and interests, and also express my deep appreciation for what I have learned from him during my study.

I do most sincerely acknowledge the financial support from University Research Grants Program (URGP) at University of Manitoba, Canada that made it possible for me to devote much more time and efforts to my thesis and finally bring it into light. Moreover, my sincere thanks go to Mr. Chad Klowak, P.Eng.,W.R. McQuade Heavy Structures Laboratory Manager, University of Manitoba for his technical support and valuable guidance. In addition, I would like to thank my colleagues, especially Mr. Hooman Kazempour for his help during the experiment and technical analysis.

Finally, I extend my heartiest gratitude to my parents for their heavenly love, care and support throughout my life. Without their unremitting encouragement and praying, I could not make it possible. Also, I sincerely thank my sister, brothers and all the rest of my relatives and friends particularly my close friend Mr. Md. Mujahedul Islam who have supported me in many ways.

Table of Contents

List of Tables

List of Figures

Abbreviation/Nomenclature

C_2S - Dicalcium silicate (belite), $2CaO\ .\ SiO_2$

C_3A - Tricalcium aluminate, $3CaO\ .Al_2O_3$

C_3S - Tricalcium silicate (alite), $3CaO\ .\ SiO_2$

C_4AF - Tetracalcium aluminoferrite, $4CaO\ .\ Al_2O_3\ .Fe_2O_3$

$\overline{S}$ - Sulfate, SO_4^{2-}

A - Aluminum oxide (alumina), Al_2O_3

C - Calcium oxide (lime), CaO

CH - Calcium hydroxide

C-S-H - Calcium silicate hydrate

DSC - Differential Scanning Calorimetry

EDX - Energy Dispersive X-ray analysis

F - Ferric oxide (iron oxide), Fe_2O_3

FA - Fly ash

NA - Nano-alumina

NS - Nano-silica

PLC - Portland-limestone cement

PSA - Physical salt attack

S - Silicon dioxide (silica), SiO_2

SCMs - Supplementary cementitious materials

SEM - Scanning Electron Microscopy

TSA - Thaumasite sulfate attack

XRD - X-ray Diffraction

1. Introduction

1.1. Overview

Since concrete is not an inert material, it interacts physically and chemically with surroundings when exposed to normal or aggressive environments. Hence, during service life, concrete elements may be vulnerable to many durability problems such as freezing-thawing cycles, alkali-silica reaction, sulfate attack, etc. External sulfate attack on concrete can occur due to physical and chemical interactions between various sulfate salts (e.g. sodium sulfate) and concrete. The former is termed physical salt attack (PSA), while the latter is referred to as chemical sulfate attack, which is further classified into conventional (ettringite) sulfate attack and thaumasite sulfate attack (TSA), depending on the nature of damage. PSA on concrete is a distress caused by the crystallization of salts in pores near drying faces or evaporative zones, which leads to progressive scaling and flaking of the concrete surface. On the other hand, conventional sulfate attack is associated with significant expansion and cracking of concrete, while TSA transforms concrete into a non-cohesive mass (mush) without any binding or loading carrying capacity. The durability concerns of sulfate attack on concrete under different environmental conditions can be mitigated by selecting suitable or innovative cementitious materials incorporating supplementary cementitious materials (SCMs) with proper mixture design based on the type of exposure to reduce the rate of deterioration and consequently life-cycle costs.

1.2. Sulfate Attack on Concrete

In conventional sulfate attack, waterborne sulfate ions chemically interact with the hydration phases of tri-calcium aluminate, tetra-calcium aluminoferrite and calcium hydroxide to form voluminous products of gypsum and ettringite (Menéndez *et al.*, 2013). Depending on the

availability of sulfate ions, the reaction of sulfate ions and hydration products proceeds to a greater or lesser extent (Neville, 2004). The pressure developed from the expansive sulfate-bearing products creates tensile stress inside the cementitious matrix which leads to cracking that allows more solution uptake and deterioration. The damage manifestations of conventional sulfate attack involve micro- and macro-cracking, expansion, and spalling.

PSA on concrete is linked to the crystallization of salts in pores near the drying surfaces, which leads to progressive surface scaling and flaking of concrete; the appearance of damage due to PSA on concrete is similar to that of freezing-thawing cycles (Haynes *et al.*, 1996). Surface scaling frequently occurs when the evaporation rate from the exposed surface of concrete is higher than the rate of solution uptake through capillarity, resulting in efflorescence (not harmful) on the surface, and subflorescence underneath the surface which is the main cause for scaling. Growth of salt crystals in the confined pore space is accompanied by crystallization pressure. It was believed that concrete exposed to soil containing salt-laden mainly suffer from chemical attack, and many field cases in North America were misdiagnosed the deterioration caused by PSA as conventional sulfate attack. Nevertheless, it has been shown that concrete in such exposures can also deteriorate at the evaporative faces (e.g. the exposed part of basement walls, piers, abutments, slabs on grade, service tunnels, etc.) due to a physical mechanism (PSA) without appreciable chemical interaction.

Thaumasite is a sulfate attack reaction product, which forms under certain conditions. It is composed of calcium silicate, carbonate, sulfate, and water. Erlin and Stark (1966) first reported thaumasite formation (TF) in portland cement concrete in 1965. It was found in sanitary sewer pipes, portland cement grout, and a pavement core. TF in cementitious systems is a complex phenomenon, which relies on multiple factors including temperature and humidity conditions,

type and concentration of sulfate salts, pH level, and type of cementitious binders and aggregates, and inclusion of limestone fillers in the binder. Excessive TF transforms cementitious system into a pulpy and non-cohesive mass that is often described as 'mush', which is a typical damage manifestation of TSA (Tsivilis *et al.*, 2007; Crammond, 2003; Hobbs, 2003). Both conventional sulfate attack and TSA are associated with volumetric expansion of concrete, which causes fine cracks parallel to the surface of concrete (Hobbs and Taylor, 2000). However, TSA is more deleterious to concrete as it disintegrates calcium silicate hydrate (C-S-H: the main hydration phase) and transforms the matrix into a soft mass without any binding capacity. The occurrence of TSA has been reported for concrete structures/elements in many parts around the world such as UK, USA, Canada, South Africa, France and Germany.

1.3. Need for Research

Extensive research has been done on conventional sulfate attack on concrete since early 1900's and led to the advent of sulfate resisting portland cements. Yet, special forms of sulfate attack such as PSA and TSA still needs further research to investigate the effects of key parameters such as w/cm, type of binder, and pore structure characteristics on the response of concrete vulnerable to these types of damage. While there are many concrete structures/elements vulnerable to PSA during their service life, there are currently no code provisions and standard test methods in North America directly addressing the issue of PSA on cement-based materials. In addition, portland-limestone cements (PLC), which contain 5-15% limestone filler, have recently been accepted in Canada (CSA A3000-08) and in USA (Barrett *et al.*, 2014). However, durability issues (e.g., TSA) may arise when adequate content of limestone materials are available in concrete serving in sulfate exposures. Inclusion of limestone fillers in cement/concrete (either blended or interground) acts as an internally rich-source of carbonate

ions which is one of the main components responsible for TSA reactions, and thus the use of PLC in sulfate environments is still controversial with more research data needed in this area.

Fly ash (a type of SCMs available in Canada) is an industrial by-product of coal-fired power plants that has the ability to improve durability and mechanical properties of concrete. When added at certain dosages, typically more than 25% by mass, it can improve the resistance of concrete to durability issues such as external sulfate attack and TSA. The rates of hardening and strength development, however, are delayed with addition of fly ash in concrete because of its slow pozzolanic reactivity. Therefore, regulatory bodies impose policy barriers on the wider use of fly ash in concrete. For example, surface works specifications in Manitoba mandate that the use of fly ash as a cement replacement in concrete pavements, curbs, sidewalks, etc. is optional, and if used, it must not exceed 15% (City of Winnipeg, 2013). Due to their ultrafine nature, nanoparticles (size scale of 1-100 billionth of a meter) can vigorously speed-up the kinetics of cement hydration and efficiently refine the pore structure of concrete (Sanchez and Sobolev, 2010). Their application in concrete (nano-modification) has a great potential to mitigate the performance issues associated with the use of higher volumes of fly ash and create innovative types of sustainable concrete with superior performance for restoring/upgrading Canadian infrastructure. Said *et al.* (2012) reported that addition of nano-silica particles to concrete containing up to 30% of binder significantly improved the kinetics of hydration and rate of strength development. Yet, there is dearth of information on the durability characteristics of concrete modified with nanoparticles (e.g. nano-silica [NS] and nano-alumina [NA]) and fly ash, such as its resistance to special forms of sulfate attack (PSA and TSA). Hence, the motive of this research, which mainly aims at capturing improvement trends and/or performance limitations of

nano-modified fly ash concrete, and thus contributing to updating current code provisions for these durability issues.

1.4. Objectives

The primary objectives of this research are to:

- Develop innovative concrete mixture designs incorporating various dosages of NA or NS and fly ash (nano-modified fly ash concrete).
- Introduce an accelerated laboratory test procedure to evaluate the resistance of the newly developed nano-modified fly ash concrete to PSA focusing on the effect of key mixture design variables (w/cm, fly ash and type of nanoparticles).
- Assess the response of the nano-modified fly ash concrete to conventional sulfate attack and TSA exposures, considering the effects of cement, fly ash and nanoparticles.

1.5. Scope of the work

To assess the durability characteristics of the newly developed nano-modified fly ash concrete, this study was split into two experimental phases. Firstly, an accelerated laboratory test procedure was designed to evaluate the resistance of concrete to PSA. Therefore, based on this exposure, concrete prepared from 30% fly ash (Class F) with or without the incorporation of 3 and 6% NS and NA by mass of the total binder content at w/cm of 0.4 and 0.5 were evaluated by visual assessment, mass change, and rapid chloride penetrability test. To identify the underlying mechanisms of damage, the alteration of microstructure in deteriorating specimens was investigated by microscopy, thermal and mineralogical analyses.

In the second phase (conventional and TSA exposures), two types of cement were used: general use (GU) portland cement and portland-limestone cement (PLC). Also, GU cement was

blended with limestone filler to produce (GUL) cement, to assess its performance relative to PLC (interground limestone with clinker). In addition to cement types, twenty four mortar mixtures were made with different dosages (15, 30 and 40%) of fly ash and nanoparticles (6% of NS or NA) to evaluate the resistance of these newly developed binders to chemical sulfate Attack. The assessment criteria were based on visual observations and physico-mechanical properties (length change, mass change, dynamic modulus of elasticity, and RCPT). To investigate the alteration of microstructure on deteriorated mortar samples, scanning electron microscopy (SEM) with energy-dispersive X-ray analysis (EDX) techniques were employed, and to identify the formation of sulfate-bearing products in the cementitious matrix X-ray diffraction (XRD-Cu-Kα) and differential scanning calorimetry (DSC) techniques were used.

1.6. Thesis structure

The thesis is divided into six chapters:

Chapter one contains introduction, overview of sulfate attack, need for research, research objectives and scope of the work.

Chapter two presents a brief literature review of conventional sulfate attack, PSA and TSA including factors affecting the problems, consequences of sulfate attack, mechanisms of PSA and TSA, available tests on sulfate attack, and durability characteristics of nano-modified concrete.

Chapter three describes the methodology, and materials and mixtures used in the test program. It also elucidates different exposure regimes for sulfate attack experiments, test procedures of fresh and hardened properties, and microstructural, mineralogical and thermal analyses.

Chapter four presents results and discussion for the PSA exposure including mechanisms of damage and effects of w/cm, fly ash and nanoparticles.

Chapter five describes conventional sulfate attack test results and discussion. In addition, it presents the results of the TSA exposure and discussion based on the effects of the type of binder, dosage of fly ash and nanoparticles.

Chapter six provides a summary of the research program, concluding remarks based on the test results and recommendations for future research.

2. Literature Review

In this chapter, a review of the literature pertinent to conventional sulfate attack, physical salt attack (PSA) and thaumasite sulfate attack (TSA) is presented. The effect of nanoparticles on the behaviour of cement-based materials is also discussed herein.

2.1. Conventional (classical) sulfate attack

2.1.1. Gypsum formation

With the availability of moisture, sulfate salts such as sodium sulfate (Na_2SO_4) and magnesium sulfate ($MgSO_4$) migrate into concrete and react with calcium hydroxide [$Ca(OH)_2$] to form gypsum ($CaSO_4.2H_2O$) according to the following equations (Skalny *et al.*, 2002; Hewlett, 1998):

$$Ca(OH)_2 + Na_2SO_4 + 2H_2O \rightarrow CaSO_4.2H_2O + NaOH \quad \text{(Eq. 2.1)}$$

$$Ca(OH)_2 + MgSO_4 + 2H_2O \rightarrow CaSO_4.2H_2O + Mg(OH)_2 \quad \text{(Eq. 2.2)}$$

Where ($NaOH$) and [$Mg(OH)_2$] are sodium and magnesium hydroxide (brucite), respectively. The formation of gypsum has been reported to be responsible for softening (strength reduction) of the cementitious matrix and increasing the porosity of concrete. Santhanam *et al.* (2003) have shown that gypsum also contributes to the volumetric expansion of cementitious matrices under external sulfate attack. Gypsum formed according to the above reactions can further react with hydrated calcium aluminate (C_4AH_{13}), monosulfate ($C_4A\bar{S}H_{12-18}$) or unhydrated tricalcium aluminate (C_3A) to produce secondary ettringite according to the following equations (Skalny *et al.*, 2002; Hewlett, 1998):

$$C_4AH_{13} + 3C\bar{S}H_2 + 14H \rightarrow C_6A\bar{S}H_{32} + CH \quad \text{(Eq. 2.3)}$$

$$C_4A\bar{S}H_{12-18} + 2C\bar{S}H_2 + (10-16)H \rightarrow C_6A\bar{S}H_{32} \quad \text{(Eq. 2.4)}$$

$$C_3A + 3C\bar{S}H_2 + 26H \rightarrow C_6A\bar{S}H_{32} \quad \text{(Eq. 2.5)}$$

Secondary ettringite has an expansive nature which can lead to the destruction of concrete. In addition, secondary ettringite stimulates thaumasite sulfate attack via the Woodfordite route.

2.1.2. Ettringite formation

In the presence of calcium hydroxide and water, ettringite ($C_6A\bar{S}_3H_{32}$) forms as a reaction product of monosulfate hydrate or calcium aluminate hydrate with sulfate (Kurtis and Monteiro, 1999). Equation 2.6 shows the formation of ettringite from monosulfate:

$$Ca_4Al_2(OH)_{12}.SO_4.6H_2O + 2Ca^{2+} + 2SO_4^{2-} + 20H_2O \rightarrow$$

$$3CaO.Al_2O_3.3CaSO_4.32H_2O \quad \text{(Eq. 2.6)}$$

Ettringite is a typical reaction product of conventional sulfate attack on concrete which consumes calcium aluminate hydrates (CAHs) from the cementitious matrix during the reaction. Also, ettringite is considered as a voluminous phase associated with expansion, cracking and spalling of concrete. Moreover, expansion and softening from conventional sulfate attack, can be attributed to gypsum ($CaSO_4.2H_2O$) formation (Tian and Cohen, 2000). Although the mechanisms of conventional sulfate attack are complex and controversial, there is a general consensus that dissolution of the main phases of hydrated cement paste and formation of ettringite and gypsum are primarily responsible for the damage of cementitious systems under conventional sulfate attack.

2.1.3. Factors affecting conventional sulfate attack

Ettringite and gypsum might form from both internal and external sources of sulfate ions. The internal sources of sulfate might originate from cements, aggregates and different supplementary cementitious materials (SCMs). For example, Araújo *et al.* (2008) reported internal sulfate attack due to iron sulfides from oxidation of aggregates in Spanish concrete dams. In external sulfate attack, however, sulfate ions might be drive in from ground water, brackish water, water of rivers, lakes and sea, soil, landfill, atmospheric sulfur dioxide, and other sources; while susceptibility of damage always depends on the concentration of the sulfate ions along with the velocity of ground water flow (Marchand *et al.*, 2004).

Ettringite formation needs a source of aluminate, which essentially comes from the tricalcium aluminate of cement clinker. Therefore, sulfate resistant portland cement (SRPC), with limited C_3A content minimizes the formation of ettringite. Supplementary cementitious materials (SCMs), such as slag, fly ash and silica fume, which are typically industrial by-products with pozzolanic and/or latent hydraulic properties, dilutes the C_3A content and improves the performance and long-term durability when incorporated in concrete. In the cementitious matrix, SCMs react with CH to produce secondary C-S-H gel with low calcium-to-silicate ratio of ~1.1, which increases strength and stability of concrete exposed to chemical environments. As explained earlier, CH reacts with sulfate solutions to produce gypsum, which can further react to produce ettringite (Eqs. 2.3-2.5). Also, transformation of CH refines the pore structure of concrete and densifies the interfacial transition zone (ITZ) (Hewlett, 1998), which reduces the ingress of moisture and aggressive ions into concrete, and hence minimizes the risk of sulfate attack.

Deterioration of concrete attributed to sulfate attack depends on the topography and mineral composition of soil and groundwater. In addition, environmental conditions including humidity and temperature, and location of structure accelerate or decelerate the deterioration rate of concrete due to sulfate attack. To complete the sulfate reactions, a source of water is needed for transporting the ions in the reaction site which might come from the internal or external sources. Occasionally, water table in subgrade contains sulfate salts have substantial influence on concrete substructures due to continuous rise and drop of water level (Clifton *et al.,* 1999). Even concrete above the soil or water can be subjected to sulfate attack because of the migration of salt carrying sulfate ions through the capillary pores of concrete.

2.1.4. Consequences of conventional sulfate attack

Conventional/classical sulfate attack (i.e., ettringite related) creates expansion in the "core" of concrete and fine cracks parallel to the surface of concrete because of the volumetric reaction between hydrated and/or unhydrated cement grains, and sulfate ions (Hobbs and Taylor, 2000). The damage attributable to ettringite formation in the paste increases when pressure exerted by ettringite causing tensile stress on the pore wall of the cementitious matrix. The deterioration accompanied by the continuously growing ettringite results in cracks when increase in pressure exceeds the tensile capacity of the mortar/concrete. The reaction process progresses as the cracks allow the sulfate solution to directly enter into the matrix which inevitably deteriorates more on the cementitious materials. Therefore, conventional sulfate attack degrades the concrete by chemical means and causes expansion, cracking and spalling of concrete.

2.1.5. Conventional sulfate attack tests

In North America, the resistance of cement-based materials to sulfate attack is usually evaluated by ASTM C1012-13 (expansion of mortar prisms). In this test, mortar specimens (25×25×285

mm) are immersed in 5% (50 g/l) sodium sulfate solution at 23°C, without controlling the pH, and expansion is regularly measured. The expansion (failure) limit stipulated by ASTM C1012 is 0.10% at 12 months. This test method has been specified for blended cements and for cementitious systems comprising supplementary cementitious materials (SCMs). For blended binders subjected to Class 3 sulfate exposure (more than 10,000 ppm), the ACI 201.2R: Guide to Durable Concrete permits an expansion of up to 0.10% after 18 months of exposure following the ASTM C1012 procedure (ACI 201.2R, 2008).

The currently used ASTM test methods for evaluating the sulfate resistance of cement-based materials have been criticized for a long time. There is a general consensus that the ASTM C1012 test overlooks important parameters affecting the field performance of concrete structures exposed to sulfate attack such as temperature and humidity conditions, pH level and type of sulfate solutions (Clifton *et al.*, 1999). It is already acknowledged in the standard that the mechanisms of sulfate attack observed in the test are pertinent to the composition of the sulfate solution used. Hence, modified versions of the sulfate attack test have been reported in the literature to account for the effect of temperature and humidity variations (e.g., Sahmaran *et al.*, 2007), pH level (e.g., Cao *et al.*, 1997), type of cation (e.g., Bassuoni and Nehdi, 2012; Lee *et al.* 2005; Matthews, 1994) and solution concentration (e.g., Matthews, 1994).

Since extensive research studies have been carried out on mitigating conventional sulfate attack by incorporating SCMs in concrete, the prime focus of this thesis is not on conventional sulfate attack. The main focus of this thesis is on special forms of sulfate attack: physical salt attack (PSA) and thaumasite sulfate attack (TSA).

2.2. Physical Salt Attack (PSA)

2.2.1. Overview on PSA

Salt weathering or distress is considered as one of the key deterioration mechanisms in rocks exposed to a certain environmental conditions such as in hot-arid regions and coastal zones (Rodriguez-Navarro and Doehne, 1999). The mechanical behavior of rocks' decay as a result of salt weathering has been extensively studied for the last 150 years (e.g. Cooke, 1979; Evans, 1970). For the past few decades, however, ongoing research has been carried out to minimize the adverse effects of salt crystallization (weathering) on building materials and concrete structures (Mehta, 2000). Until the initiative of Folliard and Sandberg (1994), research efforts were mainly focused on conventional sulfate attack.

Usually, salt crystallization distress is observed on the evaporative faces of concrete exposed to salt-laden soil (e.g. the exposed part of basement walls, piers, abutments, slabs on grade, service tunnels, etc.). Also, damage of concrete caused by salt crystallization is accelerated as the soluble salt content and moisture content increases in soil. Among the different terminologies available in literature, American Concrete Institute (ACI) Committee 201 (Durability of Concrete) has adopted the phrase 'physical salt attack (PSA)' for this type of damage, which might be caused by sulfate salts, carbonate salts, chloride salts or others (Haynes and Bassuoni, 2011). Each salt induces different levels of damage depending upon the nature and kinetics of crystallization pressure with sulfate salts being the most deleterious to concrete (Haynes *et al.*, 2008, 2010; Rodriguez-Navarro and Doehne, 1999).

2.2.2. Occurrence

Physical salt attack (PSA) is a common problem around the world. PSA mostly occurs in hot-arid regions where there is a variation of temperature and relative humidity; such as coastal regions where both moisture and salt is available in the atmosphere. This process of salt crystallization/salt hydration distress highly depends on the presence of salts in the surrounding environment. It might come from soil, groundwater, sea water and other sources. It is not indispensable to have higher salt concentration in the salt-laden soil. Lower concentration of salt, however, might cause PSA problem as well but this process takes longer time. The damage caused by salt crystallization might occur due to variety of salts including sodium sulfate, sodium carbonate, sodium chloride, magnesium sulfate, calcium sulfate, and calcium chloride (Haynes and Bassuoni, 2011).

Throughout the process of PSA two products are generated, which are termed as efflorescence and subflorescence, on the evaporative fronts. Efflorescence is salt crystals that deposit after the evaporation of water-soluble salts. It occurs on the surface of porous material where there is free space to accommodate the crystallization. Although, efflorescence creates cosmetic problem, most of the time it is not harmful to concrete. Subflorescence, on the other hand, takes place just below the surface and forms when the evaporative flux in the convective zone of the porous element exceeds the capillary flux (Cardell *et al.*, 2008). Usually, salt crystallization growth below the efflorescence zone causes micro-cracking in the cementitious matrix. Eventually, pressures in fine pores produced from the continuously growing salt crystals crumbles the weaker portion of surface (mortar) which leads to progressive surface scaling.

The exposure cycle of PSA can be split into multiple processes. Water-soluble salt penetrates into concrete by capillary absorption (wicking), and subsequently drawn out from the

evaporation front by vapour diffusion. Interconnected pores with evaporative front are essential to complete the capillary absorption of salt solution. In addition, the higher rate of drying/evaporation and solution uptake depends on the permeability of concrete as well as the distance salt solution needs to travel by capillary suction. Repetitive wetting and drying also promotes salt crystallization and growth, along with continual hydration of the matrix. All of these processes induce synergistic effects that progressively alter the pore structure of the matrix (Liu *et al.*, 2012).

2.2.3. Features of PSA

In the field of concrete durability, the issue of PSA was misidentified as chemical sulfate attack until recently (Haynes *et al.* 2008). Characteristically, PSA on concrete can occur due to the exerted pressure from continuous growth of salt crystals inside the pores without limited or no interaction between hydrated cement paste and salt ions, which leads to progressive surface scaling and flaking; the appearance of damage (as shown in Figure 2.1) due to PSA on concrete is similar to that of freezing-thawing cycles (Haynes *et al.*, 1996). In chemical sulfate attack, however, sulfate ions directly react with the main components of hydrated cement paste, resulting in softening, expansion, cracking, spalling and disintegration of concrete (Irassar, 2002). While concrete is a porous material, the salt crystallization or PSA frequently occurs when the evaporation rate of salt solution from the exposed surface is higher than the rate of uptake. This results in efflorescence (not harmful) on the surface and subflorescence beneath the surface of concrete which is the main cause for scaling. Furthermore, the damage attributable to salt crystallization in the subflorescence zone increases when exerted pressure is greater than the tensile strength of concrete. This crystallization pressure *(P)* equals to (Correns, 1949):

$$P = (RT/V_s)\, ln\, (C/C_s) \qquad \text{(Eq. 2.7)}$$

Where, R is the ideal gas constant, T is the absolute temperature, V_s is the molar volume of solid salt, C is the solute concentration and C_s is the saturation concentration. In a particular situation, if the salt crystallization pressure (P) calculated from the above equation exceeds (supersaturation condition) the tensile capacity of the concrete pore wall then the damage is likely to occur. This crystallization pressure depends on the pore size where higher pressure is created in smaller pores (Scherer, 2004a). Also, it was reported that concrete with very fine pore structure is vulnerable to damage by PSA (Bassuoni and Nehdi, 2009a).

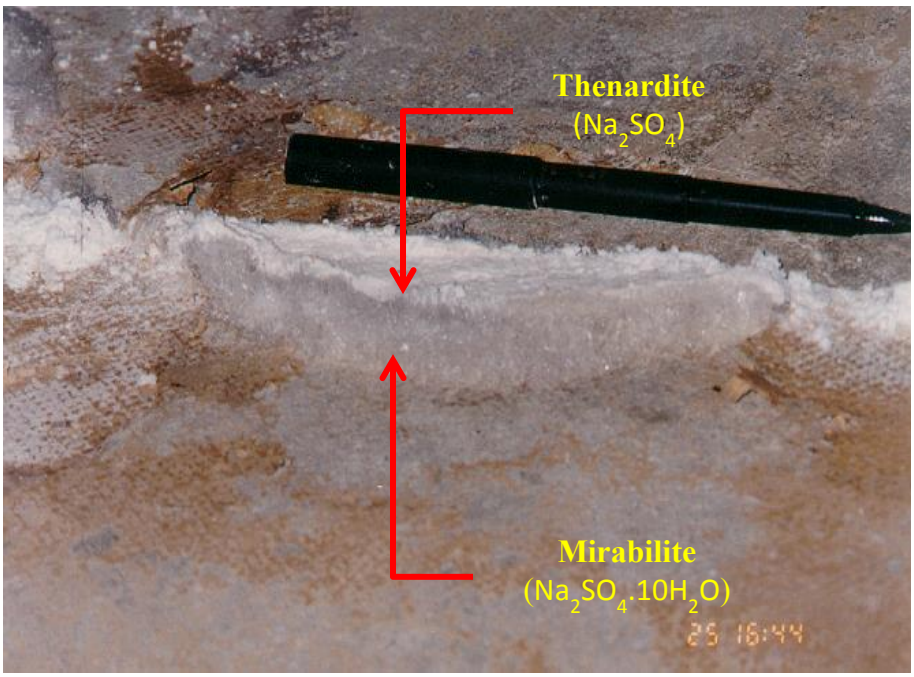

Figure 2.1: Physical salt attack on concrete ground floor (courtesy of R. Day, Calgary).

2.2.4. Factors affecting the extent of PSA

The mechanisms of PSA are complex phenomena that depend on many factors. The factors affecting the salt crystallization damage in porous building materials are salt type, evaporation rates, surface tension, vapor pressure, environmental factors, properties of the pore system, rate

of airflow, degree of supersaturation, differential thermal expansion of salts, etc. (Haynes and Bassuoni, 2011; Rodriguez-Navarro and Doehne, 1999; Smith, 1994). Also, the location of salt crystallization is an important factor; for instance, subflorescence creates higher pressure on the surface of concrete than efflorescence. Moreover, the hydration phase transformation of salt mineral is an important factor affecting the salt crystallization. For instance, the alteration of anhydrous sodium sulfate (thenardite, Na_2SO_4) to hydrous (mirabilite, $Na_2SO_4.10H_2O$) form creates volume expansion by 314% causing distress (Haynes and Bassuoni, 2011). The solubility of thenardite and precipitation of mirabilite highly depends on the temperature and humidity (Flatt, 2002). The thenardite dissolves below 32°C and at high relative humidity to mirabilite (Chatterji and Jensen, 1989), and a phase transition between two sodium sulfate salts was found by Flatt (2002) about 75% RH at 20°C (as shown in Figure 2.2). In a long experimental program (about 1130 days), Haynes *et al.* (2008, 2010) showed the importance of cyclic exposures (conversion between thenardite and mirabilite) in accelerating the damage of concrete prepared with high water-to-cementitious materials ratio (0.6) due to PSA. According to Haynes *et al.* (1996), in addition, salt crystallization is an exothermic process that increases the volume of salt crystals after the completion of reaction.

For salt nucleation, hydrated salt must be transported to the evaporative zone otherwise no distress will be occurred due to the buildup pressure of salt crystallization. Hence, availability of water (diluted salt) is required to continue the process of salt growth. Usually, salty water enters into the porous media either as liquid or vapor through two mechanisms: capillarity and/or infiltration and condensation and/or hygroscopicity (Charola, 2000). Moreover, the rate of crystallization is one of the significant factors affecting PSA on concrete and this crystallization growth depends on the salt concentration. Also, in both porous rocks and concretes, the

magnitude of damage caused by the crystallization pressure is a function of the supersaturation ratio of solution and the place of crystallization (Rodriguez-Navarro and Doehne, 1999). In addition, high rate of evaporation results higher level of supersaturation which in line increases the transient stress on the pore wall (Scherer, 2004b). Furthermore, higher supersaturated solution produces rapid growth of salt crystals than the one with less. Moreover, continuous variations of relative humidity (RH) intensify the salt concentration in pores near the drying surface. Additionally, high temperature evaporates the moisture at or near the surface that leaves the salt crystals in the pores and allows the salt crystals to grow. Also, the change in temperature and relative humidity cause pore solution to expand and contract on a continuous basis which result in fatigue on the matrix. Therefore, repetitive cycling of temperature combined with RH causes higher salt distress on concrete.

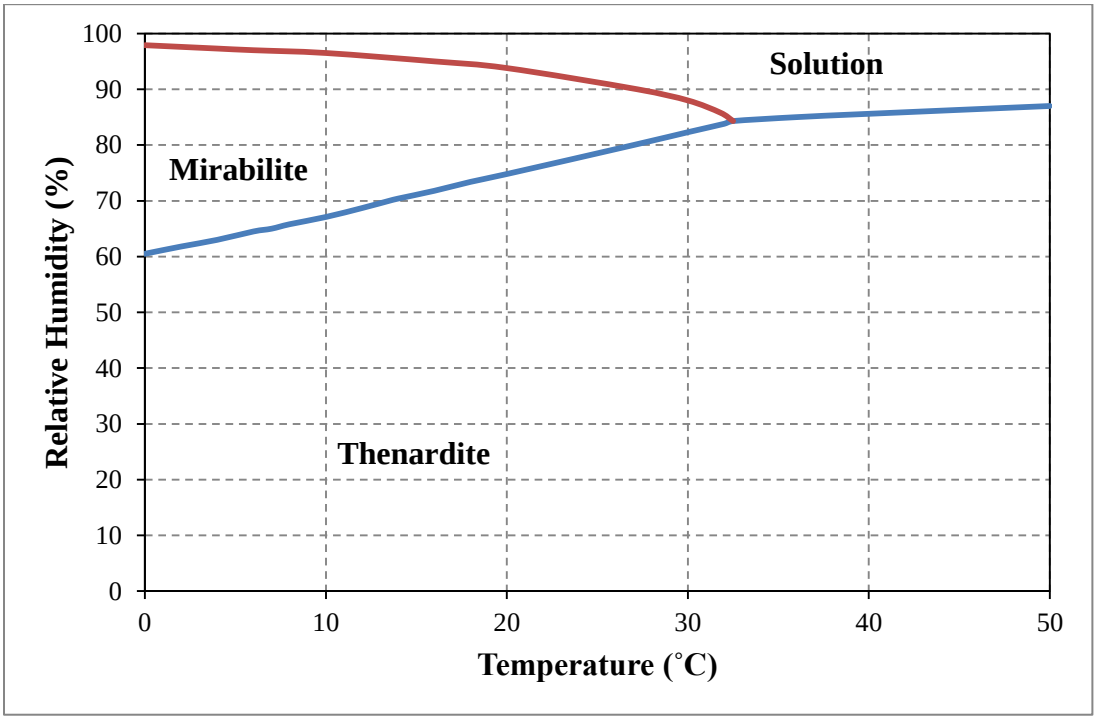

Figure 2.2: Sodium sulfate phase diagram (after Flatt, 2002).

2.2.5. Previous research on PSA on concrete

An early effort to identify the mechanisms of sulfate attack on concrete was made by the Portland Cement Association (PCA) in 1940 (Mcmillan *et al.*, 1949). Later, in 1963 Bureau of Reclamation reported in a Concrete Manual that salt crystallization in pores (PSA) might be responsible for the surface damage without any chemical interaction in between salt and hydration phases in concrete. Another long-term field test was carried out for five years on concrete specimens including fly ash, natural pozzolan and slag (Irassar *et al.*, 1996). Half of the concrete specimens were partially embedded into sulfate soil. It was concluded that the evaporative zone of concrete samples suffered from salt crystallization distress, while the immersed portion of concrete samples was vulnerable to conventional sulfate attack. In addition, high volume of SCMs in concrete decreased the resistance to PSA. Conversely, the PCA studies showed that use of SCMs in concrete has positive effect to reduce the surface scaling due to PSA (Stark, 2002).

Folliard and Sandberg (1994) studied the underlying mechanisms of salt crystallization damage. The salt crystallization occurred in different concrete specimens because of the hydration, evaporation and changes in temperature. The important finding from the study was that sodium sulfate solution created higher damage manifestation when the temperature varied from 5 to 30°C. Moreover, the hydrous phase of sodium sulfate (mirabilite) was responsible for deterioration according to the authors. In addition, Haynes et al. (2008, 2010) carried out a 3-year test program on concrete partially submerged in different solutions including sodium sulfate, sodium carbonate, or sodium chloride solutions. To promote PSA, concrete specimens were cycled in between different temperature and relative humidity conditions. In terms of aggressiveness, sodium sulfate created higher deterioration on concrete compared to other salts.

Similar to the distress occurred by sodium sulfate salt, authors found that two hydration phase transformation of sodium carbonate in between thermonatrite ($Na_2CO_3.H_2O$) to natron ($Na_2CO_3.10H_2O$) produced surface scaling; whereas sodium chloride had little impact on surface scaling. In a different cyclic exposure, Bassuoni and Nehdi (2009a) reported that concrete with very fine pore structure (prepared from quaternary binders and low w/cm of 0.38) was vulnerable to damage by PSA where the exposure was continued for 24 months. These results agreed with that of Irassar *et al.* (1996). An overview of PSA process on concrete is shown in Figure 2.3.

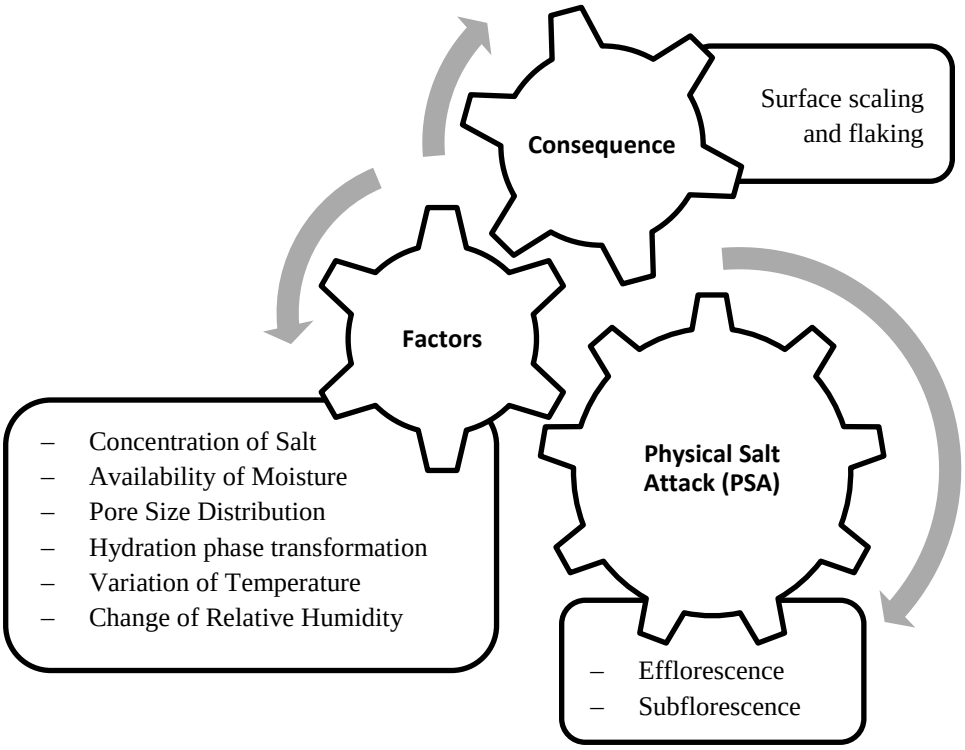

Figure 2.3: General overview of PSA process.

2.3. Thaumasite Sulfate Attack (TSA)

2.3.1. Mechanisms of Thaumasite formation

In general, thaumasite formation (TF) preferentially occurs at low temperature (≤ 15℃) with the availability of calcium silicate, sulfate and carbonate ions, and the abundance of moisture (Crammond and Halliwell, 1995; DETR, 1999). Incidental occurrence of thaumasite in fissures and voids of cementitious systems does not necessarily imply deterioration of the matrix; however, excessive formation of thaumasite within the microstructure of cementitious systems is an indication for TSA. There are two possible routes for thaumasite formation: direct and indirect. In the direct route, thaumasite is formed through the reaction of calcium silicate hydrate (C-S-H) with calcite in the presence of moisture and unbound sulfate ions, according to Eq. 2.8 (Skalny *et al.*, 2002):

$$SO_4^{2-} + 3Ca^{2+} + CO_3^{2-} + SiO_3^{2-} + 15H_2O \rightarrow 3CaO.SiO_2.CO_2.SO_3.15H_2O \quad \text{(Eq. 2.8)}$$

In the indirect (woodfordite) route, woodfordite is an intermediate solid solution in between ettringite and thaumasite (Bensted, 2003), ettringite acts as a precursor for thaumasite formation. In the presence of moisture carrying sulfate ions, ettringite forms first (e.g. Eqs. 2.3-2.5), and subsequently it reacts with C-S-H and carbonates/bicarbonates to form thaumasite, according to Eq. 2.9 (Schmidt, 2007):

$$C_3S_2H_3 + C_6A\bar{S}H_{32} + 2C\bar{C} + 4H \rightarrow 2C_3S\bar{C}\bar{S}H_{15} + C\bar{S}H_2 + AH_3 + 4CH \quad \text{(Eq. 2.9)}$$

Progressive formation of thaumasite has been correlated to the depletion of ettringite (Gaze and Crammond, 2000; Taylor, 1997). It was postulated that TF takes place after the consumption of Al ions to form ettringite at a molar ratio of SO_3/Al_2O_3 greater than 3 (Schmidt *et al.*, 2008). In addition, other phases such as gypsum, tricalcium aluminate (C_3A) and calcium

aluminoferrite (C_4AF) affect TF (Schmidt, 2007). It is unlikely that TF occurs without the formation of ettringite and most case studies of TSA related deterioration show that thaumasite and ettringite coexist (sometimes termed as solid solution) in the microstructure of concrete. The potential sequence (Irassar, *et al.*, 2003; González and Irassar 1998) of TF in cement-based materials is schematically shown in Figure 2.4. The indirect route shown in this figure is responsible for quicker TF than the other one because of the chemical structure (octahedral skeleton) of already formed ettringite; however both direct and indirect routes are mutually relying on each other (Bensted, 2003). In addition, TF is a continuous process and it does not stop even when there is scarcity of ettringite inside the cementitious matrix (Bensted, 2003). The continuance of TF occurs in accordance with the presence of carbonate or atmospheric CO_2 via direct route.

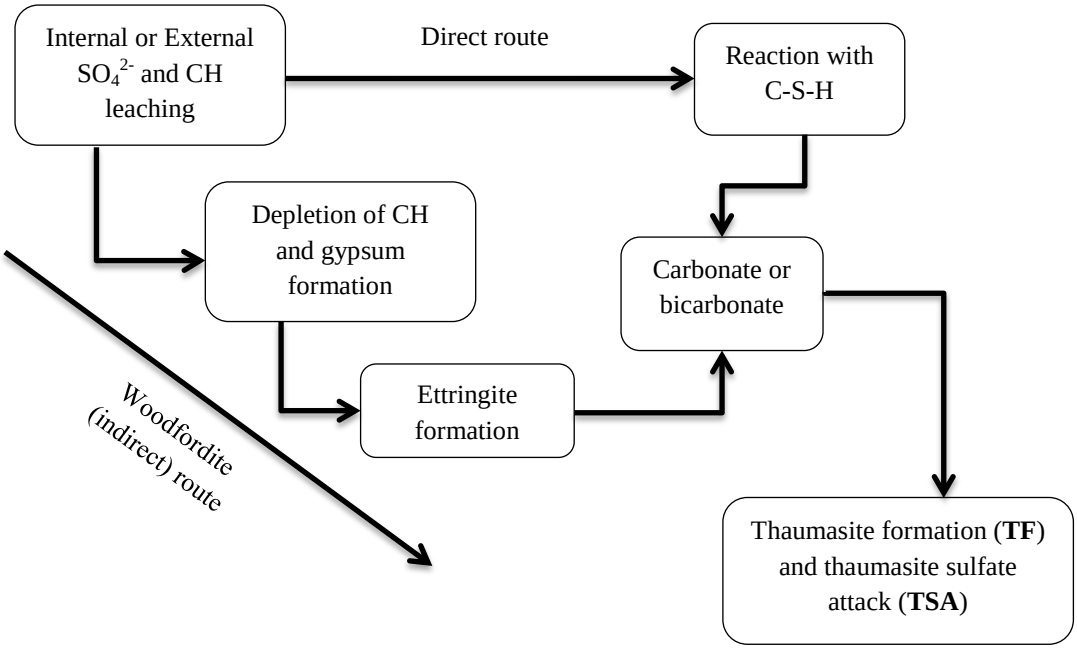

Figure 2.4: Possible direct and indirect routes of TF and TSA.

2.3.2. Features of TSA

If the source of sulfate is external to the pore structure of concrete, deterioration caused by TSA starts from the surface of concrete and progressively moves toward the sound core. In an experimental study, Higgins and Crammond (2003) described the features of TSA as a mushy white mass on the surface of specimens which was also found as residue in the test containers; they indicated that softening and erosion of the paste matrix loosened the bond with aggregates, and thus the aggregates were also vulnerable to degradation. Also, in a field case study the Thaumasite Expert Group (TEG) identified a degraded zone (up to 25 mm) due to TSA in a 29 year-old buried concrete structure enclosed by reworked clay (DETR, 1999). This structure was made of high quality concrete with a mixture of dolomitic and oolitic limestone coarse aggregate and quartz sand. The visual features of damage were generally similar to that of the laboratory specimens described earlier. The TEG indicated that progressive ionic diffusion within the deteriorated zone and subsequent TSA led to loss of strength and stiffness of concrete. Figure 2.5 shows deterioration (cracking, spalling, soft and non-cohesive mass) of precast concrete retaining wall units due TSA; in this case the source of sulfate was internal from contamination of fine aggregate with gypsum.

Figure 2.5: Visual features of precast concrete retaining wall units damaged by TSA (courtesy of Willems, T., CTLGroup, IL, USA).

2.3.3. Factors affecting the extent of TSA

There are multiple factors affecting TSA on concrete, which can be grouped into field/test related parameters (e.g. sulfate solutions, pH) and mixture design parameters (w/cm, constituent materials).

2.3.3.1. Field/Test related parameters

Temperature

The stability of thaumasite depends on temperature and usually takes place at low temperatures (5-15˚C). Favorable TF occurs at low temperatures because (Crammond, 2003): (a) thaumasite is much more insoluble, (b) the six coordinated $Si(OH)_6$ groups are more stable, (c) solubility of CO_2 in water increases, and (d) portlandite is more soluble. Nevertheless, TSA was also reported

in laboratory and field studies at higher temperatures (e.g. Bassuoni and Nehdi, 2009a; Collepardi, 1999). However, TSA is stable once formed and is thermally decomposed at about 110˚C to form thaumasite glass which is a disorganized crystal structure (Bensted, 1999).

pH level

The likelihood of TF is strongly related to the pH of sulfate bearing solution in the sense that the risk of TSA increases with pH level (Zhou *et al.*, 2006; Hobbs and Taylor, 2000). In addition, it was concluded that the combination of relatively high sulfate concentrations and alkalinity can significantly accelerate the kinetics of TSA on concrete (Zhou *et al.*, 2006; Hill *et al.*, 2003). Based on field and experimental data, Gaze and Crammond (2000) reported that thaumasite does not form at a pH level below 10.5, especially it forms above 13. If the pH drops below 10.5, thaumasite disintegrates and popcorn calcite forms in the deteriorated matrix (Clark and Thaumasite Expert Group, 2002). Comparatively, another study indicated that absence or presence of acids does not stimulate thaumasite formation (Hill *et al.*, 2003). Hobbs and Taylor (2000) postulated that pH of 12.5 is necessary for TF, when calcium hydroxide is depleted from the surface of concrete. A laboratory study showed that thaumasite reacted with different ions in the test solutions; nevertheless, the reactivity of thaumasite with phosphate, carbonate and bicarbonate ions decreased with the increase of the pH level and it was highly stable with minimum reactivity at pH greater than 12.45 (Jallad *et al.*, 2003).

Exposure Conditions

For concrete elements partially embedded in or in contact with salt-rich soils, salt crystallization can coexist with TSA (e.g. Rollings *et al.*, 2006). In these elements, there is a continual supply of sulfate ions and evaporation surfaces are created within which supersaturation of salt leads to their crystallization and consequently progressive disruption to the cementitious matrix. This

deterioration mechanism has been observed in basements of residential dwellings, slabs on grade, service tunnels and dams (e.g. Haynes and Bassuoni, 2011; Price and Peterson, 1968). In an experimental study, Bassuoni and Nehdi (2009a) observed the effect of different sulfate attack exposure regimes (full immersion, wetting/drying, and partial immersion with wetting/drying) on concrete. It was observed that for concrete comprising limestone filler exposed to partial immersion and wetting/drying, the drying portion above the solution level was damaged by crystallization of sodium sulfate, while the immersed portion of those specimens suffered significant expansion and softening due to TSA. In the case of full wetting/drying, specimens from those binders were damaged due the synergistic effects of salt crystallization, conventional sulfate attack and TSA (Bassuoni and Nehdi, 2009a).

Moreover, in other experiments which combined sulfate attack with frost action, salt crystallization, conventional sulfate attack and TF were detected in intimate assemblages in the microstructure of concrete comprising limestone filler (Bassuoni and Sonebi, 2010; Nehdi and Bassuoni, 2008). This complex damage scenario may also occur in concrete elements in tidal zones. These combined damage experiments reproduced TSA in laboratory, corresponding to some filed case studies listed in ***Appendix C*** (Table A.1) [e.g. Hagelia *et al.*, 2003; Romer *et al.*, 2003; Clark and Thaumasite Expert Group, 2002; Rogers, 1997].

2.3.3.2. Mixture design and materials related parameters

w/cm and curing

One of the key mixture design parameters of concrete is w/cm which primarily controls its physical resistance (characteristics of pore structure) to the penetrability of moisture and aggressive ions including sulfate. To improve the resistance of concrete to any type of chemical

attack (including TSA), low w/cm (typically less than 0.45) is required to discount ingress and movement of ionic species and moisture, which stimulate chemical reactions with the hydrated cement paste (Skalny *et al.*, 2002). Low w/cm ratio produces concrete with less porosity, and finer and disconnected pore structure which reduces the susceptibility to TSA. For example, Brueckner *et al.* (2012) found that the deterioration rate of concrete affected by TSA was directly dependent on the mixture design and it was significantly reduced with the reduction of w/cm. Yet, the efficacy of mixture design parameters such as w/cm is a function of curing practices. Initial curing has a profound effect on the microstructural development of concrete, and consequently its resistance to chemical attack in aggressive environments. Proper curing enables efficient hydration reactions by retaining available water within the cementitious matrix, and thus helps achieving target strength and microstructural characteristics.

Carbonate

Carbonate is one of the essential compounds needed for TF. It can originate from internal sources such as cement, coarse and/or fine aggregates and admixtures or external sources such as groundwater and atmospheric CO_2 (Sims and Huntley, 2004). High dosages (typically more than 10% by mass of binder) of finely divided carbonate (limestone filler) increases vulnerability of concrete to TSA (Lee *et al.*, 2008; Torres *et al.*, 2006; Hartshorn *et al.*, 1999). However, incorporation of limestone filler in OPC at replacement level of 5 to 10% does not show significant change on sulfate performance of concrete (Irassar, 2009). The presence of monocarbonate (from limestone) and ettringite provoke TSA (Schmidt *et al.*, 2008). Nevertheless, it is not necessary that limestone inclusion in cement will always cause TSA. Even concrete prepared with ordinary cement (limestone content is less than 5%) has shown vulnerability to TSA. This statement is supported by previous studies in which researchers

observed some level of deterioration because of TF in ordinary cement systems exposed to sodium sulfate or magnesium sulfate solutions (e.g. Irassar *et al.*, 2005). It was suggested that deterioration of concrete without limestone inclusions might be due to atmospheric CO_2, which causes TF through the formation of bicarbonate ions in the matrix (Collett *et al.*, 2004).

C_3A Content

Thaumasite formation (TF) has been correlated to alumina content in synthetic solutions, in the sense that an increase of alumina content accelerates TF even though the composition of thaumasite may not contain alumina. This is attributed to the fact that alumina increases the potential for ettringite formation, and subsequently increases the potential for TF via the woodfordite route as explained earlier (Barnett *et al.*, 2002). However, sulfate resistant portland cement (SRPC), with limited C_3A content was also found to be susceptible to TSA (Nobst and Stark, 2003), probably due to the formation of thaumasite through the direct route. Gaze and Crammond (2000) stated that thaumasite was typically generated from the preceding formation of ettringite in both magnesium and potassium sulfate solutions. Other studies showed that ettringite activated TF, where excessive expansion and cracking associated with ettringite facilitated the ingress of additional CO_2 resulting in TF (e.g. Brown *et al.*, 2004; Hartshorn *et al.*, 1999). Borsoi *et al.* (2000) showed that the combination of sulfate solutions and blended cements with 10-20% limestone filler altered ettringite to thaumasite. Also, it was observed that the vulnerability of specimens prepared from portland-limestone cement (PLC) to TSA depended on its C_3A content (Tosun-Felekoğlu, 2012). Though, Irassar (2009) explained that reactive alumina phases in PLC systems may be minimized due to the dilution effect that reduces the C_3A content and chemical interaction between $CaCO_3$ and C_3A to form calcium carboaluminate hydrate.

However, the author suggested that the dilution of C_3A content does not have significant effect on the long run when the structures are vulnerable to sulfate attack.

Supplementary Cementitious Materials (SCMs)

The beneficial effect of SCMs on improving the resistance of concrete to TSA has been reported by many authors (e.g., Higgins and Crammond, 2003; Tsivilis *et al.*, 2003; Borsoi *et al.*, 2000). Depending on the type of SCMs, their combinations and maximum limits stipulated in different codes, usually higher dosages of SCMs minimize the risk of TSA. Higher replacements levels of ordinary and limestone cements with SCM also dilute the C_3A content, which should reduce ettringite and thaumasite formation. For example, a recent study (Ramezanianpour and Hooton, 2012) has shown that replacing either ordinary cement or PLC with 50% slag makes concrete highly resistant to TSA. The CSA A3000 (2008) allows the use of PLC blended with SCMs but the average expansion limit of mortar bars, tested using CSA A3004-C8, exposed to moderate sulfate exposure shall not be exceeded (0.10% after 12 months). However, for high sulfate exposure, the expansion limit was reduced to 0.05% at 6 months.

As explained earlier, CH reacts with sulfate solutions to produce gypsum, which can further react to produce ettringite (Eqs. 2.3-2.5) and through the Woodfordite route subsequently thaumasite (Eq. 2.9). It was indicated that in the TF process, CH acts as a reactant rather than as a product (Hartshorn *et al.*, 1999). Through thermodynamic calculations, Bellmann and Stark (2008) concluded that in the presence of CH, calcium-rich C–S–H (from hydration of ordinary cement) is under severe attack due to TF. Also, the authors reported that at moderate concentration of sulfate solutions, silicon-rich C-S-H in the cementitious matrix show higher resistance against TF. In addition, the vulnerability of concrete to TSA increases when the CH is highly available on concrete exposed to sulfate environment (Higgins and Crammond, 2003).

Comparatively, reduction of CH content in the cementitious matrix due to addition of appropriate SCMs (low calcium oxide and alumina) may improve the resistance of concrete to TSA in a similar manner to conventional sulfate attack.

2.3.4. TSA tests

As previously discussed, TSA has been reported to occur under prevailing low temperatures. Hence, to study the resistance of cement-based materials to TSA, many studies (e.g., Skaropoulou *et al.*, 2012) used a modified continuous immersion procedure in which the temperature was held constant at 5°C. Canadian Standards Association (CSA) A3001 introduced a standard test for TSA (CSA A3004-C8, Procedure B) in its 2010 amendment, which is an identical test to ASTM C1012 (CSA A3004-C8, Procedure A), except that the temperature was changed to 5°C. To pass the sulfate resistance requirement, the expansion should be limited to 0.10% and 0.05% for moderate and high sulfate-resistant cement at 6 months, respectively (according to CSA A3004-C8, Procedure A). However, for CSA A3004-C8 (Procedure B) the expansion limits was set at 18 months instead of 6 months and allow continuing the test up to 24 months when the expansion limit between 12 and 18 months exceeds 0.03% but for any kind of binders the limit shall not exceed 0.10%.

Similar to the case for ASTM C1012, CSA A3004-C8, Procedure B only considers one unique situation in which mortar/concrete is constantly exposed to a continual supply of sulfate ions at a constant low temperature (e.g., buried elements). This, however, might not be the only case under which TSA can occur. Indeed, TSA occurs under different environmental conditions involving variable/cyclic temperature and humidity (e.g., partially embedded structures, tunnels). Some studies investigated the effect of TSA on cement-based materials, for example they considered different types of solutions (e.g. Brueckner *et al.*, 2012; Barker and Hobbs, 1999),

exposure/temperature conditions (e.g. Skaropoulou *et al.*, 2012; Bassuoni and Sonebi, 2010) and pH levels (e.g., Zhou *et al.*, 2006). For example, Yamada *et al.* (2006) exposed concrete prepared with various proportions of ordinary cement, limestone filler and ground granulated blast furnace slag (GGBS) to artificial seawater (solutions containing Cl^-, Mg^{2+}, Ca^{2+} and SO_4^{2-} ions with concentrations comparable to that of natural seawater) at temperatures of 20℃ and 5℃ for 6 months. Also, to explore field performance, concrete specimens were placed in a tidal zone in Japan, where the annual daily average temperature was 2.6°C. They concluded that TF was suppressed due to the effect of chloride ions. The beneficial effect of SCMs was found by Day and Middendorf (2011), where they soaked mortars produced from GU cement and 30% fly ash (both Type F and CI) in 0.35 M Na_2SO_4 solution for up to 3 years at 20˚C which performed better in reducing expansion than the one with only GU cement mortars. In a series of laboratory studies, Bassuoni and coworkers (2008, 2009a, 2009b and 2010) investigated the effect of TSA on self-consolidating concrete made from binders containing limestone filler using a combined damage approach involving sodium sulfate attack with other factors existing in the field such as frost action, wetting/drying, and cyclic environments (alternating freezing/thawing and wetting/drying cycles). Under all exposure conditions, concrete mixtures comprising 15% limestone filler deteriorated due to TSA.

2.4. Code provisions for sulfate attack on concrete

To date, there is no specific recommendation in the last version of the American Concrete Institute (ACI) 201.2R-08: Guide to Durable Concrete on TSA or PSA. However, this document gives general guidance for improving the resistance of concrete to conventional sulfate attack, which is also applicable to the case of PSA and TSA considering the factors discussed in the preceding sections. In addition to proper construction and curing practices, ACI201.2R-08

provides guidance based on the severity of sulfate exposure, where w/cm varies from 0.50 (low concentration of sulfate in soil or water) to 0.40 (high concentration of sulfate in soil or water). Also, the type of cement depends on the severity of exposure. Generally, sulfate resisting portland cements with low C_3A content and SCMs (or equivalent) are recommended for severe exposures based on their performance in the ASTM C1012 test. For example, for blended binders subjected to Class 3 sulfate exposure (more than 10,000 ppm in water), the ACI 201.2R permits an expansion of up to 0.10% after 18 months of exposure following the ASTM C 1012 procedure.

Canadian Standards Association (CSA) A23.1 (2009) follows a similar approach to that of ACI201.2R to improve the resistance of concrete to conventional sulfate attack based on the severity of exposure. Provision for PSA is implicitly considered by reduction of w/cm with the severity of sulfate exposure. To mitigate the risk of TSA on concrete, the current version of CSA 23.1 provides an explicit statement on preventing the use of portland-limestone cements (PLC) or mineral fillers of calcium or magnesium carbonate, where sulfate is prevalent. The modified version of CSA A3000-08 (2010 amendment) included the minimum requirement of SCMs to make sulfate resistance PLC. According to CSA A3000, for binary blended moderate and high sulfate resistant PLC, the minimum amount of Type F fly ash, slag and metakaolin shall be 25, 40 and 15%, respectively. However, for ternary blended PLC, 5% Type SF silica fume shall be added with a combination of 25 % slag or 20% Type F fly ash. In addition, the CSA A3004-C8 test method (both procedures A and B) has to be performed to qualify binders for moderate and severe sulfate exposures.

For moderate to severe sulfate exposures at temperatures between 5-25°C, European standard (EN 206-1) imposes some limitations on maximum w/cm ratio (0.55-0.45), minimum

cement content (300-360 kg/m^3) and minimum strength (30-35 MPa) (BS EN 206-1, 2000). The European standard EN 197-1 (2000) for cement, classifies different types of PLC in which the content of limestone filler ranges from 6% to 35%. Also, the standard classifies blast furnace cements, portland fly ash cement and pozzolanic (siliceous fly ash) cements as sulfate resisting cements (including the thaumasite form). Whereas PLC cements can only be used in Class XA1 (< 200 and ≤ 600 ppm SO_4^{2-} in water), sulfate resisting cements are recommended for Classes XA2 (< 600 and ≤ 3000 ppm SO_4^{2-} in water) and XA3 (< 3000 and ≤ 6000 ppm SO_4^{2-} in water) (EN, BS. 197-1, 2000).

Based on the aforementioned information, it is suggested that the resistance of concrete to different forms of sulfate attack can be improved by the combination of physical and chemical aspects. Producing concrete with limited penetrability (physical resistance: low w/cm, adequate cement content, SCMs, proper placement and consolidation, adequate curing) is the first line of defense against sulfate attack to slow down the migration of moisture, sulfate and CO_2 into concrete. Furthermore, the chemical resistance of concrete to sulfate attack can be improved by limiting the contents of C_3A, CH and limestone, which can be achieved by using adequate dosages of SCMs. For instance, Class F fly ash with minimum percentage (25%) dilutes the chemical phases of OPC and reduces the CH content in the hydrated cement paste.

2.5. Durability of nano-modified concrete

Advancement of nanotechnology has introduced new materials to the concrete industry termed as "nanoparticles" (less than 100 nm) which have novel properties (Sanchez and Sobolev, 2010). These materials alter the microstructure of cementitious composites at the nano level to improve the fresh and physico-mechanical properties, and durability of concrete. The main advantage of using nanoparticles is that nanoparticles potentially act as nucleation sites to improve the kinetic

of hydration (Birgisson *et al.*, 2012). Also, nanoparticles vigorously react with the hydration products because of their high surface area to volume ratio. Furthermore, nanoparticles reduce the porosity of concrete by producing more hydrated products and densifying the microstructure including the interfacial transition zone (ITZ) [Garas *et al.*, 2010]. However, the effects of nanoparticles are valid only if effectively dispersed in the cementitious matrix (Nazari and Riahi 2011).

Most studies on the effect of nanoparticles on the properties of concrete have focused on nano-silica, nano-titanium oxide, nano-iron, nano-alumina, nano-zirconium dioxide and nano-clay particles (Safiuddin *et al.*, 2014). Among these, nano-silica (NS) was found to have the most promising effect on improving the microstructure, and reducing the metastable CH phase in the matrix to produce more primary hydration phase (C-S-H) (Sanchez and Sobolev, 2010). The effect of NS addition to increase the compressive strength and aging resistance is significant (Zhang *et al.*, 2002). Moreover, incorporation of NS increases both early-age and long-term strength and activates the pozzolanic activity of slow pozzolans (e.g., fly ash) [Li, 2004]. It accelerates the hydration reaction of the C_3S phase, which is the main phase responsible for strength and stability of the matrix (Bjornstrom *et al.*, 2004). NS also acts as a filler to improve the microstructure (Jo *et al.*, 2007). As a result, this particle packing effect of NS densifies the nano- and micro-structures of the cementitious matrix. It was found that NS improves consistency and cohesiveness of self-consolidating concrete, and reduces bleeding and segregation of mixtures (Collepardi *et al.*, 2002). Moreover, NS addition in cement-based grouts reduced the plastic shrinkage up to 24 hours because of the acceleration of hydration and reduction of dormant period (Sonebi *et al.*, 2014).

In recent durability studies, NS reduced the physical penetration depth of chloride ions in concrete as a result of refining the pore structure and reducing the connectivity of pores (Said *et al.*, 2012). Also, Ji (2005) found that NS reduced the water permeability and improved the microstructure of concrete. It was found that NS addition in mixtures reduced the threshold pore diameters compared to the mixtures without NS (Said *et al.*, 2012). This refinement increased when the percentages of NS increased in the mixtures. A recent study by Duran *et al.* (2014) showed that high dosages of NS addition in lime mortars reduced vulnerability to freeze–thaw cycles and magnesium sulfate attack. In an experimental study, Atahan and Dikme (2011) observed that only 2% NS improved the resistance of mortars to external sulfate attack and limited the length expansion below 0.03%. Also, authors found that 4-6% NS in mortars were enough to resist the internal sulfate attack after 12 months of exposure.

The incorporation of nano-alumina (NA) reduces the workability of fresh concrete and increases the normal consistency (Nazari *et al.*, 2010; Lange *et al.*, 1997). It was reported that the addition of 5% nano-alumina (NA) significantly improved the modulus of elasticity of mortars up to 143% (Li *et al.*, 2006). Also, it was found that NA incorporation in cement-based mortars at a dosage of 1.25% by mass of cement increased the compressive strength significantly at 3 and 7 days (Oltulu and Remzi, 2011). In the same study, however, it was found that incorporation of 2.5% NA led to lower compressive strength at early ages but higher compressive strength at later ages. It was stated that the increase of NA content up to a maximum limit of 1.25% has a similar effect on improving long-term strength to SCMs. An experimental study by Behfarnia and Salemi (2013) showed that the addition of NA in concrete improved the frost resistance because of the densifying effect on improving the microstructure. This may be attributed to its effect on reducing the penetrability of concrete (He and Shi, 2008). It was reported that NA decreased the

total absorption, chloride penetration and generally improved the durability of concrete (Shekari and Razzaghi, 2011).

Up till now, research efforts have been mainly focused on studying the fresh and mechanical properties of concrete modified with NS and NA but limited data are available on the effect of these nanoparticles on key durability issues, such as sulfate attack. Few studies involved the use of NS in concrete exposed to sulfate environment. For example, Moslemi *et al.* (2014) investigated the effect of the dosages of NS in concrete exposed to 5% sodium sulfate solution for 180 days. They concluded that the addition of 8% NS improved the resistance of concrete to sulfate attack. However, the assessment criterion was mainly based on mass loss, with limited microstructural analysis. Zeidan (2013) investigated the effect of NS on fly ash concrete under a sulfate exposure conductive to PSA. He reported that NS had mixed effect on the resistance to PSA; incorporation of NS with GU cement improved the resistance to PSA while addition of NS with binary binders (GU cement and fly ash) diminished the effect of improvement on the resistance to PSA. Baoguo *et al.* (2014) used NS and two types of limestone to evaluate the resistance of concrete to TSA. In their experimental program, they did not assess the cementitious materials based on the length expansion result which is the primary test used to determine the resistance of concrete to TSA in North America. The authors concluded that mortars exposed to magnesium sulfate solution severely deteriorated; while no damage manifestation on mortar samples was found when exposed to sodium sulfate solution.

2.6. Closure

Extensive research has been done on conventional sulfate attack as reflected by the evolution of code provisions to this concrete durability issue. Yet, special forms of sulfate attack such as PSA and TSA still needs further research to investigate the effects of key parameters such as w/cm,

type of binder, and pore structure characteristics on the response of concrete vulnerable to these types of damage. On the other hand, the advent of nanoparticles to the concrete industry has a promising impact to improve the long-term performance of concrete infrastructure. However, research on nano-modified concrete is still in its infancy and has mainly focused on hydration kinetics and physico-mechanical properties. To date, there is dearth of information on the durability characteristics of nano-modified concrete, such as its resistance to special forms of sulfate attack. In particular, no published work has focused on investigating the effect of nanoparticles (e.g. NA and NS) combined with SCMs on the response of cement-based materials to physical salt attack and thaumasite sulfate attack. Hence, the motive of this research, which mainly aims at capturing improvement trends and/or performance limitations of nano-modified fly ash concrete, and thus contributing to updating current code provisions for these durability issues.

3. Experimental Program

This chapter describes the materials, mixture designs, exposures and experimental methods in this research program.

3.1. Materials and Mixtures

3.1.1. Physical salt attack (PSA)

In this part of the experimental program, general use (GU) portland cement and fly ash (Class F) meeting the requirements of CAN/CSA-A3001-08 standard were used as the main components of the binder. In addition, two ultrafine nanoparticles [nano-silica (NS) and nano-alumina (NA)] were also used at different dosages in some mixtures. Both ultrafine particles were used in colloidal form (already dispersed) with NS and NA solid contents of 50% and 20% by mass, respectively. The chemical composition and physical properties of the cement and fly ash are given in Table 3.1 and the physical characteristics of nanoparticles are shown in Table 3.2. The target consistency of fresh concrete was achieved by a high-range water reducing admixture (HRWRA) based on polycarboxylic acid and complying with ASTM C494-13 Type F. This HRWRA was added at different dosages (0 to 75 ml per 0.009 cubic meter of concrete) to the mixtures in order to maintain a slump range of 50 to 100 mm. Locally available natural gravel (max. size of 9.5 mm) was used as coarse aggregate; its specific gravity and absorption were 2.65 and 2%, respectively. The fine aggregate was well graded river sand with a specific gravity, absorption, and fineness modulus of 2.53, 1.5% and 2.9, respectively.

Sixteen concrete mixtures were tested in this study; the total binder content in all mixtures was kept constant at 400 kg/m^3. The mixture design variables were w/cm (0.4 and 0.5),

type of binder (GU cement or GU cement blended with fly ash) and ultrafine particles (nano-silica or nano-alumina). Single binder (control) mixtures were prepared from 100% GU cement, while blended binder mixtures incorporated 70% GU and 30% fly ash as a replacement of the total binder content. The colloidal nano-silica and nano-alumina were added at 3 and 6% replacement levels by mass of the total binder content to prepare the binary (comprising GU cement and nanoparticles) and ternary binders (comprising GU cement, fly ash and nanoparticles). Table 3.3 shows the mixture design proportions of the concrete tested in this study. Concrete was mixed in a mechanical mixer and cast in cylindrical moulds (75×150 mm) to prepare two replicates for each mixture. The concrete cylinders were demoulded after 24 hours, and then cured for 28 days at standard conditions (22 ± 2˚C and 98% RH) according to ASTM C192-07. A recent study (Said et al., 2012) has shown that addition of nanoparticles to concrete containing 30% fly ash accelerates the rate of hydration and microstructural development to a level comparable to concrete prepared from single binders containing 100% ordinary cement. Hence, the curing period for the fly ash concrete was not extended in the current study, which also provides a uniform basis for comparison among all the mixtures.

3.1.2. Conventional and Thaumasite sulfate attack (TSA)

In part of the experimental program, two types of cement were used: general use (GU) portland cement and portland-limestone cement (PLC), meeting CSA A3000-08 (Cementitious Materials Compendium) specifications to produce various mortar mixtures. GU cement was mixed with limestone filler to produce blended limestone cement (defined as GUL hereafter) at a cement replacement level of 13%. The dosage of limestone filler in GUL was selected similar to that in PLC, which was produced by intergrinding limestone filler with clinker. Class F fly ash (FA) was used in some (binary and ternary) binders at replacement levels of 15, 30 and 40% of the

total binder content. Also, two types of nanoparticles [nano-silica (NS) and nano-alumina (NA)] were used at a dosage of 6% by the total binder content to produce ternary binders. The solid content of the colloidal NS and NA are 50 and 20% by mass, respectively. The chemical composition and physical properties of cements, fly ash and limestone filler are given in Table 3.1, and the physical characteristics of nanoparticles are presented in Table 3.2. The target flow of fresh mortar was achieved by a high-range water reducing admixture. This HRWRA was added at different dosages (0 to 30 ml per 5.5 kg of mortars) to the mixtures in order to maintain a flow table value of 110 ± 5%, according to CSA A3004-C1-08. Similar to the PSA experiment, the fine aggregate used in this study was well graded river sand with a specific gravity, absorption, and fineness modulus of 2.53, 1.5% and 2.9, respectively.

Table 3.1: Chemical composition and physical properties of the cements, fly ash and limestone filler

	GU	**PLC**	**Fly Ash**	**Limestone Filler**
Chemical Composition				
SiO_2 (%)	19.8	18.9	56.0	--
Al_2O_3 (%)	5.0	4.4	23.1	--
Fe_2O_3 (%)	2.4	3.2	3.6	--
CaO (%)	63.2	63.4	10.8	--
MgO (%)	3.3	0.7	1.1	--
SO_3 (%)	3.0	2.7	0.2	--
Na_2O (%)	0.1	0.3	3.2	--
$CaCO_3$ (%)	--	--	--	95.0
$MgCO_3$ (%)	--	--	--	2.0
Physical Properties				
Blaine (m^2/Kg)	410	454	290	475
Specific Gravity	3.17	3.11	2.12	2.71

Table 3.2: Physical characteristics of nano-silica and nano-alumina

	Nano-silica (NS)	**Nano-alumina (NA)**
Solid content, wt%	50	20
pH	9.5	--
Viscosity, cP	8	--
Density, g/cm^3	1.40	1.19
Na_2O, wt%	0.2	--
Mean Particle Size (nm)	35	50

Twenty four mortar mixtures with a fixed water-to-binder ratio of 0.485 were prepared in this study. The mixture design proportions were 1 part of binder (GUL or PLC, fly ash and nanoparticles) to 2.75 parts of sand according to the standard test procedure of CSA A3004-C8-08 (similar to ASTM C 1012-13). The mixture design variables were types of binder (GU, GUL or PLC), dosages of fly ash and ultrafine particles (nano-silica and nano-alumina). The mixtures were classified into six groups (A to F). Groups A, B, and C included single binder mixtures made from 100% GU or GUL, binary binder mixtures incorporating GU or GUL with different dosages of fly ash and ternary binder mixtures incorporating GUL, fly ash and NS or NA. The type of binder (single, binary and ternary) in groups D, E and F were similar to that of groups A, B, and C expect that PLC cement was used instead of GU or GUL. Table 3.4 shows the mixture design proportions of the mixtures tested. Mortar was mixed in a mechanical mixer and cast in prism (25×25×285 mm) and cube (50×50×50 mm) moulds to manufacture four and six replicates for each mixture, respectively. Subsequently, the moulds were immediately sealed and placed in the curing room at 23 ± 2°C after casting to prevent evaporation from the top surface of freshly mixed mortar. The mortar prisms and cubes were demoulded after 24 hours and placed in water saturated with lime solution at 23 ± 2 °C for 28 days, to furnish for a uniform basis of comparison on the same period of curing.

Table 3.3: Proportions of mixtures per cubic meter of concrete (PSA Exposure)

Mixtures	Cement (kg)	Water* (kg)	Fly Ash (kg)	NS (kg)	NA (kg)	Coarse Aggregate (kg)	Fine Aggregate (kg)	Compressive Strength (MPa)
w/cm = 0.4								
GU-0.4	400	160	--	--	--	1200	580	44
F-0.4	280	160	120	--	--	1200	540	42
GUS3-0.4	388	148	--	24	--	1200	575	52
GUA3-0.4	388	112	--	--	60	1200	590	43
FS3-0.4	268	148	120	24	--	1200	530	42
FS6-0.4	256	136	120	48	--	1200	530	43
FA3-0.4	268	112	120	--	60	1200	540	46
FA6-0.4	256	64	120	--	120	1200	545	46
w/cm = 0.5								
GU-0.5	400	200	--	--	--	1200	480	34
F-0.5	280	200	120	--	--	1200	435	23
GUS3-0.5	388	188	--	24	--	1200	470	38
GUA3-0.5	388	152	--	--	60	1200	485	31
FS3-0.5	268	188	120	24	--	1200	425	32
FS6-0.5	256	176	120	48	--	1200	420	30
FA3-0.5	268	152	120	--	60	1200	435	30
FA6-0.5	256	104	120	--	120	1200	445	34

Notes: "*" This is the adjusted amount of water used in the mixing after considering the absorption of coarse and fine aggregate, and the water content of NS and NA.

Table 3.4: Proportions of the binders (in mass percentage) used in the mortar mixtures (Conventional and TSA exposures)

Mixture ID.	GU	GUL	PLC	Fly Ash	NS (%)	NA (%)	*fc'* at 28 days
GU/GUL							
Group A							
GU	100	--	--	--	--	--	55
GUL	--	87	--	--	--	--	52
GUF15	85	--	--	15	--	--	50
GULF15	--	74	--	15	--	--	46
GULF15S6	--	69	--	15	6	--	46
GULF15A6	--	69	--	15	--	6	38
Group B							
GU	100	--	--	--	--	--	55
GUL	--	87	--	--	--	--	52
GUF30	70	--	--	30	--	--	49
GULF30	--	61	--	30	--	--	48
GULF30S6	--	56	--	30	6	--	49
GULF30A6	--	56	--	30	--	6	37
Group C							
GU	100	--	--	--	--	--	55
GUL	--	87	--	--	--	--	52
GUF40	60	--	--	40	--	--	40
GULF40	--	52	--	40	--	--	39
GULF40S6	--	47	--	40	6	--	44
GULF40A6	--	47	--	40	--	6	28
PLC							
Group D							
PLC	--	--	100	--	--	--	60
PLCF15	--	--	85	15	--	--	57
PLCF15S6	--	--	79	15	6	--	62
PLCF15A6	--	--	79	15	--	6	45
Group E							
PLC	--	--	100	--	--	--	60
PLCF30	--	--	70	30	--	--	52
PLCF30S6	--	--	64	30	6	--	48
PLCF30A6	--	--	64	30	--	6	43
Group F							
PLC	--	--	100	--	--	--	60
PLCF40	--	--	60	40	--	--	45
PLCF40S6	--	--	54	40	6	--	42
PLCF40A6	--	--	54	40	--	6	37

3.2. Exposures

3.2.1. Physical salt attack

After the standard curing, concrete cylinders were air-dried (at 20°C and 50% RH) for 48 hours to determine their initial properties (mass, strength and dynamic modulus of elasticity) before the PSA exposure. Subsequently, the concrete cylinders were partially immersed up to one-third of the total height in plastic containers with air tight lids containing a high-concentration (10%) sodium sulfate solution (Figure 3.1). To minimize the evaporation of solution, the lids were cut circularly to provide an opening equal to the diameter of cylinder. The very high concentration of solution was selected to accelerate the test procedure. Moreover, the exposed (drying) portion of specimens was subjected to cyclic temperature and humidity conditions based on the phase diagram of sodium sulfate to provoke repetitive crystallization of the salt from anhydrous (thenardite) to hydrous (mirabilite) states, which is associated with volume increase (Figure 2.2). The exposure continued for 120 days, where each cycle (24 hours) consisted of two consecutive stages: an 8-hour hot/dry stage (40±2℃ and 35±5% RH) followed by a 16-hour temperate/humid stage (20±2℃ and 90±5% RH) [Figure 3.1]. This range of temperature and humidity can be correlated to seasonal variations in many geographic locations around the world (e.g. southern parts of Canada and United states). Continuous absorption of the solution, especially during the drying stages reduced the solution level in the containers; the solution was therefore frequently replenished in order to maintain the solution level to one-third of the height of cylinders. Also, the solution was replaced with a fresh one every 30 cycles (days).

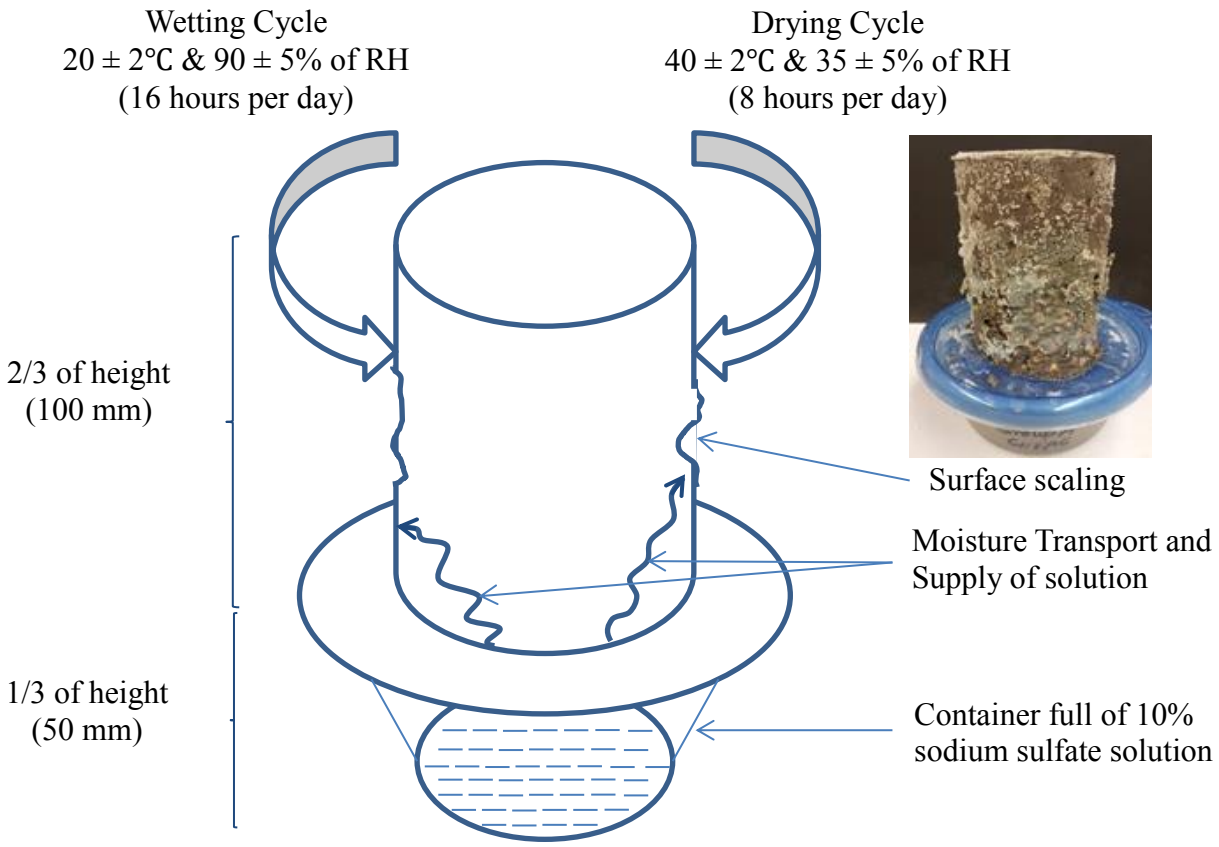

Figure 3.1: Schematic diagram showing the PSA exposure of a concrete specimen.

3.2.2. Conventional sulfate attack

In a similar procedure to CSA A3004-C8-08 (Procedure A), the mortar bars and cubes (two replicates per mixture) were immersed in 5% sodium sulfate (Na_2SO_4) solution at 23°C for 12 months. Solutions were renewed each three months, and the pH was controlled at a range of 6.0-8.0 by titration with diluted sulfuric acid solutions at regular time intervals (5 days). Regular stirring was conducted to allow for a homogenous distribution of the solutions. While controlling the pH of the sulfate solution was not specified in CSA A3004-C8, the importance of a controlled pH (6.0-8.0) of a sulfate solution correlates to field conditions in which concrete exists in a neutral environment with continual supply of sulfate ions (Skalny *et al.*, 2002; Mehta, 1992).

3.2.3. Thaumasite sulfate attack (TSA)

To provoke thaumasite sulfate attack on mortar specimens, the modified version of CSA A3004-C8 (Procedure B) test procedure was generally followed. This procedure is similar to the CSA A3004-C8 (Procedure A), except the temperature was kept at 5°C instead of 23°C. Similar to the conventional sulfate attack exposure, two replicates of mortar bars and cubes per each mixture were tested in the TSA exposure up to 12 months (uniform basis of comparison with the conventional sulfate attack exposure). Also, renewal of solution and pH control was done in a similar manner as the conventional sulfate attack exposure.

3.3. Tests

3.3.1. Tests on Concrete Mixtures (PSA exposure)

In the PSA exposure, plastic properties (i.e., slump) and physico-mechanical properties (i.e., mass and compressive strength) of concrete were evaluated. At the end of initial curing, concrete specimens from each concrete mixture were tested for compressive strength in accordance with ASTM C39-12a (Standard Test Method for Compressive Strength of Cylindrical Concrete Specimens).

To evaluate the penetrability of the pore structure of the concrete mixtures, the rapid chloride penetrability test (RCPT: ASTM C1202-12, Standard Test Method for Electrical Indication of Concrete's Ability to Resist Chloride Ion Penetration) was performed at 28 days on duplicate specimens from all mixtures. Concrete discs (100×50 mm) were mounted between cathodic (3% NaCl solution) and anodic (0.3 N NaOH solution) compartments under a potential difference of 60 V DC for 6 hours. The data acquisition system connected to the cells automatically collected charges passing through the discs (in coulombs) during the test period.

To avoid the electrolysis bias of this method, the penetration depth of chloride ions into concrete, which better correlates to the physical characteristics of the pore structure, was determined according to Bassuoni *et al.* (2006). After the RCPT, the specimens were axially split and sprayed with 0.1 M silver nitrate solution, which forms a white precipitate of silver chloride in approximately 15 minutes, to measure the physical penetration depth of chloride ions. The average depth of the white precipitate was determined at five different locations along the diameter of each half specimen. This depth is considered to be an indication of the ease of ingress of chloride ions, and thus the connectivity of the microstructure (Bassuoni *et al.*, 2006).

During the PSA exposure, the specimens were monitored at regular time intervals (every 12 to 15 cycles). After the hot/dry exposure period, salt efflorescence and debris were carefully removed from the surface of the specimens using a nylon brush. The specimens were then left to dry in lab conditions for about six hours before visual inspection and recording their masses. The visual assessment was determined using a numerical scale from 0 (no scaling) to 5 (severe scaling) in a similar manner to ASTM C672-12 (Scaling Resistance of Concrete Surfaces Exposed to Deicing Chemicals). Also, a pictorial visual rating scale was developed based on experimental trials as shown in Figure 3.2.

3.3.2. Tests on Mortar Mixtures (Conventional and TSA exposures)

In these exposures, fresh properties including flowability (CSA A3004-C1), visual observations and physico-mechanical properties (length change, mass change, dynamic modulus of elasticity, compressive strength, and RCPT) of mortar were evaluated. At the end of initial curing (28 days), 50 mm replicate mortar cubes from each mixture were tested for compressive strength in accordance with CSA A3004-C2 standard. The compressive strength results at 28 days are listed

in Table 3.4, which were in the range of 28 to 62 MPa. These values are well above the minimum strength (20 MPa) required by CSA A3004-C8 before exposure.

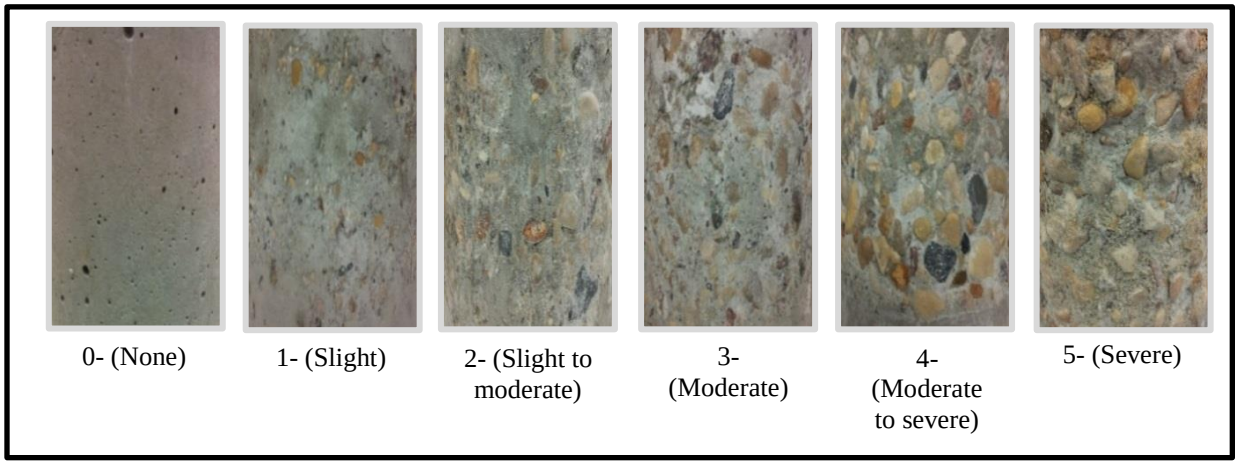

Figure 3.2: Visual rating of concrete deterioration based on experimental trials.

Similar to the RCPT on concrete specimens in the PSA exposure, the penetrability of chloride ions into mortar mixtures was evaluated by RCPT at 28 days according to ASTM C1202-12. Although this test is prescribed for concrete specimens, it was used herein to qualitatively assess the interconnectivity of pores in the mortar mixtures, and thus their penetrability. Further details regarding the test procedure was described in section 3.3.1.

To study the effect of both exposures on the expansion of specimens, this study focused on determining the length change of the mortar bars (Figure 3.3) at different time intervals (1, 2, 3, 4, 8, 13, and 15 weeks, and subsequently at 4, 6, 9, and 12 months) of exposure in compliance with the standard's recommendation. Also, the change of mass of mortar bars was determined at the same time intervals. In addition, the change in the dynamic modulus of elasticity (DME) of mortar cubes over time (during the exposure) was determined from ultrasonic pulse velocity (UPV) [Figure 3.4] measurements, according to ASTM C597-09 (Eq. 3.1).

$$\vartheta = \sqrt{\frac{E_d(1-\mu)}{\rho(1+\mu)(1-2\mu)}} \text{ Or, } E_d = \frac{\vartheta^2\rho(1+\mu)(1-2\mu)}{(1-\mu)} \quad \text{(Eq. 3.1)}$$

Where, ϑ = Pulse Velocity (PV), E_d = Dynamic Modulus of Elasticity (DME), ρ = Mortar density, V = Volume of the mortar cubes, μ = Dynamic Poisson's ratio. Furthermore, the relative dynamic modulus of elasticity (RE_d) of mortar mixtures was calculated by comparing the DME at different time intervals of the exposures to the initial values (before the exposure) and plotted against the time of exposure.

Figure 3.3: Length comparator utilized for determining the change in length of mortar bars.

Figure 3.4: Ultrasonic Pulse Velocity (UPV) test apparatus used to determine the DME.

3.4. Microstructural, Mineralogical and Thermal Analyses

To identify the underlying mechanisms of damage, the alteration of microstructure in deteriorating specimens was studied by microscopy, and thermal and mineralogical analyses. To detect PSA, fracture concrete surfaces were extracted from the surface (up to 20 mm depth) of the drying and immersed portions of selected specimens to be examined by scanning electron microscopy (SEM) [Figure 3.5] assisted with energy-dispersive X-ray analysis (EDX). Nonetheless, deteriorated mortar samples were used for the same test to investigate conventional and thaumasite sulfate attack. The samples were coated with a fine layer of carbon before performing the analysis to make the surface conductive and to improve the sample imaging. To complement the analysis from the SEM, the reaction products within the cementitious matrix, were analyzed by X-ray diffraction (XRD, Cu-Kα) [Figure 3.6] and differential scanning calorimetry (DSC) [Figure 3.7] on powder samples collected from the surface (0-20 mm from

the exposed surface) of selected specimens. This powder was prepared from carefully extracted fracture pieces (not including large coarse aggregate) of specimens, which were pulverized to fine powder passing through sieve #200 (75 μm). While, mortar pieces were collected from the deteriorated mortar bars and cubes, and pulverized to fine powder to detect the formation of sulfate-bearing products in cementitious matrix. For XRD, scan speed of 2°/min and sampling interval of 0.01° 2θ was used for all the samples. Furthermore, the samples were heated up to 500°C with a ramp temperature of 5°C/min in the DSC tests.

Figure 3.5: SEM sample chamber where the fracture pieces were mounted.

Figure 3.6: XRD instrument where the powder samples were mounted.

Figure 3.7: DSC instrument where the powder samples were mounted.

4. Results and Discussion for Physical Salt Attack

4.1. Results

4.1.1. Rapid Chloride Penetrability Test

After completing the RCPT, the physical penetration depth of chloride ions was measured for concrete specimens prepared from all the mixtures. The whitish precipitate indicating the penetration depth of chloride ions was clearly visible, as for example shown in Figure 4.1. The average passing charges, chloride ion penetrability class according to ASTM C1202-12 and average penetration depth of the mixtures are listed in Table 4.1. It can be noted that the trend of passing charges and penetrability class is consistent with that of the penetration depth in the sense that high passing charges corresponded to large penetration depth and vice versa.

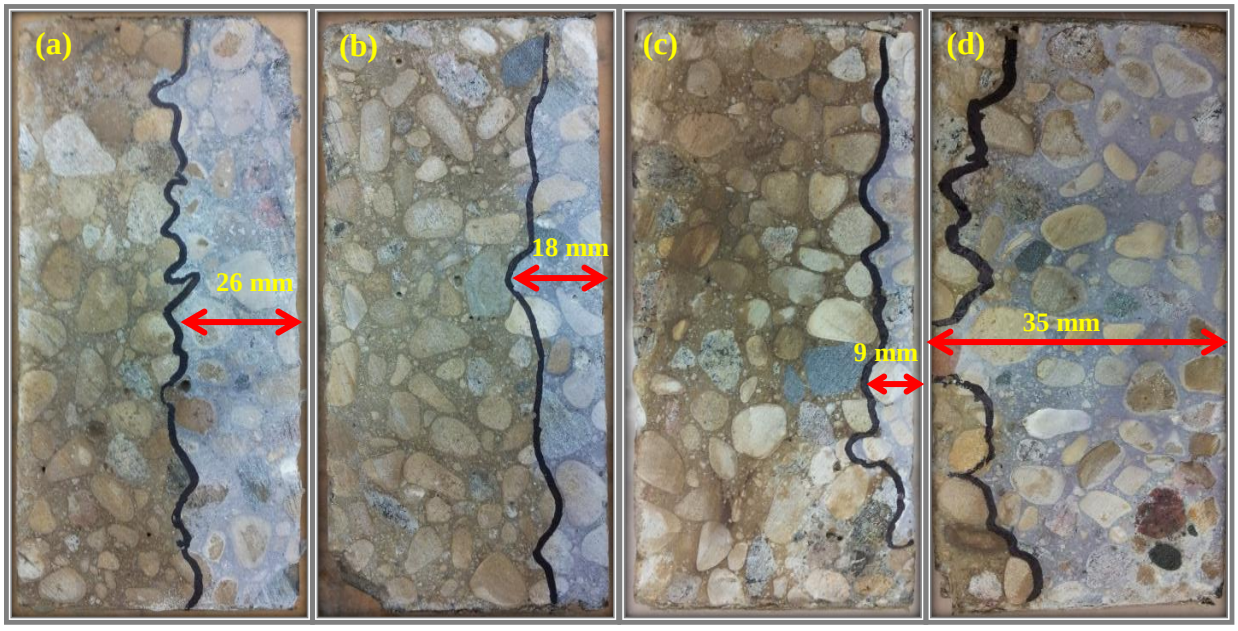

Figure 4.1: Whitish precipitate showing the penetration depth of chloride ions in mixtures: (a) GU-0.4, (b) F-0.4, (c) FS3-0.5 and (d) FA6-0.5.

Table 4.1: RCPT results

Mixture	**Charges Passed** (coulombs)	**Chloride Ions Penetrability Class** (ASTM C1202)	**Average Penetration Depth** (mm)
w/cm = 0.4			
GU-0.4	4086	High	26
F-0.4	2254	Moderate	18
GUS3-0.4	1854	Low	9
GUA3-0.4	5508	High	29
FS3-0.4	921	Very Low	6
FS6-0.4	522	Very Low	4
FA3-0.4	2241	Moderate	14
FA6-0.4	3185	Moderate	23
w/cm = 0.5			
GU-0.5	5144	High	32
F-0.5	4285	High	27
GUS3-0.5	2693	Moderate	14
GUA3-0.5	6539	High	44
FS3-0.5	984	Very Low	9
FS6-0.5	744	Very Low	7
FA3-0.5	2301	Moderate	23
FA6-0.5	5114	High	35

The average penetration depth for the mixtures prepared with w/cm of 0.4 and 0.5 was in the range of 4 to 30 mm and 7 to 44 mm, respectively. Conforming to the well-documented trend of the effect of w/cm on the penetrability of concrete, all specimens with 0.5 w/cm yielded higher penetration depth than that of corresponding specimens prepared with w/cm of 0.4. For example, the penetration depth in the control specimens prepared from GU-0.5 mixture was about 23% higher than that of the control specimens from GU-0.4 mixture, which was 26 mm. Compared to single binder (control) mixtures, the incorporation of fly ash in binary binders (F-0.4 and F-0.5) significantly reduced the penetration depth at both w/cm (Table 4.1), even at 28 days. The results show that NS addition reduced the chloride penetration depth (less than 15 mm) compared to the other mixtures in each group of mixtures (w/cm of 0.4 and 0.5). Also, increasing the dosage of NS up to 6% in the ternary binders (FS6-0.4 and FS6-0.5) led to further reduction

in the penetration depth. On the contrary, the addition of NA markedly increased the penetration depth, especially at the higher w/cm. For example, specimens from mixture GUA3-0.5 had the highest penetration depth of 44 mm, which is about 38% higher than that of the control specimens from mixture GU-0.5.

4.1.2. Visual assessment

Specimens exposed to the PSA regime was continuously observed throughout the test period. During the hot/dry stage of the cycles, the rate of solution uptake was higher due to faster evaporation of moisture from the surface of the top (drying) portion of specimens, which caused salt deposition on the surface of specimens. After 3 to 5 cycles of exposure, efflorescence started to notably grow on the drying portion of specimens, followed by progressive surface scaling and flaking. For instance, Figure 4.2 shows enormous amount of efflorescence on the evaporative zone of deteriorated concrete cylinders at the end of exposure. At the initial stage of deterioration, surface scaling started above the level of the solution (lid) and then it propagated toward the top of specimens. At the end of exposure, the cross section of specimens was considerably reduced as a consequence of progressive surface scaling of concrete. The sequence of deterioration of concrete specimens (e.g. see ***Appendix A***) over time is for example shown in Figure 4.3.

The visual ratings of specimens at different ages of exposure, according to the rating shown in Figure 3.2, are listed in Table 4.2. After about 15 cycles, coarse aggregate began to appear in some specimens (e.g., FS3-0.5, FA6-0.5). The drying portion of all specimens started to notably scale off after 30 cycles (visual rating equal to or greater than 1), while the immersed portions were intact except for specimens incorporating NA that showed minor cracking and spalling at the end of exposure. The latter symptoms are typical of the progression of chemical

sulfate attack. Visual assessment showed that almost all specimens suffered from PSA distress. The specimens had slight to moderate deterioration (visual rating between 1 and 3) after 30 cycles, which was aggravated to moderate-to-severe deterioration (visual rating between 3 and 5) after 60 cycles (mid-period of exposure). Eventually, all the mixtures had a visual rating of 5 (severe scaling) at the end of exposure.

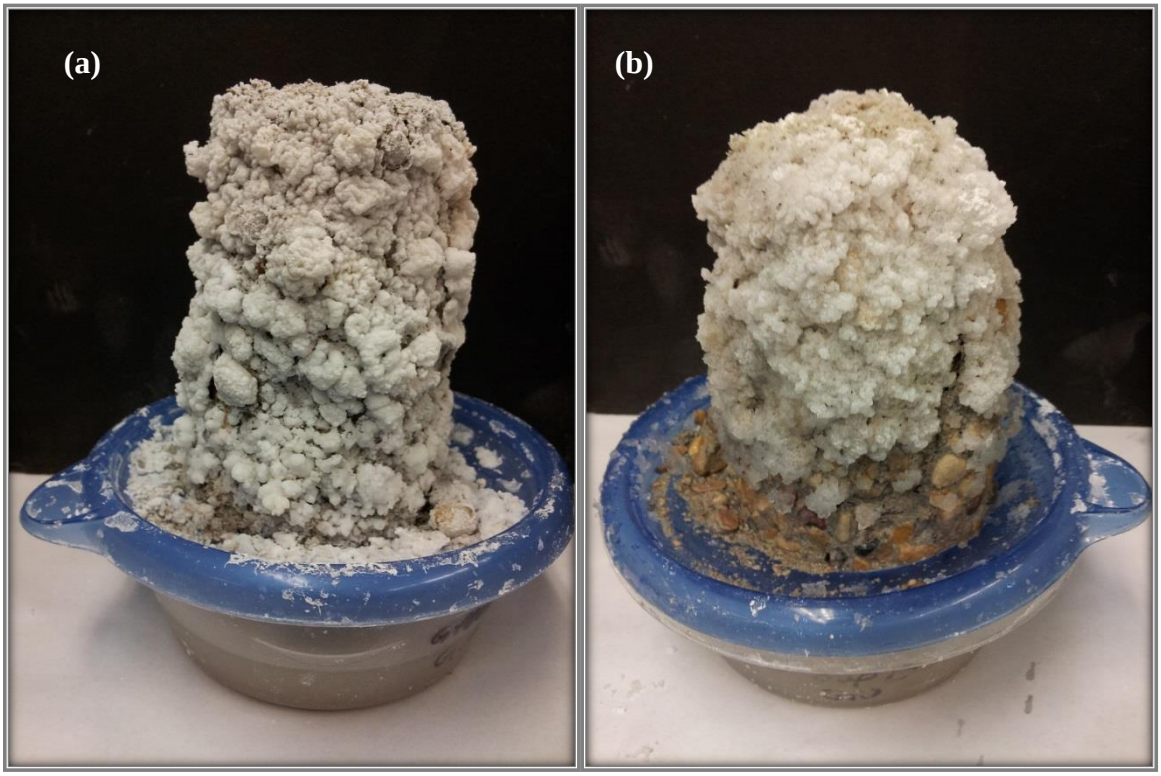

Figure 4.2: Efflorescence on specimens after 120 cycles: (a) GU-0.4 and (b) GU-0.5.

The NS addition reduced the amount of scaling at the early stage of exposure but starting from 75 days all the specimens with w/cm of 0.5 were severely deteriorated (visual rating of 5). The incorporation of NA in concrete mixtures with w/cm of 0.4 showed a distinct pattern in the visual rating results. Both 3 and 6% NA addition at w/cm of 0.4 reduced the surface scaling; in particular, the 6% NA is one of the best mixtures in term of visual rating and mass loss.

However, FA6-0.5 mixture severely deteriorated at 45 days along with the control mixtures at the same w/cm ratio. The FA3-0.5 specimen also deteriorated severely at 60 days (visual rating of 5) and lost a huge quantity of its mass (23%) at the end of experiment. However, the visual assessment method could not distinctively capture the variable performance of the concrete mixtures at the end of exposure (almost all mixtures had a visual rating of 5), and thus it must be supplemented by a physical indicator reflecting the exact amount of scaled material from each specimen (mass loss).

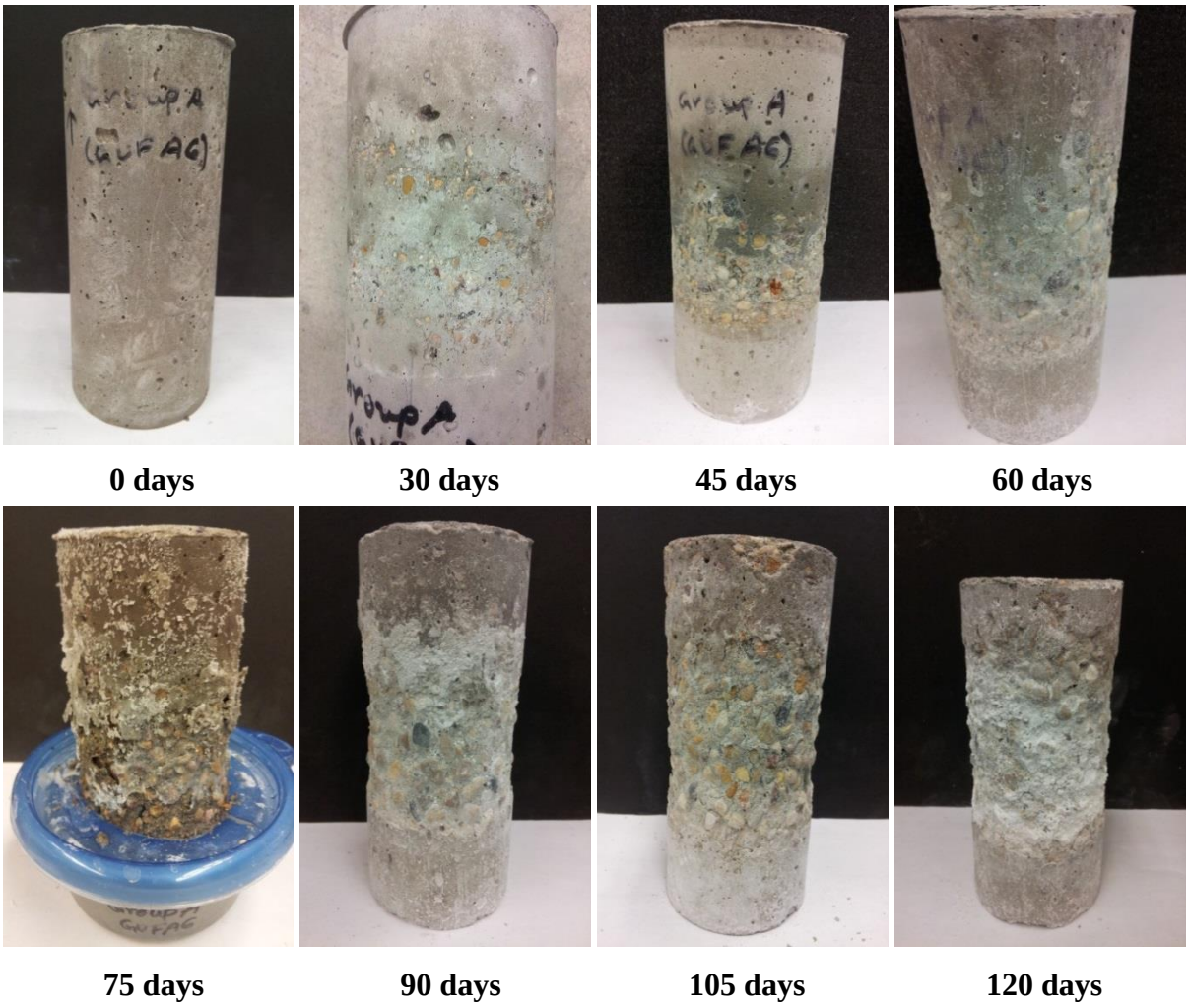

Figure 4.3: Progressive degradation of a specimen (75×150 mm) from mixture FA6-0.4 at different ages.

Table 4.2: Visual rating of damage at different ages of exposure

Mixture ID	Days							
	0	**30**	**45**	**60**	**75**	**90**	**105**	**120**
w/cm = 0.4								
GU-0.4	0	1	3	5	5	5	5	5
F-0.4	0	1	2	3	4	4	4	5
GUS3-0.4	0	1	2	3	4	4	4	5
GUA3-0.4*	0	1	4	5	5	-	-	-
FS3-0.4	0	2	3	4	5	5	5	5
FS6-0.4	0	1	2	3	4	5	5	5
FA3-0.4	0	1	3	4	5	5	5	5
FA6-0.4	0	1	3	3	3	4	4	5
w/cm = 0.5								
GU-0.5	0	2	5	5	5	5	5	5
F-0.5	0	2	4	5	5	5	5	5
GUS3-0.5	0	1	4	4	5	5	5	5
GUA3-0.5*	0	1	4	5	-	-	-	-
FS3-0.5	0	2	4	5	5	5	5	5
FS6-0.5	0	2	4	5	5	5	5	5
FA3-0.5	0	2	4	5	5	5	5	5
FA6-0.5	0	3	5	5	5	5	5	5

* Specimens were fractured/disintegrated during the PSA exposure.

4.1.3. Mass loss

The mass loss of specimens was determined at different ages as shown in Figures 4.4 and 4.5. For most of the mixtures, the rate of mass loss was low up to 30 cycles, and then it significantly accelerated up to the end of exposure conforming to the visual assessment trend. By comparing Figure 4.4a to Figure 4.4b and Figure 4.5a to Figure 4.5b, it can be noted that the increase of w/cm from 0.4 to 0.5 led to higher surface scaling of specimens prepared from similar binders. For example, specimens from mixture F-0.5 prepared with the binary binder comprising GU cement and 30% fly ash had three times higher mass loss to relative the corresponding specimens with a w/cm of 0.4 (F-0.4).

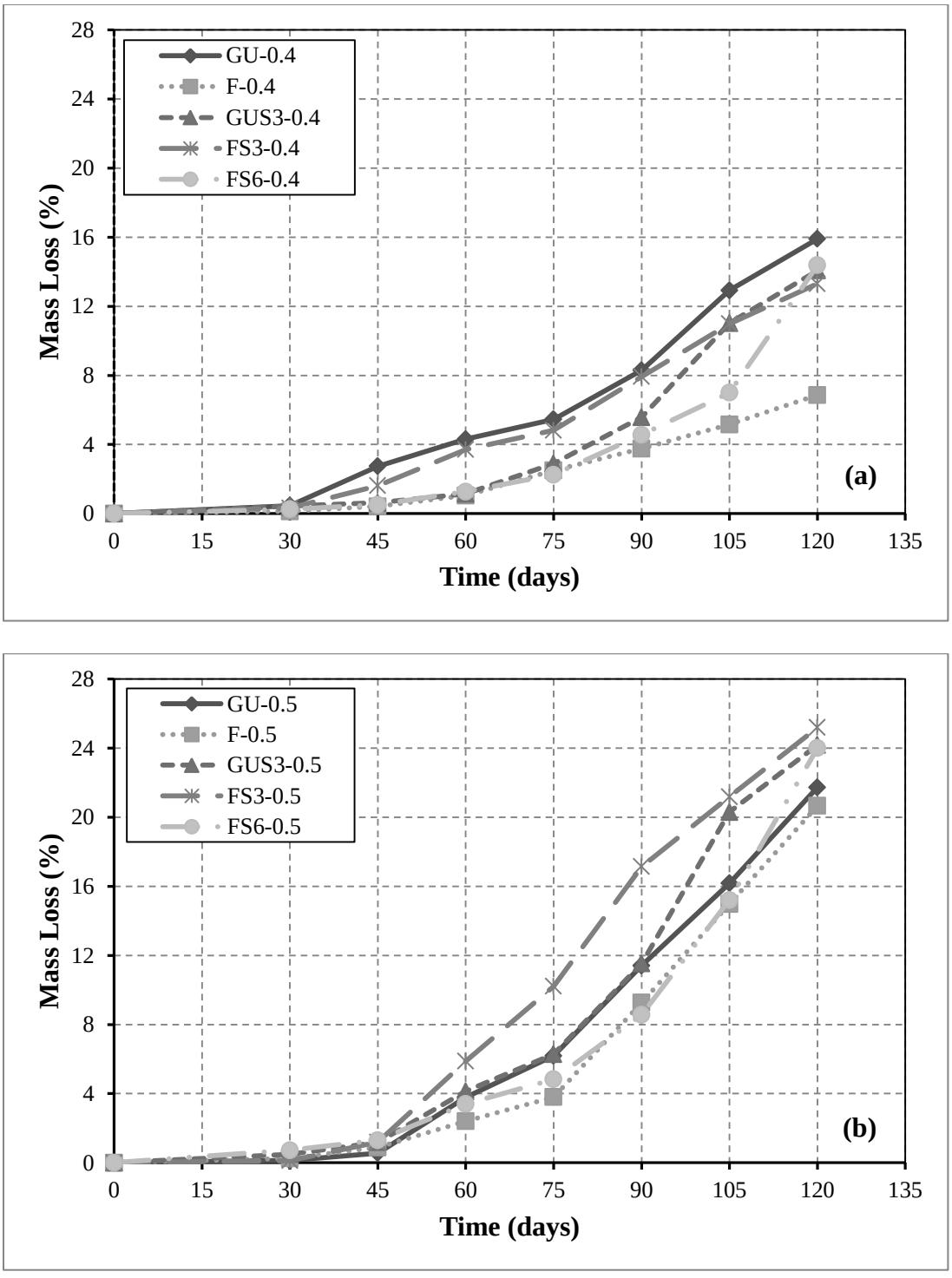

Figure 4.4: Mass loss of control and NS mixtures: (a) w/cm = 0.40 and (b) w/cm = 0.50.

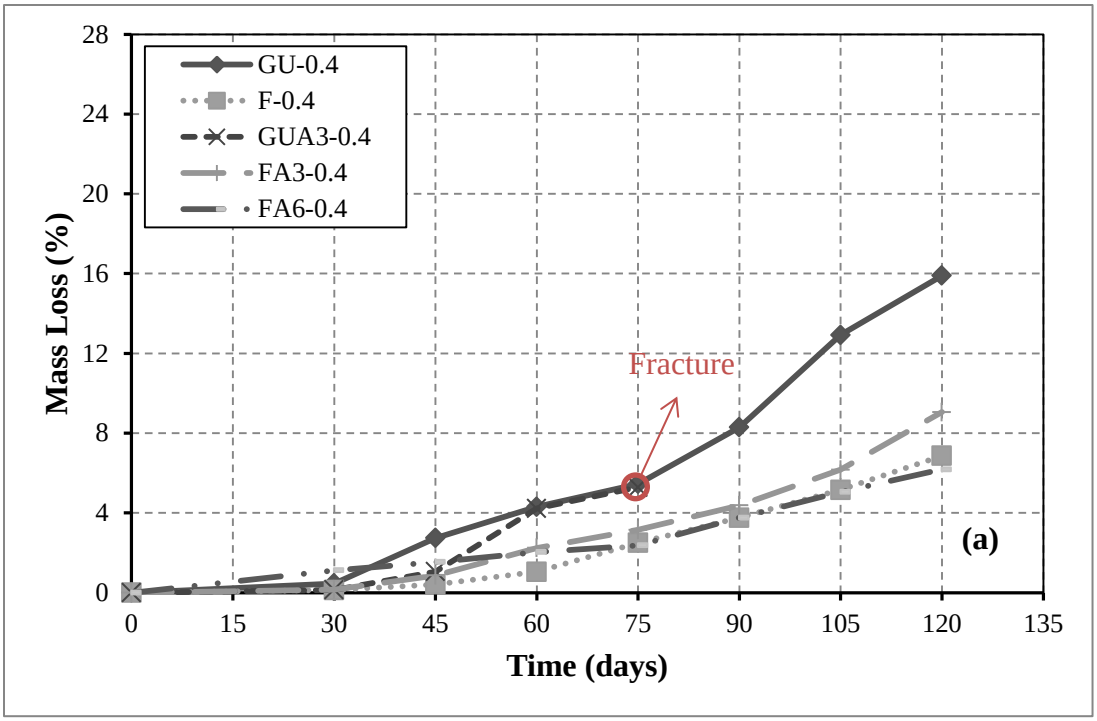

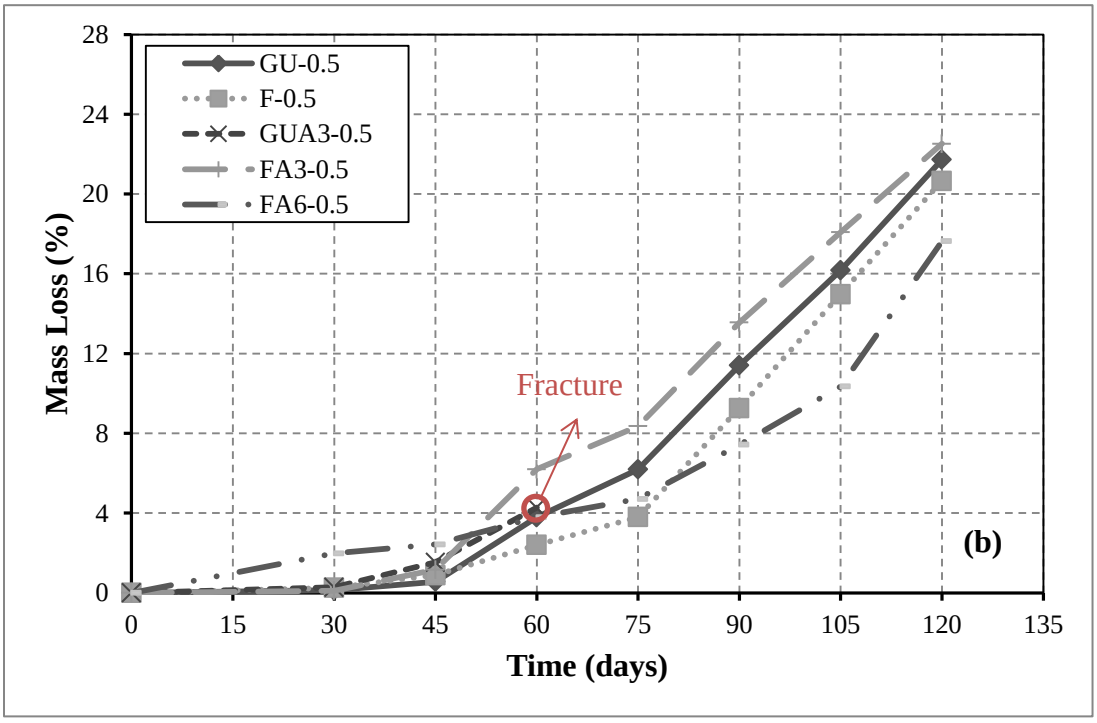

Figure 4.5: Mass loss of control and NA mixtures: (a) w/cm = 0.40 and (b) w/cm = 0.50.

The effect of fly ash on the mass loss results was mixed depending on the w/cm and incorporation of nanoparticles. At a w/cm of 0.4, specimens from binary binders comprising GU cement and fly ash (F-0.4) had better resistance to PSA (mass loss of 7%), relative to specimens from the control and ternary binders incorporating NS (Figure 4.4a). This trend was maintained for specimens comprising ternary binders with GU cement, fly ash and NA (Figure 4.5a). At a w/cm of 0.5 (Figures. 4.4b and 4.5b); however, ternary binders comprising GU cement, fly ash and NA (FA3-0.5) had the highest mass loss (about 23%) among NA mixtures.

Irrespective of the type of binder (binary or ternary), all the specimens comprising NS had comparable mass loss (average of 14%) at a w/cm of 0.40 after 120 days, without a clear effect of the NS dosage. At w/cm of 0.5, specimens incorporating NS started to deteriorate markedly after 45 days (Figure 4.4b). However, the highest percentage of mass loss (about 25%) was recorded for specimens from the ternary binders with the lower dosage of NS (FS3-0.5).

At a w/cm of 0.4, the increase in NA dosage from 3 to 6% in ternary binders led to reducing the mass loss results by 30% (mixtures FA3-0.4 and FA6-0.4 in Figure 4.5a). Furthermore, at both w/cm, specimens prepared from ternary binders with the highest dosage of NA (FA6-0.4 and FA6-0.5) had the lowest mass loss (6% and 18%, respectively) among all the mixtures tested. Comparatively, there was no improvement on the resistance of concrete prepared from ternary binders incorporating 3% NA to PSA at w/cm of 0.4 and 0.5. In addition, a specimen from GUA3-0.5 mixture was broken by a transverse macro-crack in the mid-height of the drying portion after 58 days (Figure 4.6), and the other replicate was broken at 65 days. Similarly, both specimens from GUA3-0.4 mixture were broken after 75 days of exposure during handling.

Figure 4.6: A specimen (75×150 mm) from GUA3-0.5 after breakage at 58 days.

4.2. Discussion

4.2.1. Mechanisms of damage

To detect the underlying mechanisms of damage, DSC, XRD and SEM analyses were conducted on the drying and immersed portions of several specimens after the exposure. DSC on powder samples collected from the surface of drying and immersed portions of specimens showed sodium sulfate occurrence (at an average temperature of 270°C) with sulfate-bearing compounds (ettringite and/or gypsum, at average temperatures around 90 and 110°C, respectively). Rasmussen *et al.* (1996) previously described the transition of polymorphous phases V-I of sodium sulfate crystals at 270°C using DSC. A semi-quantitative analysis based on the enthalpy concept (integration of heat flow peaks over temperature) can determine the relative phase formation, as the enthalpy of each phase is directly related to its amount (Brown and Gallagher, 2011).

The relative amount of sulfate-bearing compounds and sodium sulfate salt depended on the particular location in specimens as well as constituent materials. For example, Figure 4.7 shows that the enthalpy of sulfate-bearing products formed in the immersed portion is about thrice that of the drying portion, while the enthalpy of sodium sulfate crystallized in the drying portion is about 43 times that of the immersed portion.

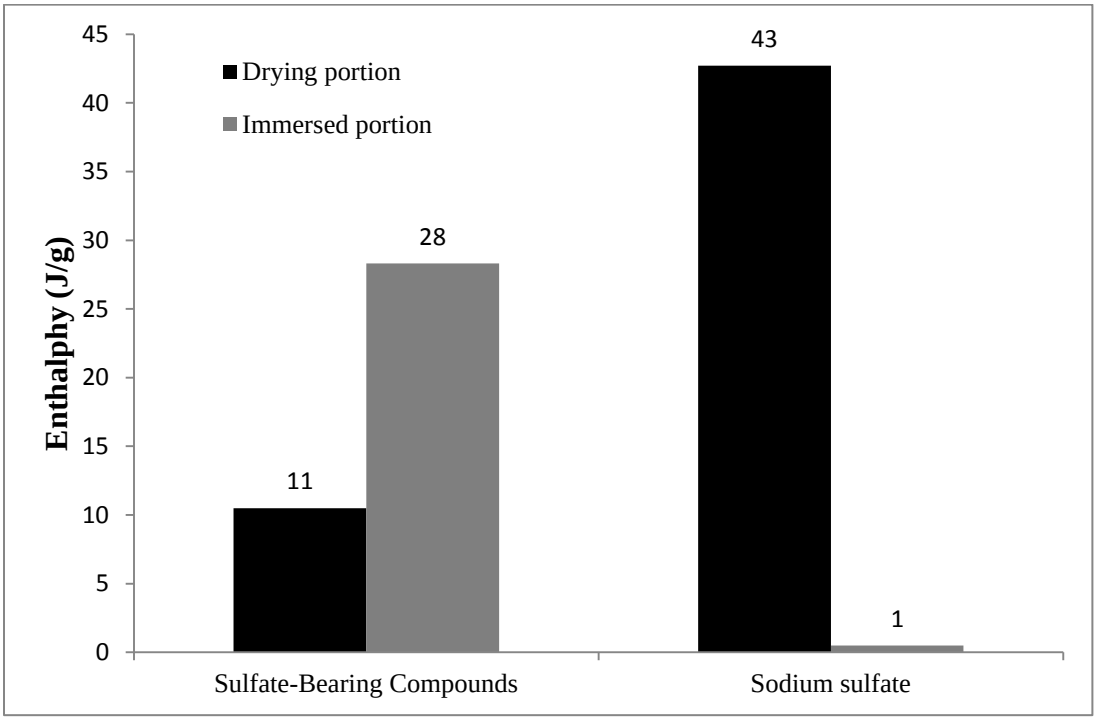

Figure 4.7: Enthalpies of sulfate-bearing compounds and sodium sulfate formed in the drying and immersed portions of an FS3-0.5 specimen after exposure.

Correspondingly, XRD analysis consistently showed a dominant pattern of sodium sulfate salt in the drying portion with traces of sulfate reaction products (e.g. Figure 4.8), suggesting significant salt accumulation within the evaporative zone of specimens. While traces of sulfate reaction products were detected by XRD in the immersed portion, there was no symptom of expansion, disruption, and spalling of concrete, which are the typical features of

chemical sulfate attack at advanced stages. To qualitatively assess the relative amounts of phases obtained from XRD, Rietveld Analysis was performed on different powder samples collected from the drying portion. The results showed that majority of the samples' masses were composed of thenardite (anhydrous Na_2SO_4), which supports that salt crystallization was the driving mechanism for the surface distress of specimens, conforming to DSC trends. As the powder sample was air-dried before performing the XRD tests, no mirabilite (hydrated Na_2SO_4) was detected in the diffractograms. This is because of the rapid transformation of unstable mirabilite to thenardite that takes place at room temperature and relative humidity (22±2°C and 55±5% RH) in accordance to the sodium sulfate phase diagram (Rodriguez-Navarro *et al.*, 2000). In addition, for specimens comprising GU and NA (GUA3-0.4 and GUA3-0.5), which were fractured during the exposure, significant amount of ettringite coexisted with thenardite in the drying portion, suggesting interaction between chemical sulfate attack and PSA, as will be explained later in the text.

SEM analysis complied with the DSC and XRD findings. For instance, Figure 4.9 shows micro-cracks emanating from a band of growing salt crystals beneath the surface (in the subflorescence zone). Abundant sodium sulfate crystals, with different morphologies and variables sizes, were typically detected at or near (within 15 mm) the surface. Also, sulfate-bearing products (ettringite and/or gypsum) were incidental features in the samples extracted from the drying portions of specimens, complying with the DSC and XRD results, which shows a minor degree of sulfate attack.

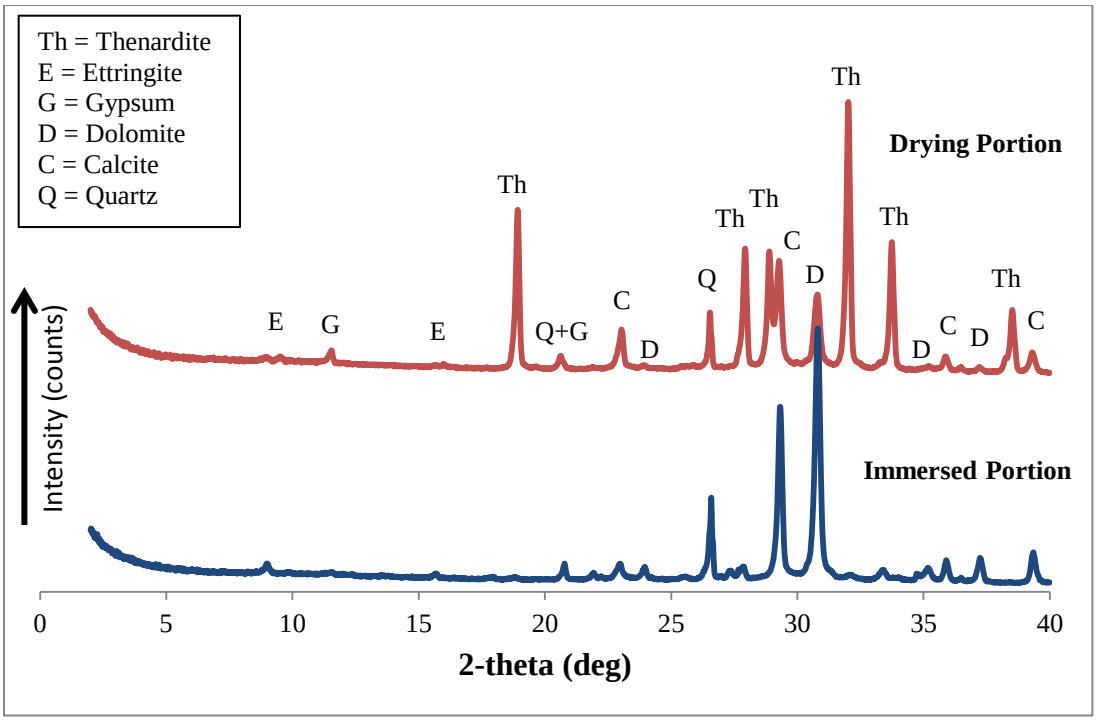

Figure 4.8: XRD analysis of FS6-0.5 specimen showing the difference between drying and immersed portions.

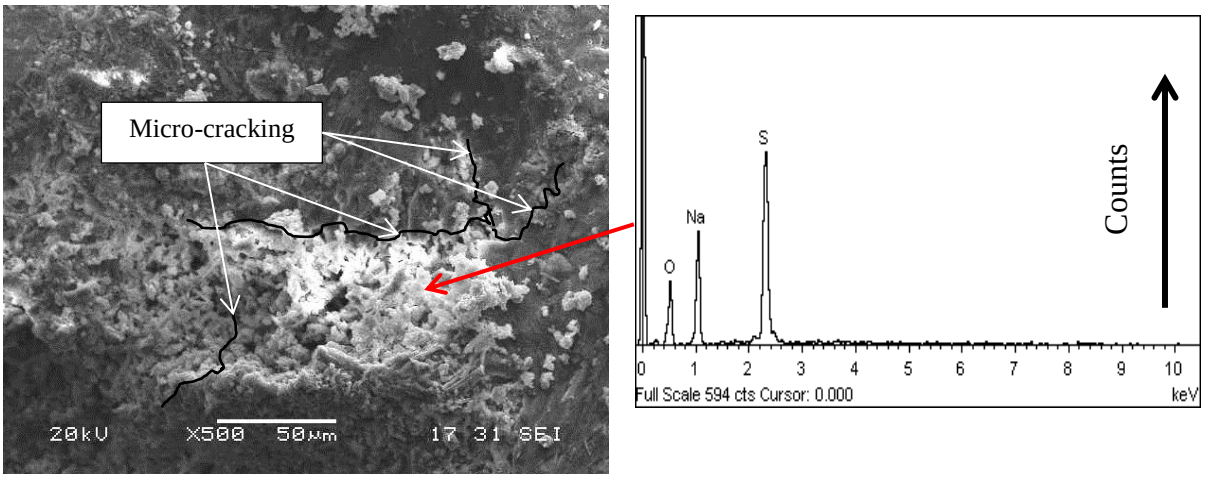

Figure 4.9: SEM micrograph showing salt crystallization bands along with propagation of cracks in the subflorescence zone of the drying portion in a GU-0.5 specimen.

Comparatively, the samples taken from the immersed portion of specimens contained only reaction products which are typical of chemical sulfate attack (e.g. Figure 4.10). These phases in the samples were acicular ettringite and round or tabular gypsum which preferentially lined in voids. However, minor damage manifestations including lack of swelling, cracking and spalling on the surface of the immersed portions of concrete and limited occurrence of ettringite and gypsum in the matrix indicated that the kinetics of chemical sulfate reactions at this location were insignificant, considering the test period of this exposure (120 days). The concomitant occurrence of salt crystallization in the above solution portion and sulfate-bearing products in the immersed portion of cylinders were also observed by Bassuoni and Nehdi (2009a) in a partial immersion exposure that continued for 24 months. However, in that study, the sodium sulfate concentration was 5%, and the temperature and humidity cycles were 20°C with 50% RH and 40°C with 35% RH. The abundance of sodium sulfate salt in the drying surface of concrete cylinders as detected by DSC, XRD and SEM with EDX substantiated that PSA was the main cause of damage for the drying portion of concrete tested in this study.

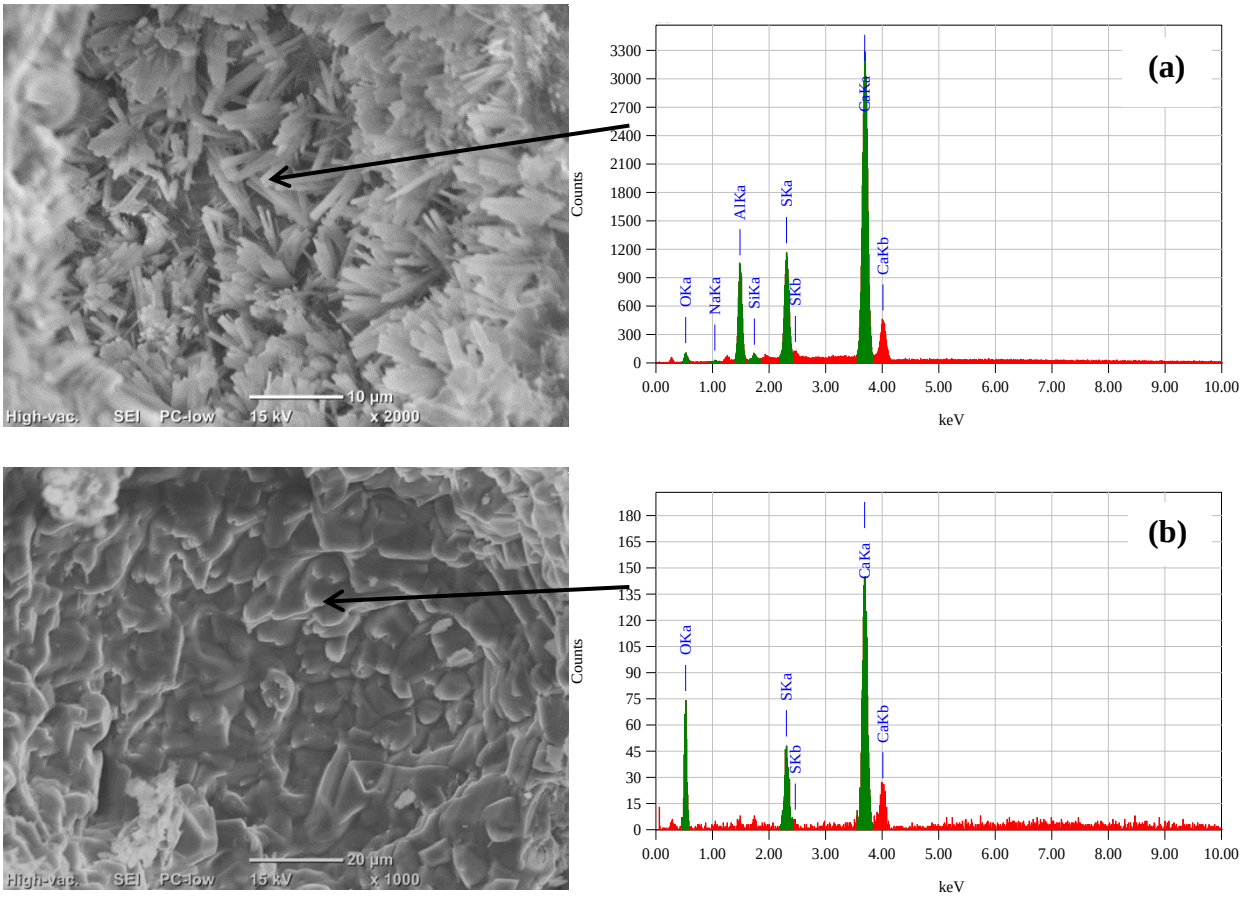

Figure 4.10: SEM micrographs and associated EDX spectrums of fracture surfaces from the immersed portion of FA6-0.5 specimen showing: (a) ettringite and (b) gypsum.

4.2.2. Effect of w/cm

The mass loss results indicated that the resistance of concrete to PSA was significantly affected by the w/cm. This was statistically supported by the analysis of variance (ANOVA) at a significance level (α) of 0.05. For instance, ANOVA for the mass loss results showed that changing the w/cm from 0.4 to 0.5 in ternary mixtures had an F value of 110.2 compared to a critical value (F_{cr}) of 6.0. According to Montgomery (2013), exceeding the F_{cr} for an F-distribution density function indicates that the variable tested has a statistically significant effect on the average results.

Higher w/cm increased the cumulative mass loss and reduced the resistance of concrete to PSA, which can be attributed to the penetrability of concrete. The general relationship of average penetration depth from RCPT and total mass loss for fly ash mixtures at both w/cm is presented in Figure 4.11. At w/cm of 0.4 and 0.5, the mass loss results were strongly correlated (coefficients of determinations of 0.97 and 0.90, respectively) to the penetrability of the mixtures. It is worth mentioning that this relationship could not be established for the GU mixtures without fly ash, since all replicates containing GU and NA (GUA3-0.4 and GUA3-0.5) failed before the end of exposure due to interaction with chemical sulfate attack, as will be explained in the next section. For the mixtures comprising fly ash with or without nanoparticles, the increase of w/cm led to increasing the penetration depth and consequently mass loss of specimens (the trend line is shifted to upwards). As evident by the penetration depth results, higher w/cm made the concrete more porous and enhanced pore connectivity, which conforms to the well-documented effect of w/cm on the capillary porosity of concrete (Mehta and Monteiro, 2013). This facilitated more solution uptake, salt crystallization and eventually led to severe surface scaling, as explained below.

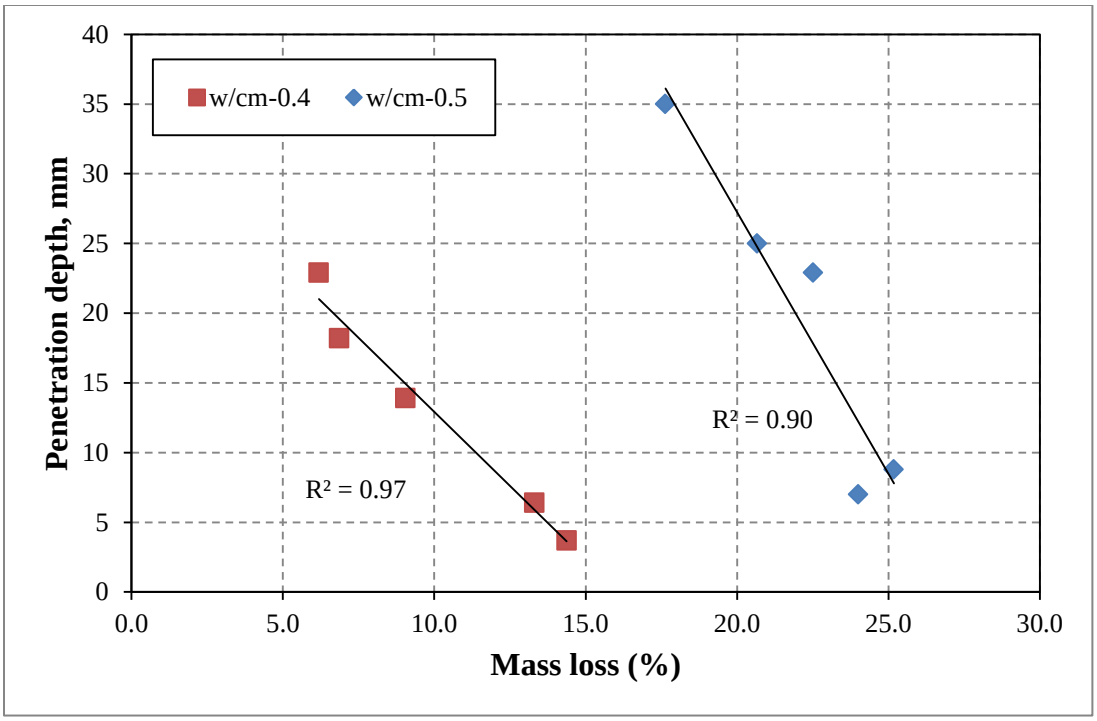

Figure 4.11: General relationship between average penetration depth and mass loss of fly ash mixtures.

The DSC curves of powder samples showed mineral phases present in the cementitious matrix after the exposure. For example, Figure 4.12 shows the abundance of sodium sulfate salt, due to salt crystallization, as indicated by the endothermic peaks at 270˚C and traces of gypsum and ettringite in the samples collected from the drying portion of specimens prepared from the ternary binders comprising GU cement, fly ash and 3% NA at both w/cm (FA3-0.4 and FA3-0.5). The occurrence of sulfate-reaction products highlights the possibility for the interaction of chemical sulfate attack with PSA. It can be observed that the enthalpy of sodium sulfate for the mixture with w/cm of 0.5 is 1.5 times higher than that of the corresponding mixture with w/cm of 0.4. This agrees with the mass loss results since FA3-0.5 specimens lost about 23% of its mass, which is about 2.5 times higher than that of FA3-0.4 specimens. The corroborated trends

from the penetration depth, mass loss and DSC show that higher w/cm enhanced the solution penetrability/uptake, which increased the amount of salt deposition within the evaporative surface of concrete, and consequently led to more surface scaling.

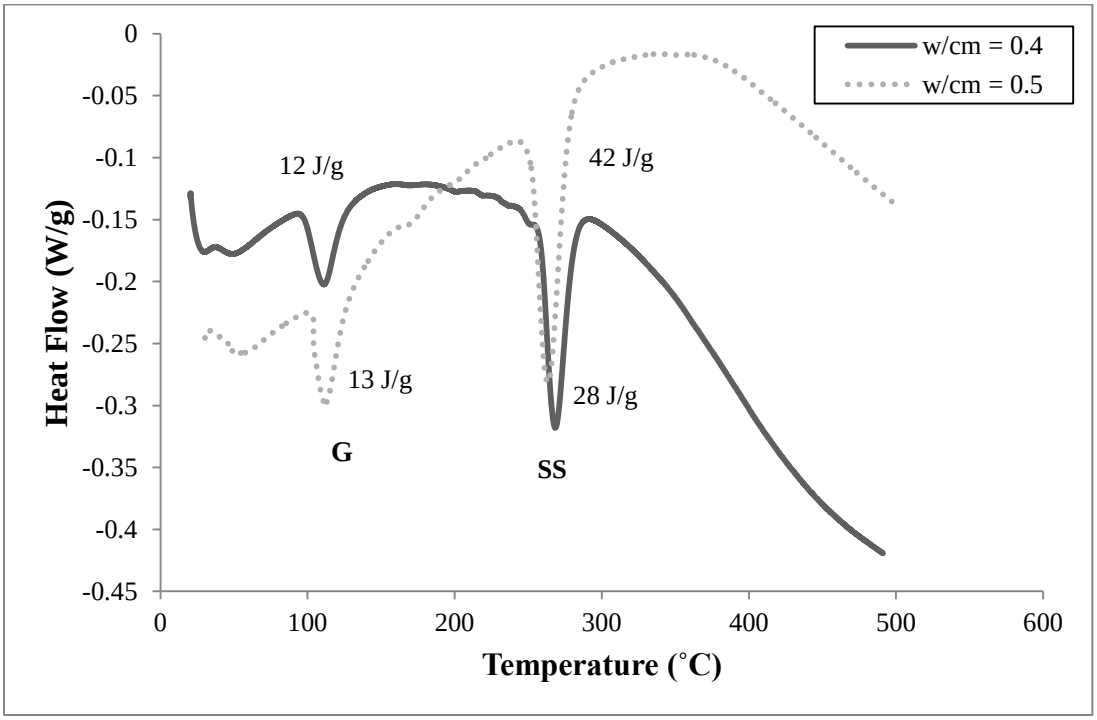

Figure 4.12: Exemplar DSC curves showing the effect of w/cm on samples from FA3-0.4 and FA3-0.5 specimens (G = Gypsum; SS = Sodium sulfate).

4.2.3. Effect of fly ash and nanoparticles

The effect of fly ash on improving the resistance of concrete to PSA was prominent at a w/cm of 0.4 (Figs. 4.4a and 4.5a), especially for the binary binder without nanoparticles (F-0.4) or ternary binders with NA (FA3-0.4 and FA6-0.4). This was confirmed by ANOVA for the mass loss results at a significance level (α) of 0.05, where changing the type of binder from single (GU) to binary (GU and fly ash) at a w/cm of 0.4 had an F value of 34.20 compared to a critical value (F_{cr}) of 18.51. The penetration depth results showed that fly ash mixtures had significantly lower

penetration depth compared to the corresponding mixtures without fly ash (Table 4.1). The increased physical resistance (lower penetrability) of fly ash mixtures can be ascribed to its pozzolanic effects on refining the pore structure and discounting the continuity of capillary pores (Berry *et al.*, 1990), as shown by the penetration depth results. Hence, fly ash mixtures had lower rate of solution uptake and consequently better resistance to PSA. At w/cm of 0.5, however, the positive effect of fly ash was relatively diminished likely because of the effects of higher w/cm and nanoparticles.

Compared to the mixtures with fly ash (binary binder), incorporation of NS in mixtures (ternary binder) further improved the microstructure of concrete by reducing the penetration depth at both w/cm. This can be attributed to the significant effect of NS on reducing the inter-connectivity of pore system and refining the microstructure of concrete system (Said *et al.*, 2012). In spite of the fact that incorporation of NS at a w/cm of 0.4 discounted the penetration depth, this reduction of penetrability corresponded to higher mass loss (Figure 4.11). Statistical analysis by ANOVA confirmed this trend at significance level (α) of 0.05. For instance, at w/cm of 0.4, the variation of NS content (0, 3 and 6%) with 30% fly ash had an F value of 11.42 compared to the critical value (F_{cr}) of 9.55. At w/cm of 0.40, excessive refinement of the pore structure due to the incorporation of NS with fly ash in mixtures FS3-0.4 and FS6-0.5, made them vulnerable to higher crystallization pressure, and more surface scaling relative to F-0.4. This behavior is in agreement with the previous findings of Irrassar *et al.* (1996), and Bassuoni and Nehdi (2009a). At w/cm of 0.5, moreover, this trend between mass loss and penetration depth for the samples with fly ash and NS (F-0.5, FS3-0.5 and FS6-0.5) were statistically significant. For example, ANOVA test results showed that variation of dosages of NS in fly ash mixtures at w/cm of 0.5 had an F value of 13.35 compared to a critical value (F_{cr}) of 9.55.

Similar to the FS6-0.5 sample, GUS3-0.5 sample lost huge quantity of mass (about 24%) at the end of experiment. Therefore, the incorporation of NS with or without the addition of fly ash did not improve the resistance to salt distress at w/cm of 0.5 rather NS addition significantly increased the mass loss.

Incorporation of NA with fly ash had a mixed effect on the mass loss results. At both w/cm, the specimens comprising 6% NA and fly ash showed higher penetration depth (i.e. coarser pore structure) compared to the corresponding specimens containing fly ash or fly ash with 3% NA. Hence, the percentages of cumulative mass loss of specimens containing 6% NA was generally lower than that of other mixtures in each w/cm group (mass loss of 6 and 18% at w/cm of 0.4 and 0.5, respectively). Comparatively, mixtures containing 3% NA with fly ash reduced the chloride penetration depth (i.e. finer pore structure) compared to only fly ash mixtures at both w/cm, and hence the mass loss of those specimens was higher. This trend has been observed in Figure 4.11, which agrees with Scherer`s theory (2004a) in the sense that lower crystallization pressure is generated in coarser pore structure. The coarser pore structure of the matrix containing 6% NA might be attributed to an agglomeration effect (inconsistent dispersion of particles), due to a relatively high dosage of ultrafine particles (specific surface of 170 m^2/g).

Specimens from mixtures GUA3-0.4 and GUA3-0.5 were broken transversely at the mid height during the exposure which involved cyclic temperature and humidity conditions. Incorporation of 3% NA with GU led to a coarser and more interconnected pore structure relative to the other mixtures at both w/cm, as these mixtures had the highest penetration depth (Table 4.1) and consequently more solution uptake, but lower crystallization pressure as previously discussed. In addition, NA blended with GU cement (high C_3A content of 9%) significantly increased the reactive alumina compounds vulnerable to chemical sulfate attack

reactions, and thus aggravating the damage. DSC analysis (e.g. Figure 4.13), showed the excessive formation of ettringite even in the drying portion of GUA3-0.4 specimens. The enthalpies of sulfate-bearing products in GUA3-0.4 sample was about 7 and 11 times higher than that in GU-0.4 and FA3-0.4 specimens, respectively. Comparatively, the enthalpy of sodium sulfate salt in GUA3-0.4 was lower compared to GU-0.4 and FA3-0.4; lower salt deposition in GUA3-0.4 specimens occurred as the specimens were broken and analyzed after 75 days of exposure. SEM analysis on fracture surfaces from GUA3-0.4 sample also confirmed the typical features of salt crystallization beneath the surface (e.g. Figure 4.14). Therefore, the deterioration of specimens comprising GU cement with NA could be attributed to the combined effects of chemical sulfate attack and salt crystallization.

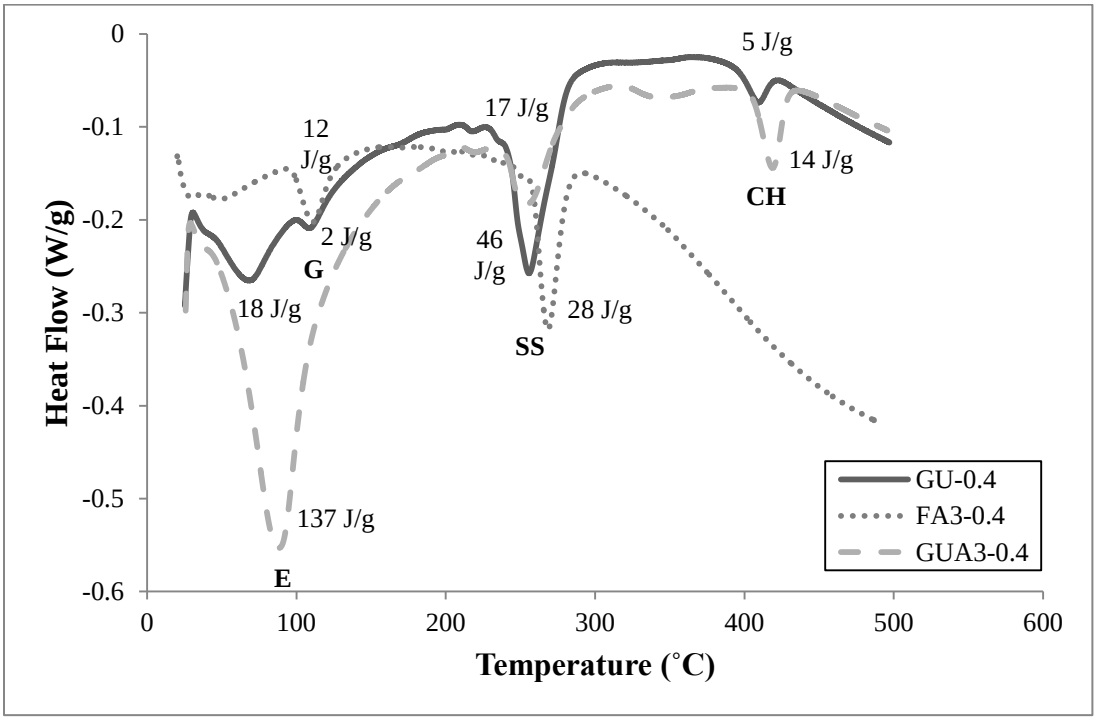

Figure 4.13: DSC curves showing the interaction of chemical sulfate attack with PSA in mixtures containing NA and GU cement (E = Ettringite; G = Gypsum; SS = Sodium sulfate salt; CH = Calcium hydroxide).

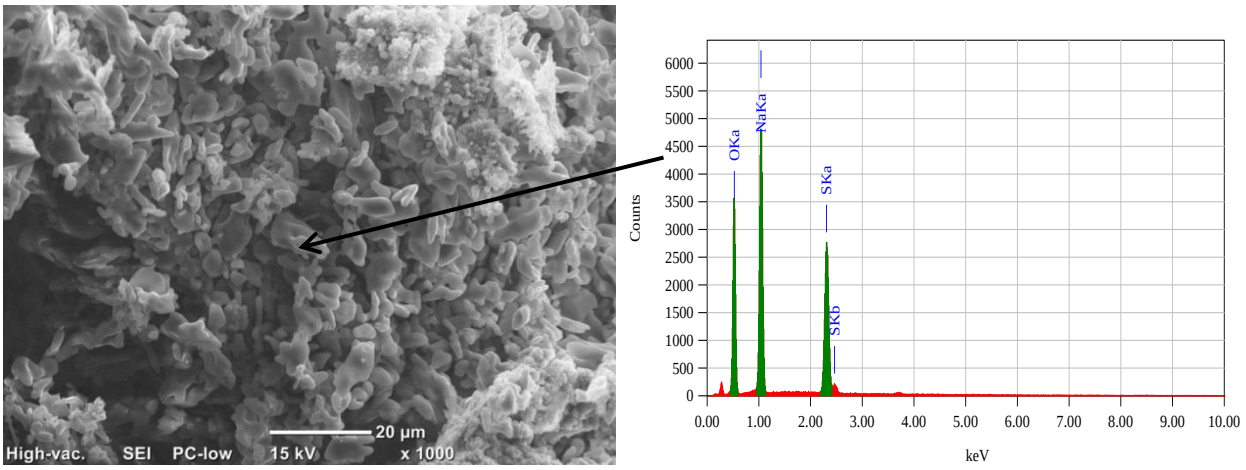

Figure 4.14: SEM micrographs and associated EDX spectrum for a fracture surface from GUA3-0.4 (drying portion) showing salt crystals in the subflorescence zone.

The improved chemical resistance of the ternary mixtures incorporating GU cement, fly ash and NA can be attributed to the effect of fly ash. Blended binders containing fly ash reduce the portlandite (CH) content in the hydrated cementitious matrix, thus improving the resistance to alkali sulfates. SCMs react with CH and water to produce C-S-H (pozzolanic reaction). Thus, blended binder matrices with lower portlandite contents can reduce the potential for gypsum formation when exposed to alkali sulfates (Skalny *et al.*, 2002). This is, for example, depicted by the lack of sulfate reaction products and CH in the thermogram of FA3-0.4 (Figure 4.13). Furthermore, cementitious materials with additional SCMs have a tendency to form hydrated alumina-bearing phases which are not susceptible to conventional sulfate attack (Skalny et al., 2002). From the mixture designing viewpoint, additionally, fly ash diluted the C_3A content from the cementitious matrix especially at a high GU replacement level (30%) in ternary binders comprising GU, fly ash and NA. Therefore, the deterioration of these systems was mainly due PSA, and lower amounts of sulfate reactions products formed in such systems (e.g. Figure 4.14).

5. Results and Discussion for Conventional and Thaumasite Sulfate Attack

5.1. Rapid Chloride Penetrability Test

Many durability issues of concrete depend on the penetrability of aggressive ions from the surrounding solution into the cementitious matrix; hence, the physical penetration depth of different mortar mixtures was measured after the RCPT to qualitatively assess their penetrability. The passing charges and penetration depths of some mortar mixtures tested in the current study are listed in Table 5.1. Example pictures are presented in Figure 5.1 showing the whitish silver chloride precipitate as an indication of penetration depth. The average penetration depth for the mixtures prepared from GUL and PLC binders was in the range of 5-43 mm and 3-39 mm, respectively. For all the mixtures tested by RCPT, specimens from the GUL group showed higher penetration depths relative to their corresponding mixtures from the PLC group except PLCF30A6 specimens which had slightly higher penetration than that of GULF30A6 specimens. This reduction of chloride penetration depth of PLC mixtures might be attributed to the uniform dispersion of interground limestone, efficient reactivity and higher fineness, which led to more refined pore structure than that of GUL. This trend was also notable in the compressive strength results (Table 3.4).

Table 5.1: RCPT results

Mixture	**Charges Passed** (coulombs)	**Chloride Ions Penetrability Class** (ASTM C1202)	**Average Penetration Depth** (mm)
GU/GUL			
GU	7459	High	29
GUL	6790	High	33
GUF40	1783	Low	10
GULF15S6	892	Very Low	5
GULF40S6	501	Very Low	5
GULF30A6	6465	High	36
GULF40A6	6590	High	43
PLC			
PLC	6324	High	28
PLCF15	5002	High	24
PLCF15S6	393	Very Low	3
PLCF15A6	5344	High	26
PLCF30A6	6661	High	39

The positive effect of higher dosages of fly ash on improving the physical resistance (i.e. reducing penetrability) of mortar was notable in the RCPT results. For example, the mortar mixture comprising 40% fly ash (GUF40) reduced the penetration depth by about 70% relative to the control mixture (GU). The most significant improvement on the penetration depth results was due to the incorporation of NS. Irrespective of the type of binder and dosage of fly ash, considerable reduction of penetration depth as well as penetrability class was achieved when NS was added to the mixtures. For example, the PLC mixtures with 15% fly ash and 6% NS (PLCF15S6) had penetration depth of 3 mm, compared to values of 28 and 24 mm for mixtures PLC and PLCF15, respectively. Conversely, addition of NA to the mortar mixtures increased the penetration depth significantly (Table 5.1 and Figure 5.1). For all types of cement, the incorporation of NA increased the penetration depth compared to the other mixtures (tested by RCPT) in each group of mixtures. Also, it can be noted that increase of penetration depth was more pronounced with higher dosages of fly ash. For instance, GULF30A6 and GULF40A6

mixtures had penetration depths of 36 and 43 mm, respectively. It appears that NA did not improve the reactivity of fly ash in the cementitious matrix, and it rather contributed to slowing down the evolution of hydration products, as also shown in the compressive strength results (Table 3.4). This might be ascribed to an agglomeration effect of NA particles with higher dosages of FA. The NA mixtures had higher penetration depths, which indicate continuous pore structure. This suggests that NA was not dispersed uniformly into the cementitious paste and led to coarse pore structure as compared to NS. As a result, mortars made with NA allowed easier ingress of the sulfate solution.

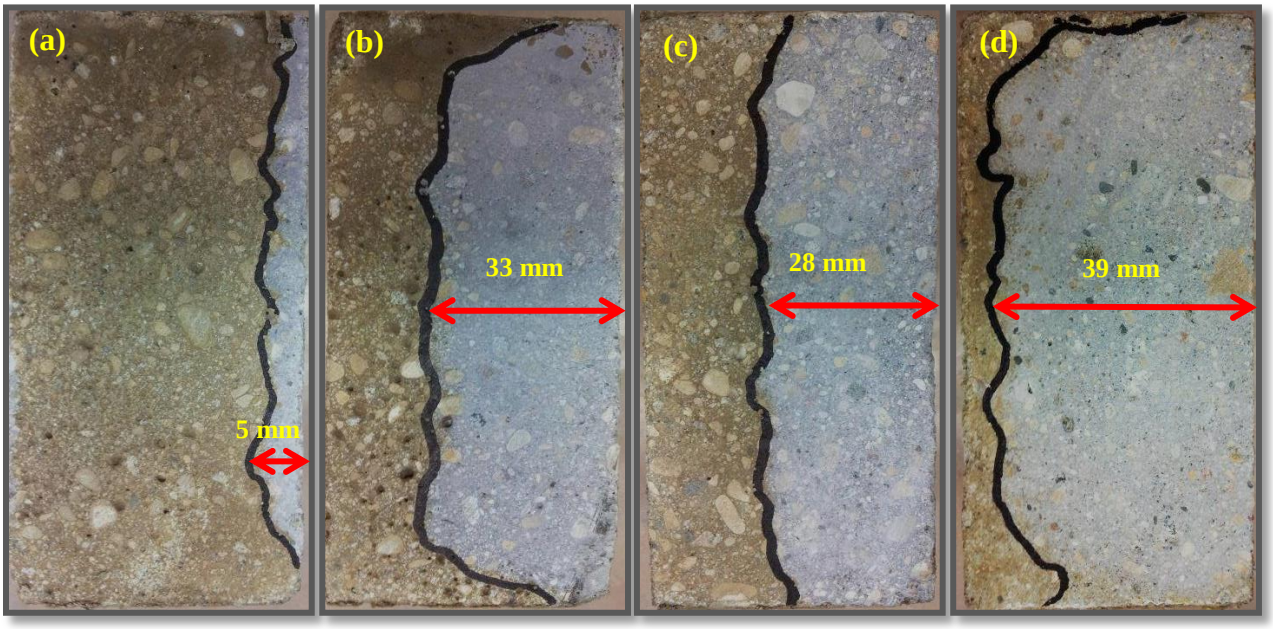

Figure 5.1: Physical penetration depth for mixtures: (a) GULF15S6, (b) GUL, (c) PLC and (d) PLCF30A6.

5.2. Conventional Sulfate Attack

5.2.1. Visual Assessment

Throughout the exposure, the preliminary manifestations of conventional sulfate attack appeared on the surface skin as cracks parallel to the mortar surface. At the end of exposure, the GU and GUL specimens had notable longitudinal and diagonal cracks. All mortar specimens containing NA showed severe signs of damage (e.g. Figure 5.2). In the GU/GUL group, only GULF15A6 specimens were broken during the test due to excessive swelling and propagation of cracks in the cementitious matrix. Cracks usually started from the corners of the mortar bars and propagated along the edges. For the PLC mixtures, few cracks at the corners and edges of the mortar bars were found in specimens made with NA and specimens prepared from PLC alone. However, these specimens remained intact and sound until the end of exposure. In general, less deterioration was observed at the corner and edges of the mortar bars made with fly ash, and the sign of deterioration decreased with the increase of fly ash dosages in mixtures.

5.2.2. Length, Mass Change and Dynamic Modulus of Elasticity

According to CSA 3000-08, cementitious binders with or without SCMs can be considered as moderate sulfate resistant if the average expansion of mortar bars is less than 0.10% at 6 months using Procedure A (23°C). For high sulfate resistance, the limit is more conservative where expansion of mortar bars cannot exceed 0.05% at 6 months or 0.10% at 12 months. Similar limits are stipulated in ACI 201.2R-08 and ACI 318-08 guidelines, and ASTM C1157-11 standard. The length change of mortar bars was determined at different ages as summarized in Table 5.2 and Table 5.3 (also see ***Appendix B***). For most of the mixtures, the rate of length change was low up to one month of exposure and then it increased notably until the end of exposure.

Figure 5.2: Cracks at the side and along the edge of GULF15A6 mortar bar (25×25×285 mm) after 120 days of exposure to conventional sulfate attack.

As anticipated, control mixtures (GU, GUL and PLC) without fly ash and nanoparticles surpassed the expansion limit of 0.10% before the end of the exposure. Compared to PLC, cumulative expansion of GUL mortar bars was 15 times higher at 12 months of exposure. In the GU/GUL group, the mortar specimens incorporating 15% fly ash failed to pass the conventional sulfate attack test limits (12 months) except for the specimens prepared from the ternary binder comprising of 79% GUL, 15% FA and 6% NS (GULF15S6). This highlights the positive effect of NS on improving the resistance to conventional sulfate attack even at a low dosage of fly ash. Comparatively, all the mixtures comprising 30% fly ash expanded less than 0.10% after 12 months of exposure. The mortar bars containing 30% FA and 6% NA marginally passed the test (expansion of 0.09%). However, the symptoms of deterioration including swelling and cracking of bars indicated that these specimens were on the verge of failure, if the time of exposure had

been extended. Thus, this mixture may not be qualified as sulfate resistant even though the expansion is within the range of 0.10%. Further improvement on the resistance of mortar mixtures to conventional sulfate attack was achieved with increasing the dosage of fly ash to 40%, even in binders incorporating NA. All the mortar bars made with PLC had expansion values lower than 0.10%, except for the ones comprising of PLC alone, and PLC with 15% fly ash and 6% NA, similar to the trends observed in the GU/GUL group.

Table 5.2: Expansion, RE_d and mass change results for GU/GUL specimens

Mixture ID.	Exposure					
	6 Months			12 Months		
	Expansion (%)	RE_d (%)	Mass Change (%)	Expansion (%)	RE_d (%)	Mass Change (%)
Group A						
GU	0.30	100	1.70	1.88	97	4.94
GUL	0.47	109	1.98	2.63	103	5.91
GUF15	0.06	107	1.31	0.39	107	2.55
GULF15	0.08	109	1.30	0.59	109	2.70
GULF15S6	0.02	99	0.66	0.04	99	1.21
GULF15A6	1.58*	109	3.00	--	--	--
Group B						
GU	0.30	100	1.70	1.88	97	4.94
GUL	0.47	109	1.98	2.63	103	5.91
GUF30	0.03	109	0.87	0.04	116	1.38
GULF30	0.03	109	0.85	0.05	109	1.45
GULF30S6	0.01	104	0.14	0.02	104	0.53
GULF30A6	0.05	109	0.86	0.09	115	1.27
Group C						
GU	0.30	100	1.70	1.88	97	4.94
GUL	0.47	109	1.98	2.63	103	5.91
GUF40	0.02	108	0.51	0.03	108	1.16
GULF40	0.02	109	0.39	0.04	108	0.89
GULF40S6	0.01	109	0.06	0.01	109	0.39
GULF40A6	0.03	110	0.35	0.04	110	0.59

*Specimens disintegrated at this age.

Table 5.3: Expansion, RE_d and mass change result for PLC specimens

Mixture ID.	Exposure					
	6 Months			12 Months		
	Expansion (%)	RE_d (%)	Mass Change (%)	Expansion (%)	RE_d (%)	Mass Change (%)
Group D						
PLC	0.04	100	0.95	0.17	100	2.07
PLCF15	0.02	108	0.86	0.04	108	1.71
PLCF15S6	0.01	100	0.74	0.02	106	1.70
PLCF15A6	0.05	109	1.05	0.18	109	2.16
Group E						
PLC	0.04	100	0.95	0.17	100	2.07
PLCF30	0.01	109	0.67	0.03	109	1.34
PLCF30S6	0.01	100	0.41	0.02	100	1.17
PLCF30A6	0.04	116	0.80	0.07	119	1.43
Group F						
PLC	0.04	100	0.95	0.17	100	2.07
PLCF40	0.01	109	0.61	0.02	109	1.21
PLCF40S6	0.01	109	0.10	0.01	109	0.49
PLCF40A6	0.02	109	0.57	0.03	109	1.02

Similar to the length change results, the change in mass was calculated at different time intervals of the exposure (e.g., see ***Appendix B***). The rate of mass gain of mortar bars was low at the initial stage of exposure but it started to increase notably after 1 month until the end of exposure. After 12 months of exposure, the GUL specimens gained the highest amount of mass (6%) followed by the control (GU) specimens which gained 5% of mass due to continual absorption of solution and generation of sulfate-bearing products in the matrix. In accordance with the length change results, fly ash reduced the rate of mass gain during the exposure. This rate was further decreased with the incorporation of NS. The results generally indicated an inverse relationship between the mass gain and dosage of fly ash (e.g. Figure 5.3). The RE_d results showed consistent increase, except for some mixtures that had slight reduction in RE_d

(Tables 5.2 and 5.3) [also see ***Appendix B***]. This conforms to the well-documented trend for conventional sulfate attack on cement-based materials (Skalny *et al.*, 2002).

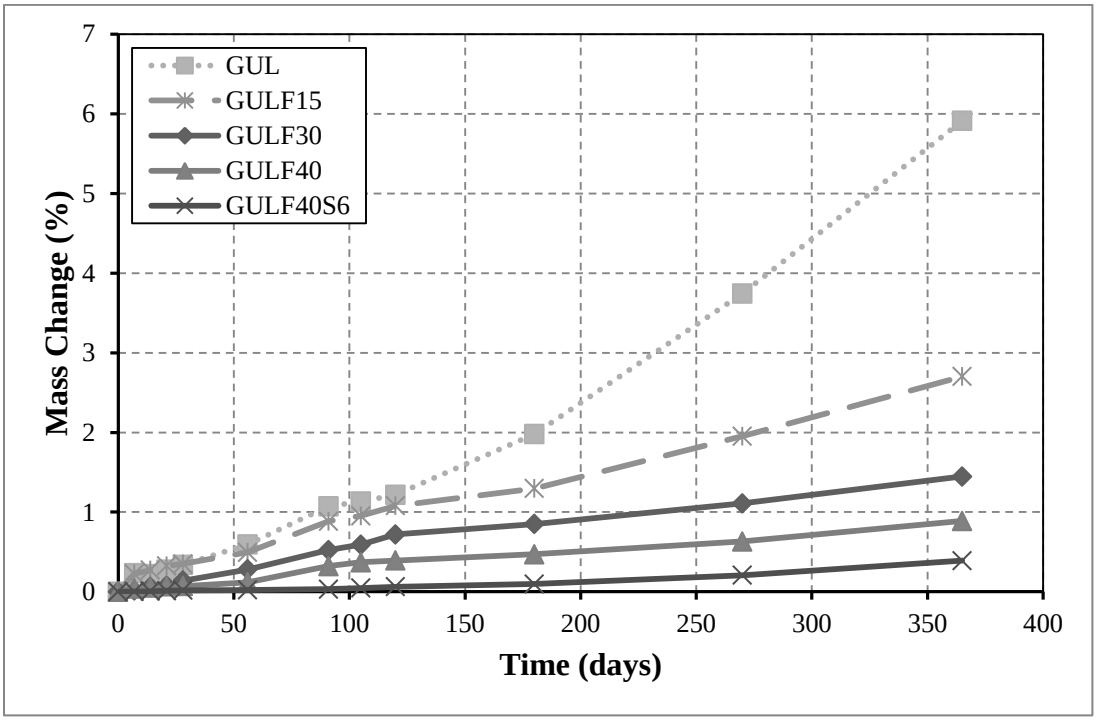

Figure 5.3: Change in mass for mixtures: (a) GUL, (b) GULF15, (c) GULF30, (d) GULF40 and (e) GULF40S6.

5.2.3. Discussion

XRD analysis on powder samples revealed the presence of different phases in the mortar specimens as shown, for example in Figures 5.4 and 5.5. Typical products of conventional sulfate attack including ettringite and gypsum, with no evidence of thaumasite, were found in the samples, irrespective of the type of binders. This indicates that the expansion and associated deterioration were primarily caused by conventional sulfate attack. In general, GU and GUL mixtures (control mixtures) had higher rate of expansion from the beginning of the exposure compared to PLC mixture. This can be attributed to the higher C_3A content in GU (9%) and

GUL cements (this content was slightly reduced in GUL due to replacement of GU with 13% limestone filler) than PLC (6%). Additionally, the penetration depth results showed that GU and GUL mixtures had higher penetration depth compared to the PLC mixture (Table 5.1). This resulted in higher penetration of the sulfate solution in the cementitious matrix of GU and GUL specimens, which led to more expansion and deterioration.

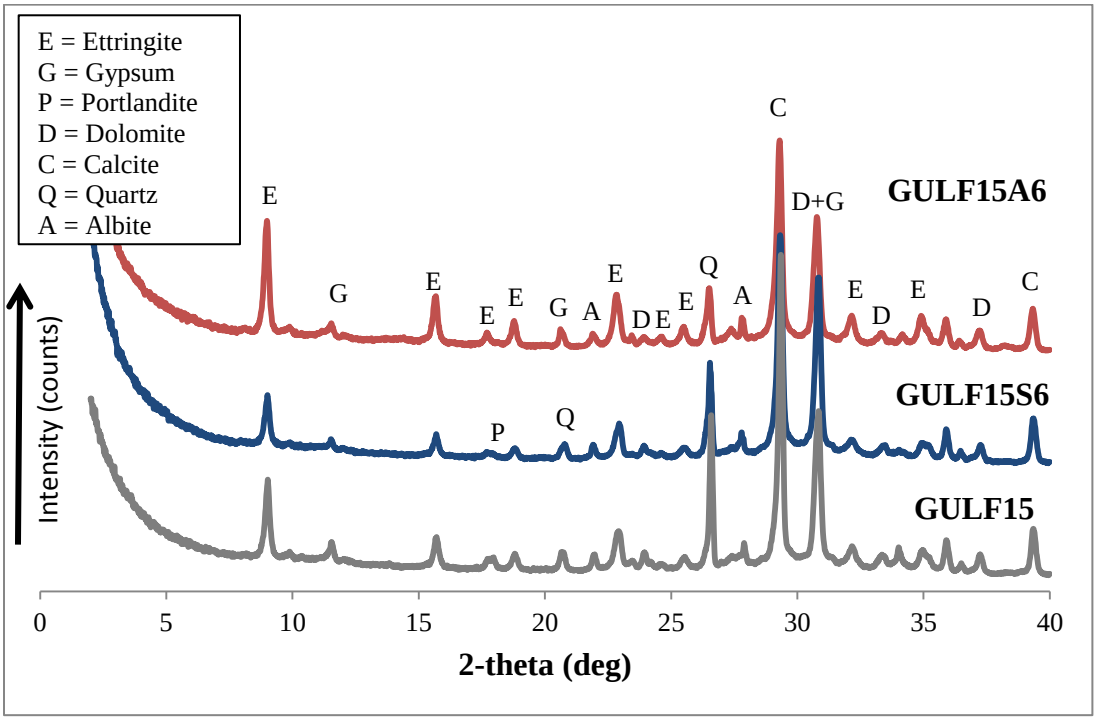

Figure 5.4: XRD of powder samples from GUL specimens exposed to sodium sulfate solution at 23°C (note: GULF15A6 was damaged after 6 months, while GULF15 and GULF15S6 were exposed for 12 months).

Fly ash (a pozzolanic SCM) was incorporated at variable dosages with GU/GUL and PLC cements to discount the CH content, especially at higher dosages, in the cementitious matrix, and thus improving the resistance to conventional sulfate attack. Fly ash reacted with CH and water to produce C-S-H (pozzolanic reaction) [Mehta and Monteiro, 2013]. The effect of fly at improving the physical resistance (i.e. reducing the penetrability) of mortar mixtures was

notable in the RCPT results, as discussed earlier. Also, there is a dilution effect (reduction of C_3A content) of fly ash in the cementitious system especially with increasing the dosage of fly ash. This reduction of CH and C_3A (chemical resistance) limited the formation of gypsum and ettringite in the cementitious matrix, and hence discounted the extent of expansion and deterioration (Tables 5.2 and 5.3). Additionally, cementitious binders with SCMs have a tendency to form stable hydrated alumina-bearing phases which are not easily engaged in sulfate attack reactions (Skalny *et al.*, 2002).

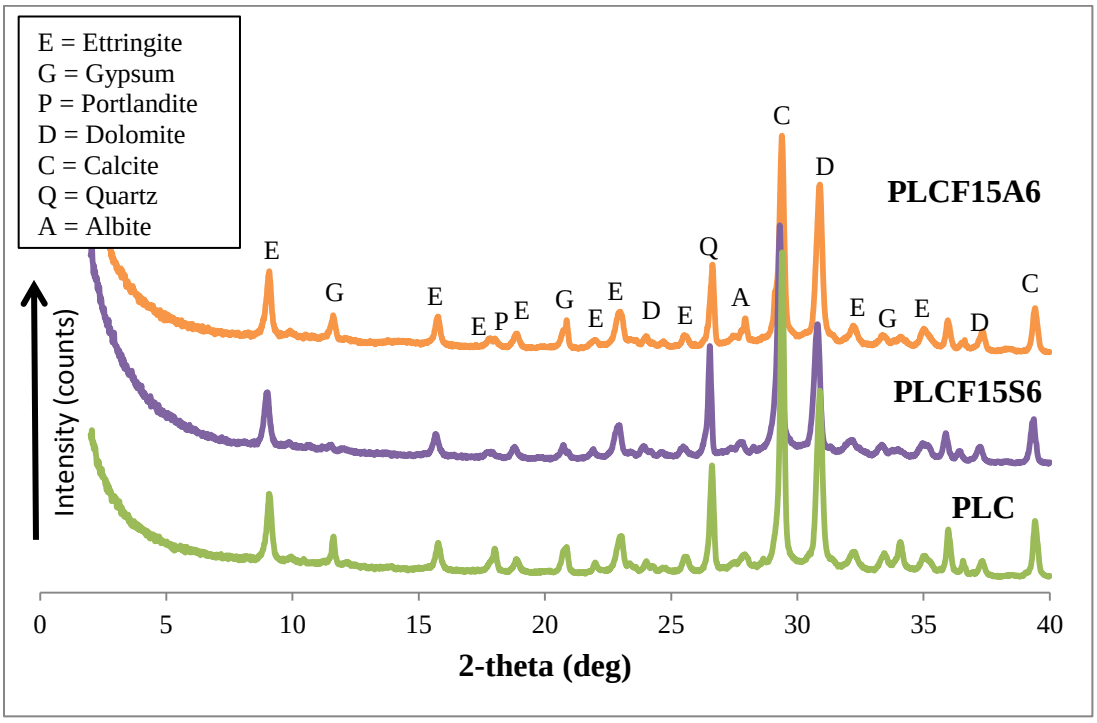

Figure 5.5: XRD of powder samples from PLC specimens after 12 months of exposure to sodium sulfate solution at 23°C.

Complying with the length change results, the XRD analysis showed that ternary mixtures incorporating NA and lower dosage of fly ash (15%) had higher intensities of ettringite (e.g., Figures 5.4 and 5.5). SEM analysis confirmed the abundance of conventional sulfate-

reaction products in these specimens (e.g. Figure 5.6). In addition to the high penetrability of mixtures incorporating NA as discussed in the RCPT section, it seems that NA acted as an additionally reactive source for sulfate attack reactions in a similar manner to binders with higher contents of C_3A (e.g. single binders of GU, GUL and PLC, which also failed the expansion limit of the test). However, this trend diminished with increasing the dosage of fly ash up to 40%, due to the dilution effect of higher fly ash dosages at improving the chemical resistance of cement-based materials to conventional sulfate attack, as explained earlier.

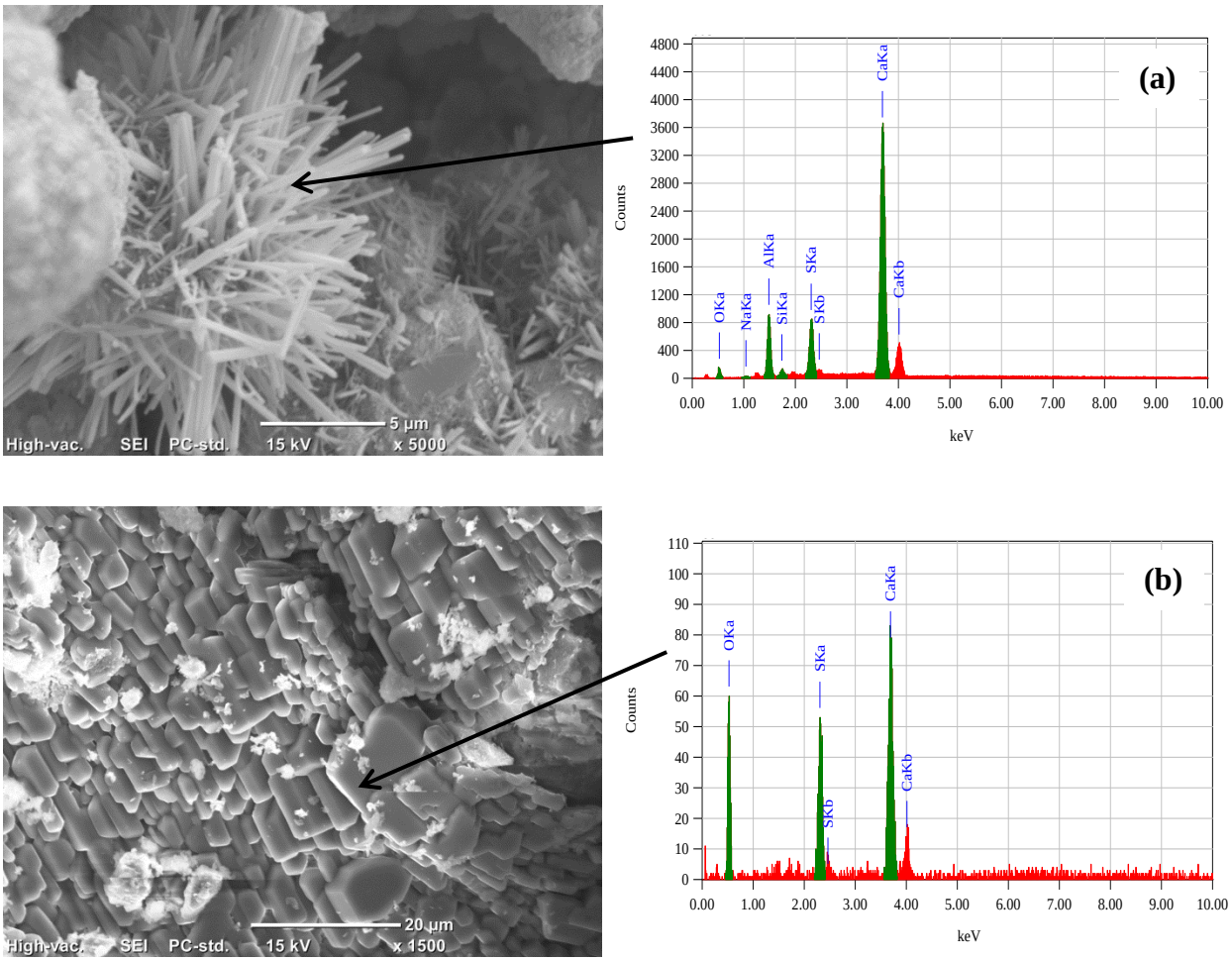

Figure 5.6: SEM micrographs and associated EDX spectrums for GULF15A6 specimen showing: (a) ettringite rosettes and (b) gypsum.

On the contrary to NA, all the mixtures incorporating NS, irrespective of the type of binder and even with a lower dosage of fly ash, had lower amounts of ettringite (e.g. Figure 5.4 and 5.5) which emphasizes the positive effect of NS on improving the resistance of cement-based materials to conventional sulfate attack. The latter effect is primarily related to improving the physical resistance of the matrix (i.e. reducing its penetrability), as discussed earlier in the RCPT section. In addition, NS has an efficient pozzolanic reactivity when combined with fly ash leading to the depletion of CH in the matrix (Said *et al.*, 2012), and in turn discounting the kinetics of sulfate reactions and resultant sulfate-bearing products. This was confirmed by DSC analysis (e.g., Figure 5.7). A semi-quantitative analysis based on the enthalpy concept (integration of heat flow peaks over temperature) can determine the relative phase formation, as the enthalpy of each phase is directly related to its amount (Brown and Gallagher, 2011). As depicted in Figure 5.7, the enthalpy of sulfate reaction products and CH in the PLC sample is much higher than that in the PLCF15S6 sample. This corresponds to the expansion results of these mixtures (0.17 and 0.02%, respectively), which signifies the role of NS at improving the chemical resistance of cementitious systems.

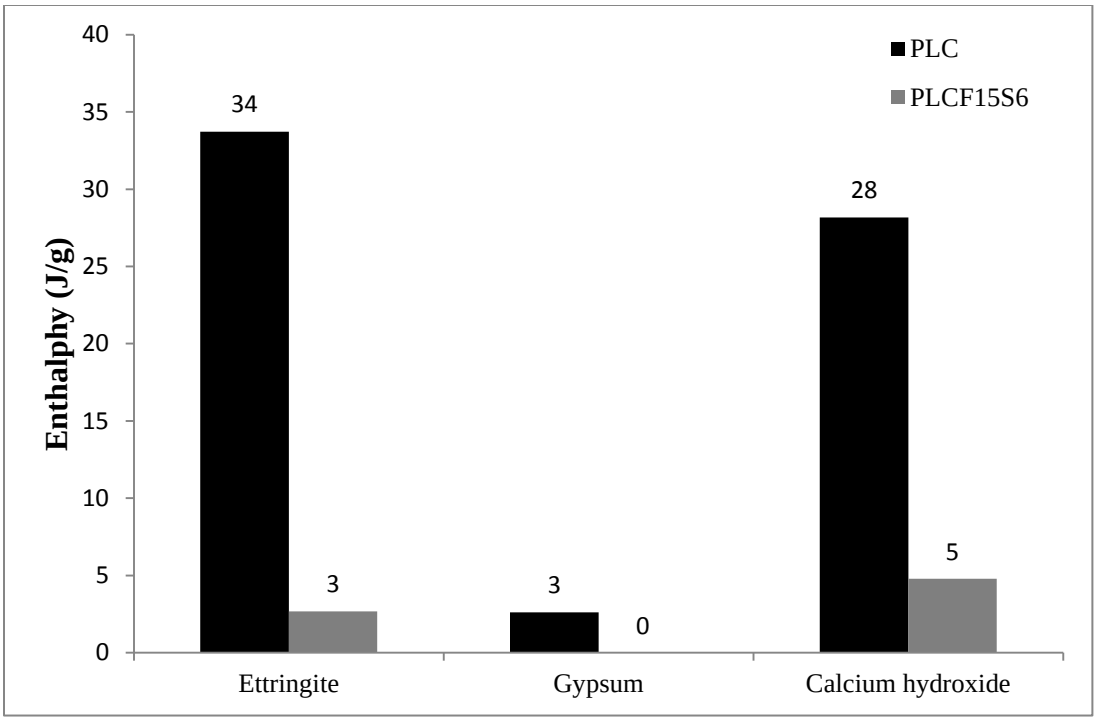

Figure 5.7: Enthalpies of sulfate-reaction products and calcium hydroxide for PLC and PLCF15S6 samples after 12 months of exposure to sodium sulfate solution at 23°C.

5.3. Thaumasite Sulfate Attack

5.3.1. Visual Assessment

At the initial stage of exposure up to 30 days, all of the mortar bars were intact without any sign of damage. Subsequently, the cracks started to appear and propagate in the specimens in proportion to the rate of expansion. For most of the specimens, the cracks started at the corner and then longitudinal cracks extended along the edges of the mortar prisms, indicating typical symptoms of sulfate attack. Together with crack formation, softening started at the surface of mortar and progressively moved towards the inner core with the ingress of sulfate solution. Figure 5.8 shows the time of disintegration/breakage (i.e., the time at which all replicates of a certain mixture disintegrated) of specimens prepared from GU/GUL binders (groups A, B and

C). For PLC binders, however, only mortar bars made with NA started to disintegrate after 160 days of exposure. Throughout the test, mushy white substance appeared on the surface of deteriorated mortar bars and cubes, and inside the container intermixed with solution and as residue (Figure 5.9), which might be indicative of TSA.

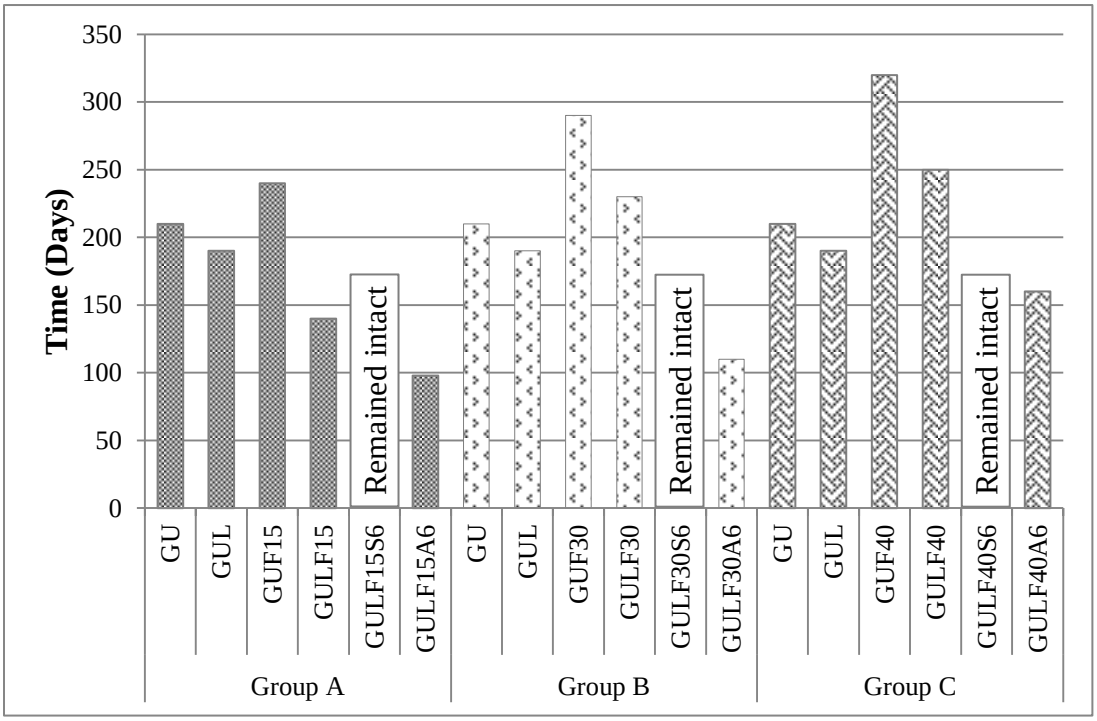

Figure 5.8: Time of disintegration/breakage of GU/GUL mortar bars exposed to sodium sulfate solution at 5°C.

Figure 5.9: Residue and deteriorated mortar specimens as a result of the sodium sulfate exposure at 5°C.

Higher intensity of cracking, bowing and deterioration were observed for the GUL specimens (e.g. Figure 5.10a). While, the incorporation of higher dosages of fly ash reduced the rate of deterioration as depicted in Figure 5.8, addition of NA accelerated the rate of deterioration from the beginning of the exposure (e.g., Figure 5.10b). Conversely, mixtures incorporating NS remained intact throughout the entire test period, irrespective of the dosage of fly ash (e.g., Figure 5.10c). Similarly, the modes of cracking and failure were observed on PLC mortar bars. However, the overall performance of the PLC mixtures was relatively better during the test in comparison to the GUL mixtures. The mortar cubes (GU, GUL and PLC mixtures) deteriorated in the same way as the mortar bars but the rate of deterioration was lower compared to mortar bars. This higher deterioration of mortar bars can be attributed to the larger surface area-to-volume ratio.

Figure 5.10: Visual features of mortar bars exposed to sodium sulfate solution at 5°C: (a) micro-cracks and expansion of a GUL specimen, (b) breakage of GULF30A6 specimens, and (c) intact PLCF15S6 specimens.

5.3.2. Length Change

The cumulative percentage of expansion for the mortar prisms comprising GU/GUL and PLC cements is shown in Figures 5.11 and 5.12, respectively. As expected, the rate of expansion of GUL mortar bars (additionally blended limestone) was higher and time-to-disintegration was earlier than GU mortar bars. On the contrary, PLC mortar specimens remained intact until the end of the experiment but exceeded the expansion limit (0.10%). This signifies that all the

control specimens (without FA and/or nanoparticles) failed to pass the test before 12 months of exposure at 5°C.

All the specimens made with 15% fly ash failed (expansion higher than 0.10%) before 6 months of exposure excluding the one with 6% NS (Figure 5.11a). The average expansion of GULF15S6 specimens was low (0.03%) after 12 months of exposure, complying with visual features of those specimens which remained intact. Comparatively, the mortar specimens comprising NA and 15% fly ash significantly expanded (more than 0.05%) after 60 days of exposure and totally disintegrated after 98 days. Similar patterns were observed for the mortar bars containing 30 and 40% fly ash irrespective of the mixture composition but the time-to-failure was delayed (Figs 5.11b-c). For example, the expansion of GULF15A6, GULF30A6 and GULF40A6 samples were 0.69% (91 days), 0.23% (105 days) and 0.18% (120 days), respectively, before disintegration. This highlighted that higher dosages of fly ash reduced the expansion and extended the time-to-disintegration. Similar to the group A specimens, samples from ternary binders comprising fly ash with NS (GULF30S6 and GULF40S6) were the only mixtures in groups B and C that showed limited expansion (about 0.01%) up to 12 months of exposure, indicating high sulfate resistance at this concentration and temperature conditions.

Relative to the average expansion results for specimens made from GU and GUL cement, specimens prepared with PLC had lower expansion values after the full-immersion exposure at 5°C (Figure 5.12). For instance, the magnitude of expansion of PLCF15S6 mortar bars was about one-third that of GULF15S6; whereas both mixtures were well below the expansion limit of 0.10%. Similar to control specimens (PLC), specimens prepared from PLC with 15% fly ash (PLCF15) exceeded the 0.10% expansion limit after about 270 days of exposure (Figure 5.12a), whereas at higher dosage of fly ash (PLCF30 and PLCF40), there was a significant reduction of

expansion up to12 months of exposure (Figures 5.12b-c). Similar to the trends observed for the GUL mixtures, PLC specimens comprising NA had an accelerated rate of expansion and exceeded the 0.10% limit, which led to disintegration of specimens starting from 160 days. Also, specimens containing PLC, fly ash and NS had limited expansion (maximum of 0.01%) up to the end of exposure.

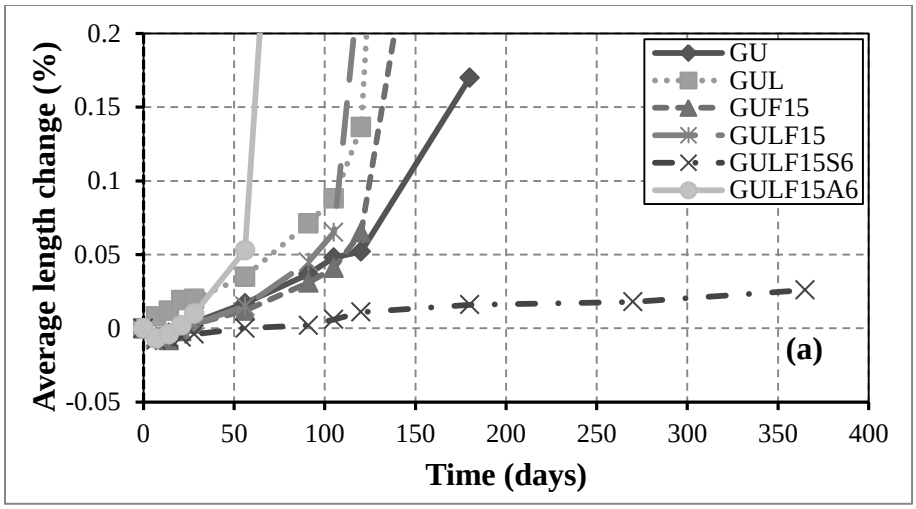

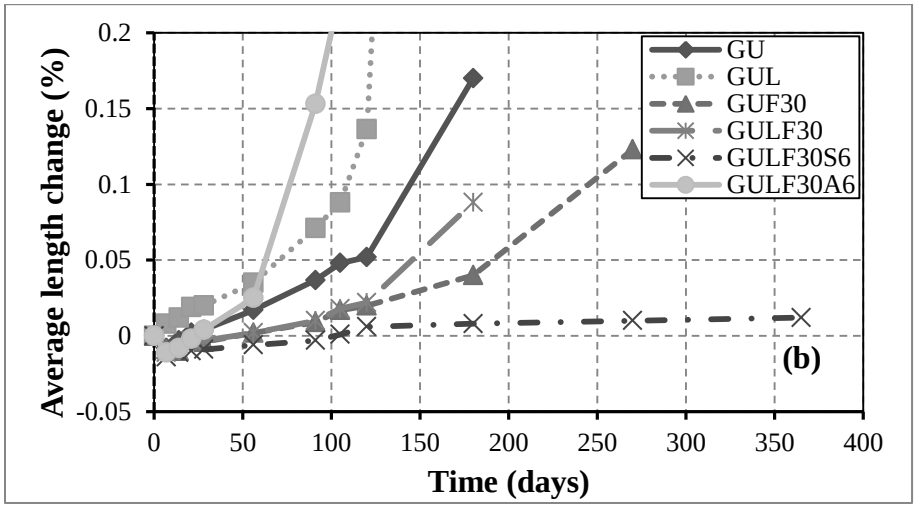

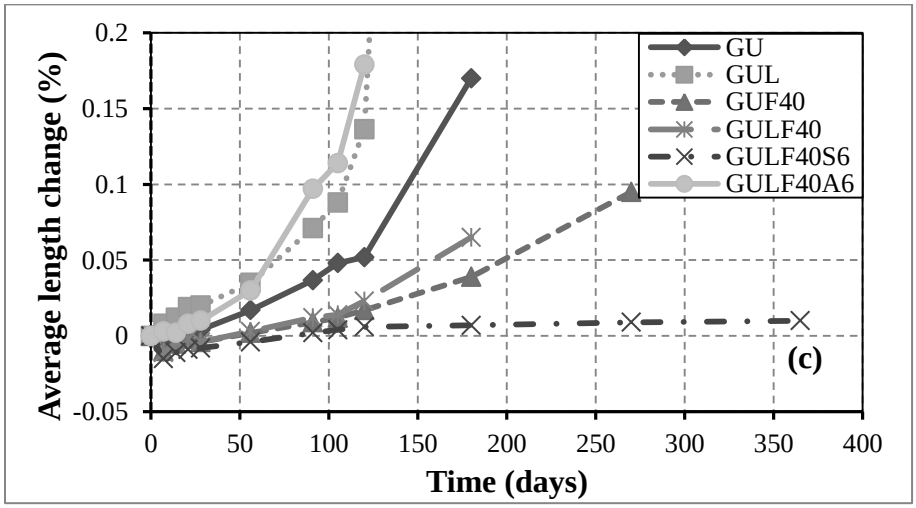

Figure 5.11: Expansion of mortar prisms exposed to sodium sulfate solution at 5°C: (a) group A, (b) group B, and (c) group C mixtures.

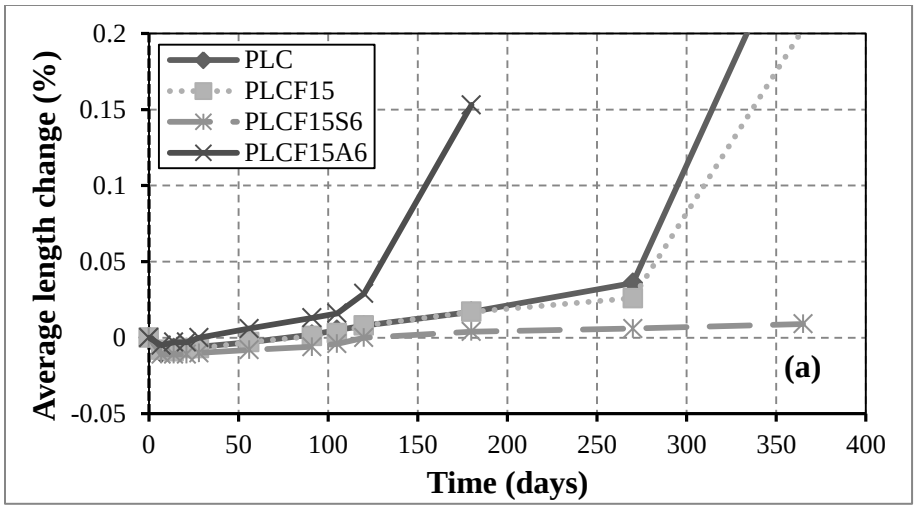

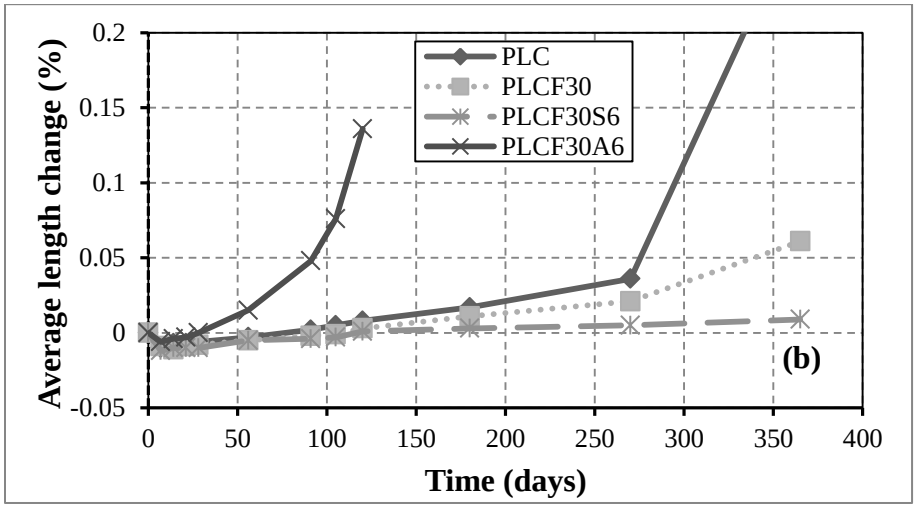

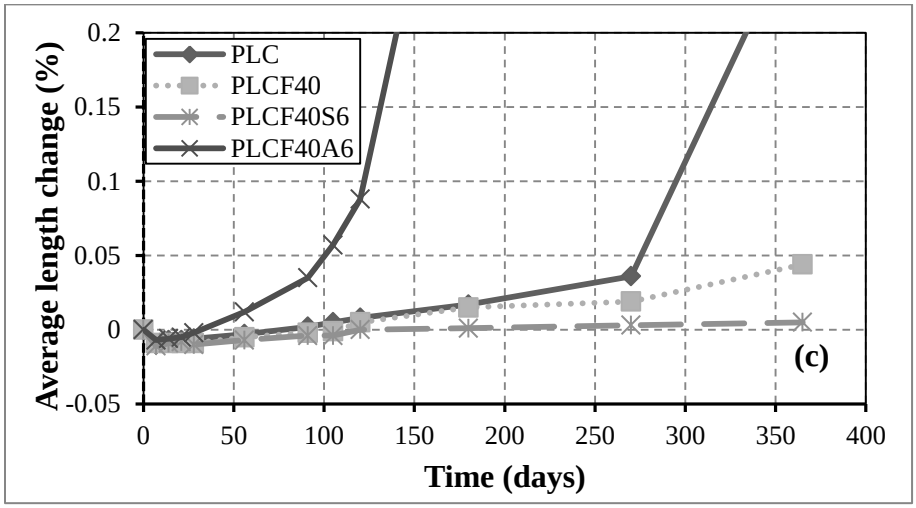

Figure 5.12: Expansion of mortar prisms exposed to sodium sulfate solution at 5°C: (a) group D, (b) group E, and (c) group F mixtures.

5.3.3. Mass Change

The mass change of the mortar bars were measured at different time intervals during the exposure similar to the length change, as for example shown in Figure 5.13 (also see ***Appendix C***). The rate of change of mass was comparable for both the GUL and PLC mixtures. For most of the specimens, the rate of mass change was low up to 30 days, and then it increased up to the end of exposure conforming to the length change trends. This slight mass gain (maximum of 3.4%) over time can be attributed to solution absorption and progressive formation of sulfate reaction products until the disintegration of some specimens. Depending upon the type of binder, however, this trend shifted downwards (e.g. GUL in Figure 5.13) after a certain period of exposure until failure/disintegration when the rate of deterioration (spalling and surface scaling) was higher relative to the rate of mass gain. However, no severe mass loss, relative to initial mass, was observed up to failure of deteriorating specimens except PLC mortar bars which lost 4.5% of mass at 12 months of exposure. Unlike the expansion results, the mass change results did not show distinctive trends among mixtures. Higher mass gain values did not necessarily correspond to higher expansion. However, specimens incorporating NS gained slightly lower mass relative to corresponding specimens, which might be indicative of their lower penetrability and slower rate of deterioration (Figure 5.13).

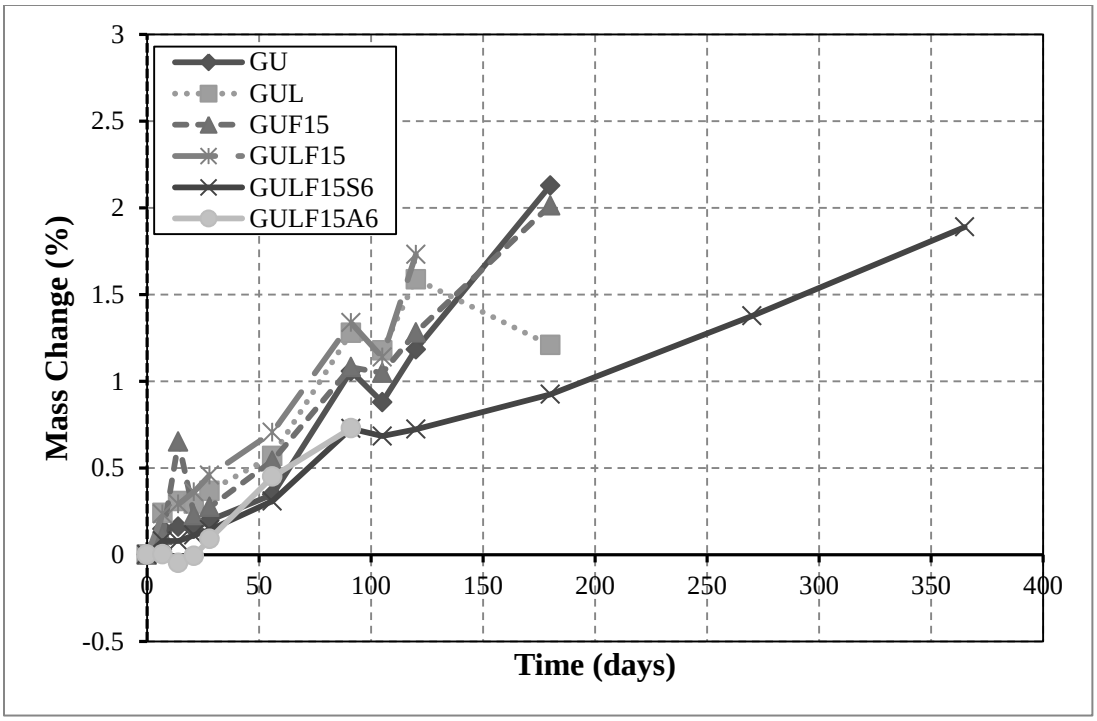

Figure 5.13: Change of mass of some GU/GUL specimens vs. the time of exposure.

5.3.4. Dynamic Modulus of Elasticity

The variation of relative dynamic modulus of elasticity (RE_d) over the time of exposure is for example presented in Figure 5.14 (also see ***Appendix C***). RE_d is indicative of the internal conditions of specimens (including micro-cracking) exposed to severe conditions (Zhang *et al.*, 2002). Up to four months, RE_d of most specimens remained constant or slightly increased (up to 10%), and then it followed a downward trend (Figure 5.14). This trend is in compliance with the progression of sulfate attack reactions, in which formation of sulfate bearing products in the matrix causes some increase in the mechanical properties at the initial stage. Subsequently, the drop of RE_d signifies that fissures had developed inside the mortar cubes due to voluminous sulfate reaction products without or with softening. It is worth noting that the rate of deterioration of mortar bars (expansion results) was higher than that of cubes (RE_d results) due to

the size effect, as explained earlier. The RE_d trends had a general agreement with the expansion results. For example, specimens comprising NS had slight reduction in RE_d after 12 months of exposure (e.g. GULF30S6 in Figure 5.14), which indicates that the core of these mortar cubes remained intact. At the end of the test, however, specimens without NS had either a higher drop in RE_d (up to 84%) due to severe deterioration, or it was not possible to measure the UPV because of the disintegration of cubes.

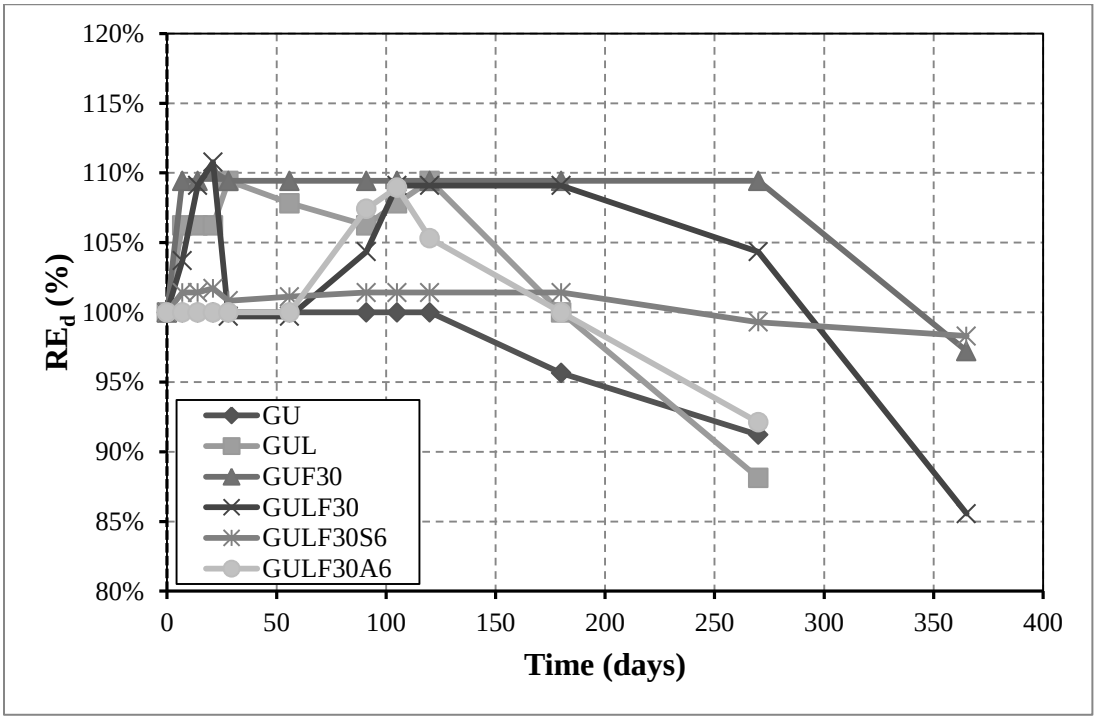

Figure 5.14: Relative dynamic modulus of elasticity of group B mortar cubes vs. the time of exposure.

5.3.5. Discussion

In this exposure (immersion in sodium sulfate at 5°C), the rate of deterioration of mortar mixtures was influenced by the key mixture design parameter. The effects of type of binder, dosage of fly ash and nanoparticles on the behaviour of specimens are discussed below.

5.3.5.1. Effect of type of binder

The type of binder had a pronounced effect on the physico-mechanical results. The specimens prepared with GUL cement had higher expansion than that of the corresponding PLC specimens. This was statistically supported by analysis of variance (ANOVA) of expansion results at a significance level (α) of 0.05. For example, ANOVA results showed that changing the cement type from GUL to PLC at a constant dosage of 15% FA had an F value of 39.17 compared to a critical value (F_{cr}) of 18.51. According to Montgomery (2013), exceeding the F_{cr} for an F-distribution density function indicates that the variables tested have a statistically significant effect on the average results.

For specimens made from GU (up to 5% limestone filler) and GUL (about 13% limestone filler) cements, the extent of deterioration was higher for the GUL specimens due to higher penetrability (Table 5.1) and limestone content, which are key factors in the process of TSA. For example, Figure 5.15 shows the XRD analysis results of GUF40 and GULF40 samples (constant fly ash content) after 320 and 250 days of exposure, respectively. Thaumasite peaks for GULF40 sample were higher than that for GUF40 sample, even after a shorter time of exposure, which indicates that addition of higher dosages of limestone filler to this binder promoted TF. In addition to ettringite and gypsum formation, TF in these specimens led to faster rate of expansion and consequently disintegration at earlier periods of exposure depending upon the limestone content in the binder (Figure 5.11c). The reason for TF in GU specimens can be related to its higher C_3A content (9%), which stimulated ettringite formation that subsequently reacted with the limestone component (up to 5%) in the GU binder or bicarbonate ions from dissolved carbon dioxide in the solution to form thaumasite [indirect or Woodfordite route] (Torres *et al.*, 2006;

Collett *et al.*, 2004). This argument, is for example substantiated by EDX analysis (e.g. Figure 5.16), which showed strong aluminum peaks in the thaumasite spectrum.

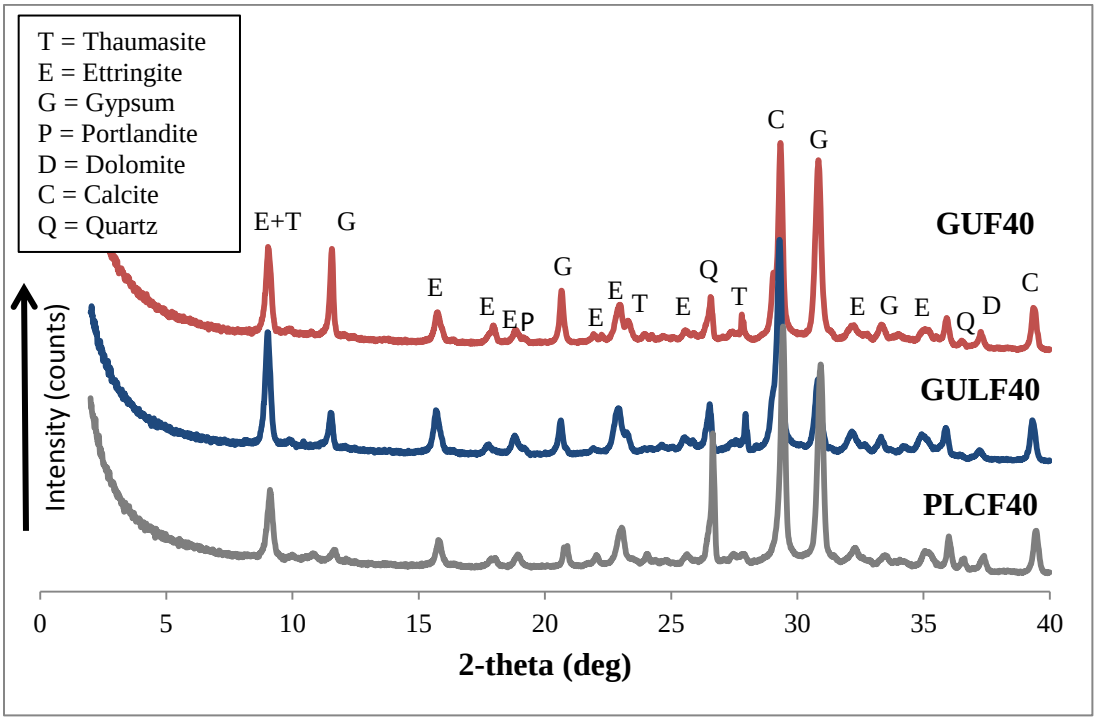

Figure 5.15: XRD of powder samples from GUF40, GULF40 and PLCF40 after 320, 250 and 365 days, respectively of exposure to sulfate solution at 5°C.

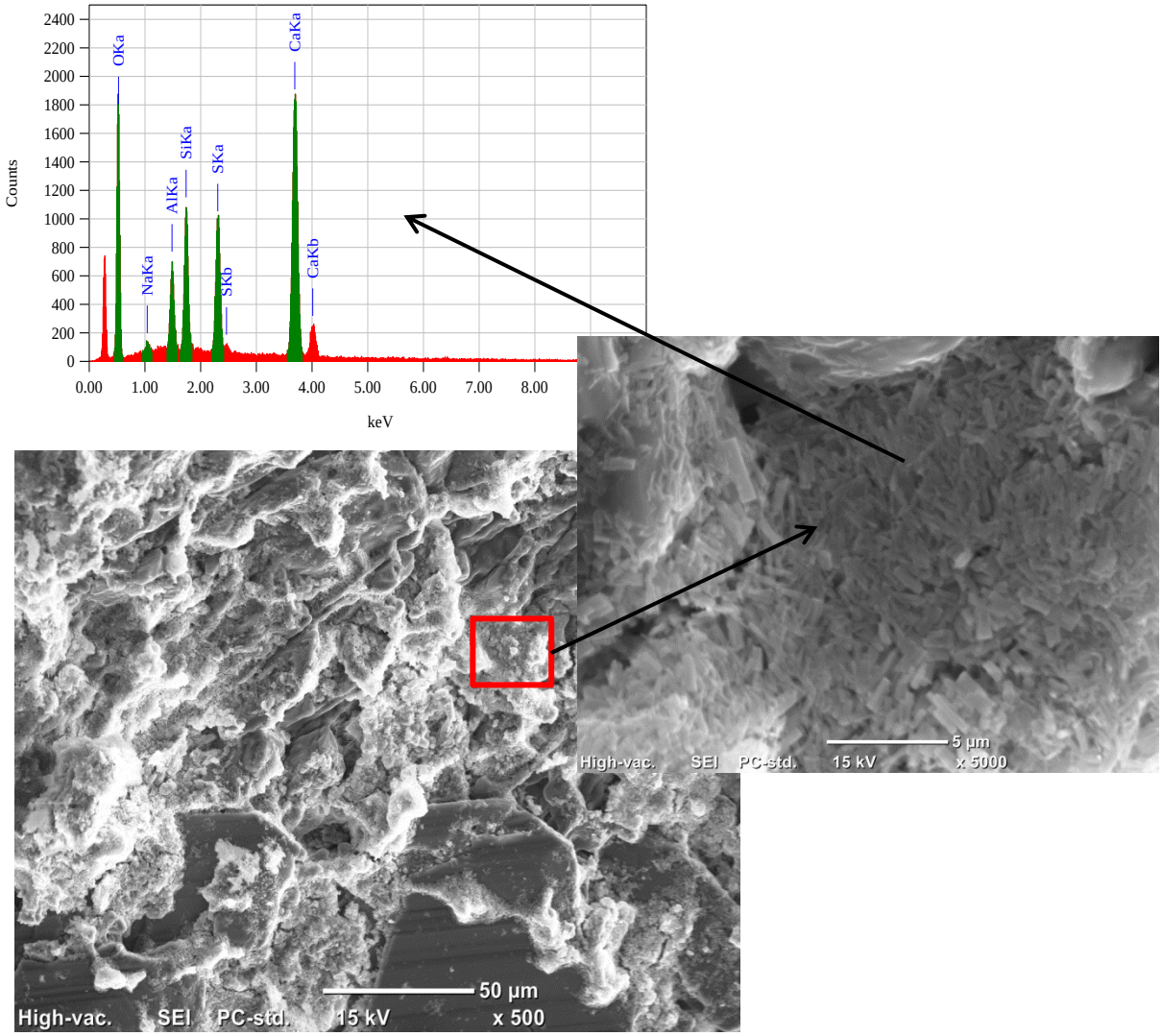

Figure 5.16: SEM micrographs and associated EDX spectrum for GU specimen after 210 days of exposure to sodium sulfate solution at 5°C showing TF.

Specimens made with GUL mixtures (excluding the mixtures with NS) were completely disintegrated during the cold temperature exposure. On the contrary, the rate of deterioration was lower in mortars prepared from PLC. This might be attributed to difference in properties between the two types of cement. Since limestone was added during the manufacturing process and interground with clinker, it produced a product (PLC) with more uniform properties, higher

fineness (454 m^2/kg) and better reactivity than that of blending coarser GU cement with 13% limestone filler at the mixer. Thus, PLC markedly reduced the volume of permeable pores in mortars (i.e. increased the physical resistance), and thus reduced the sulfate solution uptake. This is supported by the strength and RCPT results, where almost all the mortar specimens made from PLC had higher compressive strength (Table 3.3) and lower penetration depth (Table 5.1) than that of corresponding specimens prepared from GUL.

In general, the rate of TF is influenced by the amount of calcium carbonate in the mixtures. In GUL binders more carbonate particles may exist in free form and readily available for sulfate reactions, while in PLC binders the efficiency of hydration is improved, as explained earlier, and carbonate can be chemically bound in carbo-aluminate phases, which might slow down the kinetics of TF. To further verify this trend, a semi-quantitative analysis for the XRD results (e.g. Figure 5.15) was carried out by Rietveld method (e.g., Barnett *et al.*, 2002) to determine the relative amounts of phases in the XRD results. In Figure 5.15 (GULF40 vs. PLCF40), Rietveld analysis showed that the amount of thaumasite in GULF40 sample was twice that in the PLCF40 sample, which explains the higher expansion and ultimately disintegration of GULF40 mortar bars due to progressive TSA at about 250 days of exposure (Figure 5.8). On the contrary, PLCF40 specimens were intact with limited expansion up to the end of exposure. The results suggest that TSA was the main cause of damage for GULF40 specimens, while TF was still progressing in the PLCF40 specimens.

5.3.5.2. Effect of fly ash

The beneficial effect of fly ash on the resistance of mortar to sulfate attack at low temperature can be attributed to its physical and chemical effects, similar to the conventional sulfate attack exposure. The action of fly ash depended on the type of binder and nanoparticles, but increasing the dosage of fly ash generally led to discounting the rate of deterioration and associated expansion (Figures 5.11 and 5.12). This was statistically verified by ANOVA for the expansion results. For example, ANOVA for the expansion results of GU specimens showed that the variation of the fly ash dosage had an F value of 31.41 compared to a critical value (F_{cr}) of 9.55.

Considering the RCPT results (Table 5.1), it was found that fly ash mixtures had lower penetration depth than the corresponding specimens without fly ash, and further reduction in the penetration depth was achieved with higher dosages of fly ash (excluding the effect of nanoparticles). Furthermore, over the time of exposure, incorporation of higher dosages of fly ash in the cementitious matrix produced denser microstructure with less interconnected pores. This improvement in physical resistance reduced the penetrability of the sulfate solution in the cementitious matrix and delayed the rate of expansion and deterioration even at the cold temperature exposure. For example, the GU and GUF40 specimens were disintegrated at 210 and 320 days of exposure, respectively.

In the cold temperature exposure, the chemical resistance associated with increasing the dosage of fly ash is attributed to reduction of CH (pozzolanic effect), dilution of C_3A and limestone filler contents, thereby reducing the formation of sulfate-bearing products and associated damage. This was supported by the XRD analysis. For instance, Figure 5.17 shows that the intensities of ettringite, thaumasite and gypsum in the PLCF40 sample is less than that in

the PLCF15 sample, which conforms to the expansion values after 12 months of exposure (0.05 and 0.20%, respectively).

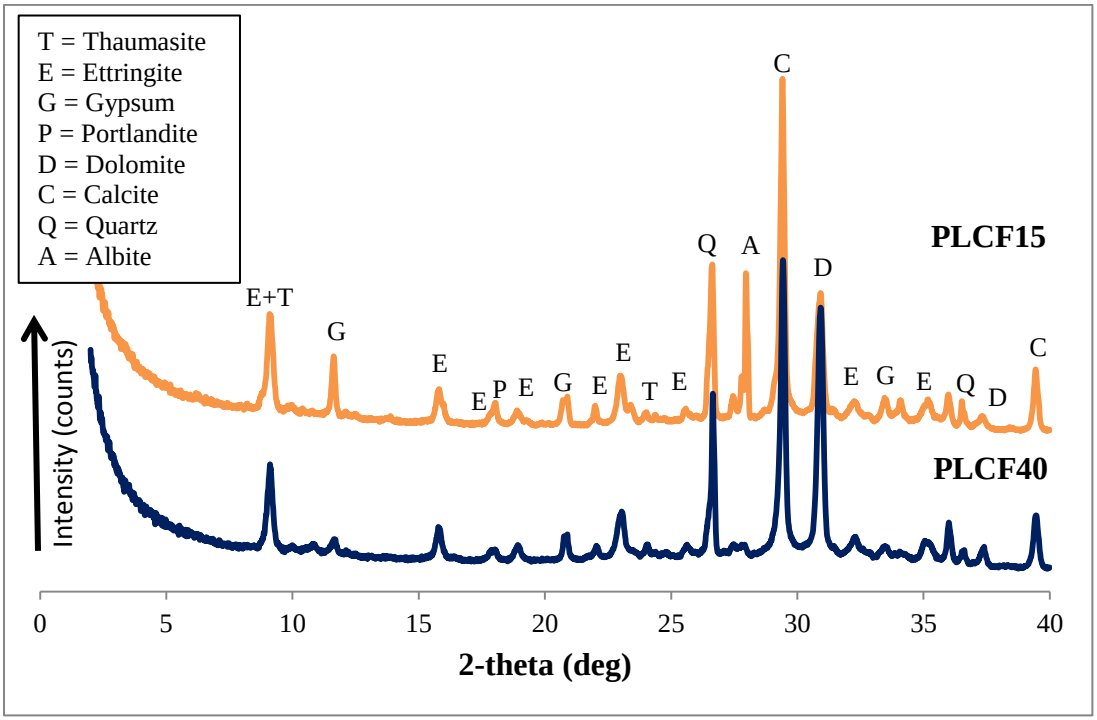

Figure 5.17: XRD of powder samples from PLCF15 and PLCF40 specimens after 12 months of immersion in sodium sulfate solution at 5°C.

5.3.5.3. Effect of nano-particles

Irrespective of the type of binder and dosage of fly ash, incorporation of NS significantly improved the resistance of mortar mixtures to sulfate attack at low temperature, since all these mixtures had limited expansion/deterioration up to 12 months (Figures 5.11 and 5.12). For instance, at a significance level (α) of 0.5, ANOVA for the expansion results showed that the addition of NS to GUL binders with 30% fly ash had an *F* value of 361 compared to a critical value (F_{cr}) of 18.51. Similar to the behaviour observed in the conventional sulfate attack exposure, this trend can be mainly ascribed to the enhanced physical resistance of the mixtures

due to the refinement and densification effects (physical filler and pozzolanic effects) of NS in the cementitious matrix, which markedly reduced the penetrability of these mixtures and limited the ingress of the sulfate solution. This behaviour is evident from the RCPT results, where the NS mixtures had limited penetration depth below 5 mm (Table 5.1). Furthermore, addition of a highly reactive pozzolan such as NS with fly ash likely led to more consumption of portlandite in the hydrated cement paste compared to fly ash alone, and thus improved the chemical resistance to alkali sulfate. This argument is substantiated by the fact that ternary binder incorporating lower dosages of fly ash (only 15%) and 6% NS had high resistance to the TSA exposure, even with high limestone contents in the GUL and PLC binders. XRD analysis (e.g. Figure 5.18) also verified this trend as mixtures containing low dosages of fly ash with NS (e.g. PLCF15S6) had less intensity for the sulfate reaction products (ettringite, thaumasite and gypsum) relative to the corresponding mixtures without NS (e.g. PLCF15), which failed the test (high expansion and/or disintegration) before or at the end of exposure. This suggests that the rate of sulfate reactions was slow, and NS effectively improved the resistance of mortar to TSA.

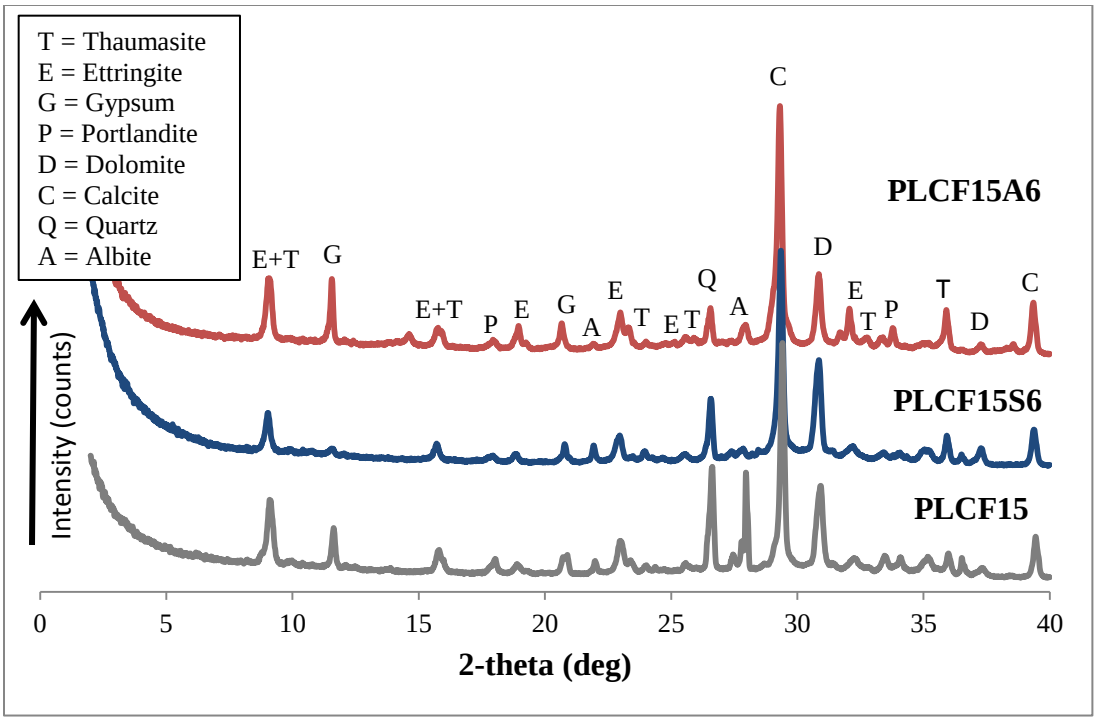

Figure 5.18: XRD of powder samples from PLCF15, PLCF15S6 and PLCF15A6 after 365, 365 and 220 days, respectively of exposure to sulfate solution at 5°C.

On the contrary to NS, addition of NA to ternary binders, irrespective of the type of cement used, aggravated the damage in this exposure. Unlike the conventional sulfate attack exposure, higher dosages of fly ash was unable to mitigate the damage of mortar in this low temperature exposure, which signifies the severity of damage in the case of TSA. For instance, ANOVA for the expansion results showed that the incorporation of NA in the GUL binders with 15% fly ash had an F value of 29.88, which is larger than the F_{cr} value of 18.51. Based on microstructural and mineralogical analyses, it was found that specimens prepared with NA failed by disintegration as a result of excessive TF which converted C-S-H gel into non-cohesive mass (e.g. Figure 5.19). Again, the existence of aluminum in the EDX spectrum suggests that thaumasite originated from the indirect (Woodfordite route) route.

As explained in the RCPT section (Table 5.1), addition of NA reduced the physical resistance (increased the penetrability) of the mortar mixture, and thus enhanced the ingress of sulfate solution in such coarse matrix. In addition, the presence of reactive alumina increased TF in the paste through the preceding formation of ettringite (indirect route), which caused magnified expansion, loss of stiffness and earlier disintegration of all the NA mixtures. This trend had been also noted in the XRD analysis (e.g. Figure 5.18) of samples comprising NA (e.g. PLCF15A6), which had higher intensities of ettringite, thaumasite and gypsum in spite of the shorter period of exposure relative to the corresponding samples without NA (e.g. PLCF15, PLCF15S6).

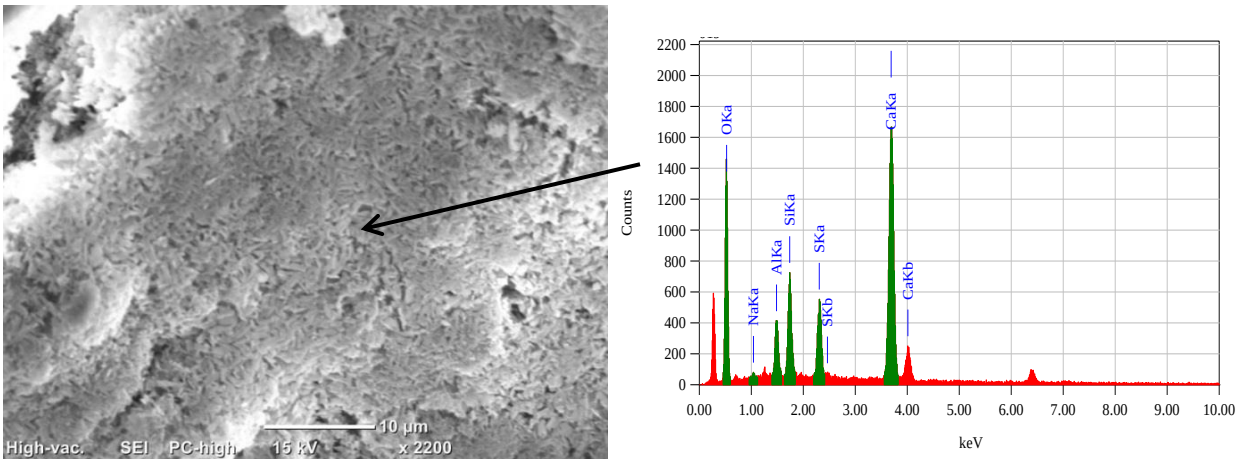

Figure 5.19: SEM micrograph and associated EDX spectrum for PLCF30A6 specimen showing thaumasite crystallites replacing the matrix.

6. Summary, Conclusions and Recommendations

6.1. Summary and Conclusions

In this thesis, two experimental studies were conducted in order to evaluate the resistance of innovative concrete mixture designs incorporating various dosages of nano-alumina (NA) or nano-silica (NS) and fly ash to external sulfate attack under different environmental conditions conductive to physical salt attack (PSA), conventional sulfate attack and thaumasite sulfate attack (TSA). For evaluating PSA on concrete, sixteen concrete mixtures were tested where the mixture design variables were w/cm (0.4 and 0.5), type of binder (GU cement or GU cement blended with 30% fly ash) and ultrafine particles (NS or NA). Based on the phase diagram of sodium sulfate, an exposure was designed to stimulate PSA by cyclic temperature (20 to 35°C) and relative humidity (90 to 40%). The assessment criteria were based on physical properties (penetration depth, visual appearance and mass loss). In addition, the alteration of microstructure was examined by microscopy and mineralogical analysis.

Twenty four mortar mixtures with a fixed water-to-binder ratio of 0.485 were prepared in the second phase of the experimental program to determine the resistance to chemical sulfate attack of nano-modified fly ash mortars. The mixtures were classified into six groups (A to F) where the design variables were types of binder (GU, GUL or PLC), dosages of fly ash (15, 30 and 40%) and nanoparticles (NS and NA). To provoke the conventional and thaumasite sulfate attack, CSA A3004-C8 (Procedure A and B) standard test procedures were generally followed. During the experiment, the mortar bars and cubes were stored in 5% sodium sulfate solution at 5 and 23°C for 12 months. The evaluation methods were based on the physical properties (visual

appearance, change in length and mass, relative dynamic modulus of elasticity and interconnectivity of pores), the alteration of microstructure by SEM with EDX and the mineralogical phases by XRD and DSC.

6.1.1. Conclusions for the PSA exposure

Physical salt attack (PSA) is a critical durability issue for concrete structures exposed to salt-rich environments and cyclic climates. The damage manifestations of PSA on concrete are surface scaling and flaking, which are typically accompanied by efflorescence. In PSA, the deterioration takes place due to salt crystallization with potential chemical interaction between salt ions and hydrated cement paste depending on the constituent materials. Based on the test procedures and mixture design variables adopted in this study, the following conclusions can be drawn:

- Damage manifestations, mass loss results and microstructural features showed that the proposed test procedure was capable of replicating PSA on concrete within a short time interval (120 days), and hence it might be used to prequalify concrete mixtures for exposures conductive to PSA.
- Except for concrete made with binary binders comprising GU and NA, the deterioration of concrete mixtures was mainly due to the crystallization of salt in pores within the drying portions of concrete cylinders. Thermal, mineralogical and microstructural analyses revealed the abundance of thenardite in the drying portion, with limited occurrence of ettringite and gypsum in the immersed portion of specimens.
- Reducing the w/cm from 0.5 to 0.4 notably improved the resistance of concrete to PSA as shown by the visual assessment and mass loss results. As observed by the physical penetration depth results, lower w/cm made the concrete less porous, which reduced solution uptake and consequently the extent of deterioration.

- Compared to the control (GU) binder, the incorporation of 30% fly ash in concrete reduced the surface scaling and mass loss at both w/cm. This improvement effect depended on the type and dosage of nanoparticles.
- For concrete mixtures incorporating fly ash without or with nanoparticles, the penetration depth was inversely proportional to the mass loss results, since more surface was obtained for mixtures with finer pore structure and vice versa.
- Mixtures incorporating GU and NA were mainly disintegrated because of the synergistic effects of chemical sulfate attack and salt crystallization; however, this trend was not replicated in the ternary mixtures containing GU, fly ash and NA due to the beneficial effect of fly ash on improving the chemical resistance of concrete.

6.1.2. Conclusions for the conventional and thaumasite sulfate attack exposures

Sulfate attack is a critical durability issue for cement-based materials exposed to sulfate-rich environments at normal and low temperatures. Conventional sulfate attack can cause expansion, cracking and spalling of concrete, whereas thaumasite sulfate attack (TSA) transforms the cementitious materials into a voluminous and non-cohesive mass without any binding capacity. Considering the different exposures and key test variables (type of binder, fly ash and nanoparticles) implemented in this study, the following conclusions can be drawn:

- The microstructural and mineralogical analyses revealed the abundance of classical sulfate-reaction products (i.e., ettringite and gypsum) in the samples exposed to sodium sulfate solution at 23°C, and thus conventional sulfate attack was the main cause of damage in this exposure.
- Irrespective of the type of binder (GU, GUL, and PLC), fly ash at higher replacement levels of 30 and 40% by mass of binder mitigated conventional sulfate attack on mortar.

- While the addition of 6% NS was effective at improving the resistance of all types of mortar to conventional sulfate attack even with the lower dosage of fly ash, addition of 6 % NA significantly increased the expansion of mortar bars due to excessive formation of ettringite.
- Damage manifestations, microstructural and mineralogical analyses revealed the abundance of thaumasite with ettringite and gypsum in deteriorating mortar specimens exposed to the sulfate solutions at 5°C. Hence, TSA was the main cause of damage in this exposure.
- The experimental results showed that GU cement (high C_3A content of 9%) blended with limestone filler (GUL) increased the susceptibility to TSA relative to PLC (moderate C_3A content of 6%), which is manufactured from intergrinding clinker and limestone.
- TSA related deterioration is directly associated with the availability and content of limestone particles in mortar/concrete. Hence, even binders incorporating fly ash with GUL cement showed inferior performance due to TSA, especially with the addition of NA.
- Among all the GU/GUL specimens, only mortar mixtures with NS were resistant to the cold temperature exposure, due to their improved physical and chemical resistance. Comparatively, PLC mixtures had better performance in this exposure, especially when sufficient dosages of fly ash (30 and 40%) and/or 6% NS were added to the mixtures.
- Similar to the conventional sulfate attack exposure, all mixtures comprising NA had inferior performance to TSA. These mixtures had high penetrability and reactive alumina source for ettringite formation and subsequently TF via the indirect (Woodfordite) route.

This trend pinpoints the key role of reactive alumina availability and content in the TSA process.

- Similar to conventional sulfate attack, reduction of penetrability of cement-based materials (for example by addition of NS) is the first line of defense against TSA. However, other key factors that control the chemical resistance to TSA are the type of binder, availability and dosage of limestone and content of reactive alumina phases in the matrix.

6.2. Recommendations for Future Work

The results and discussion presented in this study provide many useful insights for the extension of this research work. The following are recommendations for further investigations:

- Repeating the accelerated PSA test developed in this thesis on a wide range of concrete mixtures to ensure its reproducibility.
- Investigating the effect of slag, silica fume and natural pozzolans alone or their combined effect with nano-silica on the resistance of concrete to PSA, conventional sulfate attack and TSA.
- Studying the effect of other nanoparticles (e.g. nano-clay) at different dosages on external sulfate attack on concrete.
- Verifying the effect of nano-silica at different dosages with PLC on the resistance to external sulfate attack.
- Ingress of chloride ions in conjunction with sulfate ions from de-icing salts, groundwater and seawater is a natural phenomenon, which may lead to combined chloride-sulfate attack. Hence, future research on nano-modified fly ash concrete might include this aspect.

7. References

ACI 201.2R. (2008). "Guide to durable concrete." *Reported by ACI Committee 201*, Farmington Hills, MI: American Concrete Institute.

ACI 318 (2008). "Building Code Requirements for Structural Concrete and Commentary." *Reported by ACI Committee 318*, Farmington Hills, MI: American Concrete Institute.

Araújo, G. S., Chinchón, S., and Aguado, A. (2008). "Evaluation of the behaviour of concrete gravity dams suffering from internal sulfate attack." *Ibracon Structures and Materials Journal*, 1, 17-45.

ASTM C1012. (2013). "Standard Test Method for Length Change of Hydraulic-Cement Mortars Exposed to a Sulfate Solution." *ASTM International*, West Conshohocken, PA, 04.01.

ASTM C1157. (2011). "Standard Performance Specification for Hydraulic Cement." *ASTM International*, West Conshohocken, PA, 04.01.

ASTM C1202. (2012). "Standard Test Method for Electrical Indication of Concrete's Ability to Resist Chloride Ion Penetration." *ASTM International*, West Conshohocken, PA, 04.02.

ASTM C1585. (2013). "Standard Test Method for Measurement of Rate of Absorption of Water by Hydraulic-Cement Concretes." *ASTM International*, West Conshohocken, PA, 04.02.

ASTM C192. (2007). "Standard Practice for Making and Curing Concrete Test Specimens in the Laboratory." *ASTM International*, West Conshohocken, PA, 04.02.

ASTM C39. (2012). "Standard Test Method for Compressive Strength of Cylindrical Concrete Specimens." *ASTM International*, West Conshohocken, PA, 04.02.

ASTM C494. (2013). "Standard Specification for Chemical Admixtures for Concrete." *ASTM International*, West Conshohocken, PA, 04.02.

ASTM C597. (2009). “Standard Test Method for Pulse Velocity Through Concrete.” *ASTM International*, West Conshohocken, PA, 04.02.

ASTM C672. (2012). “Standard Test Method for Scaling Resistance of Concrete Surfaces Exposed to Deicing Chemicals.” *ASTM International*, West Conshohocken, PA, 04.02.

Atahan, H. N. and Dikme, D. (2011). "Use of mineral admixtures for enhanced resistance against sulfate attack." *Construction and Building Materials*, 25(8), 3450-3457.

Barker, A. P., and Hobbs, D. W. (1999). “Performance of Portland limestone cements in mortar prisms immersed in sulfate solutions at 5°C.” *Cement and Concrete Composites*, 21(2), 129-37.

Barnett, S.J, Macphee, D.E, Lachowski, E.E, and Crammond, N.J. (2002). “XRD, EDX and IR analysis of solid solutions between thaumasite and ettringite.” *Cement and Concrete Research*, 32(5), 719-730.

Barrett, T. J., Sun, H., Nantung, T., and Weiss, W. J. (2014). “Performance of Portland Limestone Cements.” In Transportation Research Board 93rd Annual Meeting.

Bassuoni, M. T. and Nehdi, M. L. (2012). “Resistance of Self-Consolidating Concrete to Ammonium Sulphate Attack.” *Materials and Structures*, RILEM, 45(7), 977-994.

Bassuoni, M. T. and Sonebi, M. (2010). “Design, Production and Placement of Self-Consolidating Concrete, *RILEM Book Series*, Springer.” In: Khayat, K. H. and Feys, D., eds., Effect of freezing-thawing cycles on the resistance of self-consolidating concrete to sulfate Attack, 1, 329-340.

Bassuoni, M. T., and Nehdi, M. L. (2009a). “Durability of self-consolidating concrete to different exposure regimes of sodium sulfate attack.” *Materials and Structures*, RILEM, 42(8), 1039-1057.

Bassuoni, M. T., and Nehdi, M. L. (2009b). “Durability of self-consolidating concrete to sulfate attack under combined cyclic environments and flexural loading.” *Cement and Concrete Research*, 39(3), 206-226.

Bassuoni, M. T., Nehdi, M. L., and Greenough, T. R. (2006). "Enhancing the Reliability of Evaluating Chloride Ingress in Concrete Using the ASTM C 1202 Rapid Chloride Penetrability Test." *Journal of ASTM International*, 3(3), 13p.

Behfarnia, K., and Niloofar, S. (2013). "The effects of nano-silica and nano-alumina on frost resistance of normal concrete." *Construction and Building Materials*, 48, 580-584,

Bellmann, F., and Stark, J. (2008). "The role of calcium hydroxide in the formation of thaumasite." *Cement and Concrete Research*, 38(10), 1154-1161.

Bensted, J. (1999). "Thaumasite — background and nature in deterioration of cements, mortars and concretes." *Cement and Concrete Composites*, 21(2), 1171-1121.

Bensted, J. (2003). "Thaumasite-direct, woodfordite and other possible formation routes." *Cement and Concrete Composites*, 25(8), 873-877.

Berry, E.E., Hemmings, R.T., and Cornelius, B.J. (1990). "Mechanisms of hydration reactions in high volume fly ash pastes and mortars", *Cement and Concrete Composites*, 12(4), 253-261.

Bickley, J. A. (1999). "The repair of Arctic structures damaged by thaumasite." *Cement and Concrete Composites*, 21(2), 155-158.

Birgisson, B., Mukhopadhyay, A. K., Geary, G., Khan, M., and Sobolev, K. (2012). "Nanotechnology in Concrete Materials: A Synopsis." *Transportation Research E-Circular*, E-C170.

Bjornstrom, J., Martinelli, A., Matic, A., Borjesson, L., and Panas, I. (2004). "Accelerating effects of colloidal nano-silica for beneficial calcium–silicate–hydrate formation in cement." *Chem Phys Lett*, 392(1-3), 242-248.

Borsoi, A., Collepardi, S., Coppola, L., Troli, R., and Collepardi, M. (2000). "Sulfate attack on blended Portland cements." *ACI Special Publications*, 192, 417-432.

Brown, M. E., and Gallagher, P. K. (2011). "Handbook of thermal analysis and calorimetry: Recent advances, techniques and applications." *Elsevier*, The Netherlands, v. 5.

Brown, P., Hooton, R. D., and Clark, B. (2004). "Microstructural changes in concretes with sulfate exposure." *Cement and Concrete Composites*, 26(8), 993-999.

Brueckner, R., Williamson, S. J., and Clark, L. A. (2012). "Rate of the thaumasite sulfate attack under laboratory conditions." *Cement and Concrete Composites*, 34(3), 365-369.

BS EN 206-1. (2000). "Concrete–Specification. Performance, production and conformity." *BSI, Gaylard and sons*, London, UK.

Bureau of Reclamation, (1963). "Concrete Manual: A Manual for the Control of Concrete Construction." 7th edition, U.S. Department of the Interior, 12-13.

Cao, H. T., Bucea, L., Ray, A., and Yozghatlian, S. (1997). "The effect of cement composition and pH of environment on sulfate resistance of Portland cements and blended cements." *Cement and Concrete Composites*, 19(2), 161-171.

Cardell, C., Benavente, D., and Rodríguez-Gordillo, J. (2008). "Weathering of limestone building material by mixed sulfate solutions. Characterization of stone microstructure, reaction products and decay forms." *Materials Characterization*, 59(10), 1371-1385.

Charola, A. E. (2000). "Salts in the Deterioration of Porous Materials: An Overview." *Journal of the American Institute for Conservation*, 39 (3), 327-343.

Chatterji, S., and Jensen, A.D. (1989). "Efflorescence and breakdown of building materials." *Nordic Concrete Research*, 8, 56–61.

City of Winnipeg (2013). "Standard Construction Specifications." Manitoba, Canada, 1053p.

Clark, L. A. and Thaumasite Expert Group. (2002). "Thaumasite Expert Group Report: Review after three years of experience." London: Office of the Deputy Prime Minister, 41p.

Clifton, J. R., Frohnsdorff, G., and Ferraris, C. "Standards for evaluating the susceptibility of cement-based materials to external sulfate attack." *American Ceramic Society*, in: J. Skalny, J. Marchand (Eds.), Material Science of Concrete — Sulfate Attack Mechanisms, Westerville, OH, 337-55.

Collepardi, M. (1999). “Thaumasite formation and deterioration in historic buildings.” *Cement and Concrete Composites*, 21(2), 147-154.

Collepardi, M., Ogoumah-Olagot, J.J., Skarp, U., and Troli, R. (2002). “Influence of Amorphous Colloidal Silica on the Properties of Self-Compacting Concretes,” *Proceedings of the International Conference*, Dundee, UK, 473-483.

Collett, G., Crammond, N. J., Swamy, R. N., and Sharp, J. H. (2004). The role of carbon dioxide in the formation of thaumasite. *Cement and Concrete Research*, 34(9), 1599-1612.

Cooke, R. U. (1979). “Laboratory simulation of salt weathering processes in arid environments.” *Earth Surface Processes*, 4(4), 347-359.

Correns, Carl W. (1949). “Growth and dissolution of crystals under linear pressure.” *Discussions of the Faraday Society*, 5, 267-271.

Crammond, N. J. (2003). “The thaumasite sulfate attack in the UK.” *Cement and Concrete Composites*, 25(8), 809-818.

Crammond, N. J., and Halliwell, M. A. (1995). “The thaumasite form of sulfate attack in concretes containing a source of carbonate ions - a microstructural overview.” *ACI Special Publications*, 154, 357-380.

CSA 3000-08 (2010). “Cementitious Materials Compendium” *Canadian Standards Association*, Mississauga, ON, Canada, Update No. 2.

CSA A23.1/A23.2. (2009). “Concrete materials and methods of concrete construction/Methods of test and standard practices for concrete.” *Canadian Standards Association*, Mississauga, ON, Canada.

CSA A3000. (2008). “Cementitious materials compendium.” *Canadian Standards Association*, Toronto, Ontario, CA.

Day, R., and Middendorf, B. (2011). “Sulfate attack and microstructural change of fly-ash mortars made with ordinary- and limestone-cements.” *Proceedings of the thirty-third international conference on cement microscopy*, San Francisco, U.S.A.

Department of the Environment, Transport, and the Regions, London, UK. (1999). "The thaumasite sulfate attack Risks, diagnosis, remedial works and guidance on new construction." report of the Thaumasite Expert Group.

Duran, A., Navarro-Blasco, I., Fernández, J. M., and Alvarez, J. I. (2014). "Long-term mechanical resistance and durability of air lime mortars with large additions of nanosilica." *Construction and Building Materials*, 58, 147-158.

EN, BS. 197-1. (2000). "Cement—Part 1: Composition, specifications and conformity criteria for common cements".

Erlin, B., and Stark, D. C. (1996). "Identification and occurrence of thaumasite in concrete a discussion for the 1965 HRB symposium on aggressive fluids." *Highway Research*, 113, 108-113.

Evans, I.S. (1970). "Salt Crystallization and Rock Weathering: a Review." *International union of geological Sciences*, Committee on geological documentation.

Flatt, R.J. (2002). "Salt damage in porous materials: how high supersaturations are generated." *Journal of Crystal Growth*, 242(3-4), 435-454.

Folliard, K.J., and Sandberg, P. (1994). "Mechanisms of Concrete Deterioration by Sodium Sulfate Crystallization." *American Concrete Institute*, Durability of Concrete, ACI SP-145, 933-945.

Freyburg, E., and Berninger, A. M. (2003). "Field experiences in concrete deterioration by thaumasite formation: possibilities and problems in thaumasite analysis." *Cement and Concrete Composites*, 25(8), 1105-1110.

Garas, V. Y., A. R. Jayapalan, L. F. Kahn, and K. E. Kurtis. (2010). "Micro-and Nanoscale Characterization of Effect of Interfacial Transition Zone on Tensile Creep of Ultra-High-Performance Concrete." In Transportation Research Record: *Journal of the Transportation Research Board*, Transportation Research Board of the National Academies, Washington, D.C., 2141, 82–88.

Gaze, M. E., and Crammond, N. J. (2000). “The formation of thaumasite in a cement:lime:sand mortar exposed to cold magnesium and potassium sulfate solutions.” *Cement and Concrete Composites*, 22(3), 209-222.

González, M. A., and Irassar, E. F. (1998). “Effect of limestone filler on the sulfate resistance of low C_3A portland cement.” *Cement and Concrete Research*, 28(11), 1655-1667.

Hagelia, P., Sibbick, R. G., Crammond, N. J., and Larsen, C. K. (2003). “Thaumasite and secondary calcite in some Norwegian concretes.” *Cement and Concrete Composites*, 25(8), 1131-1140.

Hartshorn, S. A., Sharp, J. H., and Swamy, R. N. (1999). “Thaumasite formation in Portland-limestone cement pastes.” *Cement and Concrete Research*, 29(8), 1331-1340.

Haynes, H., and Bassuoni, M. T. (2011). “Physical Salt Attack on Concrete,” *Concrete international*, 33(11), 38-42.

Haynes, H., O’Neill, R., Neff, M., and Mehta, P.K. (2008). “Salt Weathering Distress on Concrete Exposed to Sodium Sulfate Environment.” *ACI Materials Journal*, 105(1), 35-43.

Haynes, H., O’Neill, R., Neff, M., and Mehta, P.K. (2010). “Salt Weathering of Concrete by Sodium Carbonate and Sodium Chloride.” *ACI Materials Journal*.

Haynes, H.; O'Neill, R.; and Mehta, P. K. (1996). “Concrete deterioration from physical attack by salts.” *Concrete International-Design and Construction*, 18(1), 63-68.

He, X. and Shi, X. (2008). “Chloride permeability and microstructure of Portland cement mortars incorporating nanomaterials.” Transportation Research Record: *Journal of the Transportation Research Board*, 2070, 13-21.

Hewlett, P.C. (Ed.). (1998). Lea's chemistry of cement and concrete: Arnold, UK.

Higgins, D. D., and Crammond, N. J. (2003). “Resistance of concrete containing ggbs to the thaumasite sulfate attack.” *Cement and Concrete Composites*, 25(8), 921-929.

Hill, J., Byars, E. A., Sharp, J. H., Lynsdale, C. J., Cripps, J. C., and Zhou, Q. (2003). "An experimental study of combined acid and sulfate attack of concrete." *Cement and Concrete Composites*, 25(8), 997-1003.

Hobbs, D. W. (2003). "Thaumasite sulfate attack in field and laboratory concretes: implications for specifications." *Cement and Concrete Composites*, 25(8), 1195-1202.

Hobbs, D. W., and Taylor, M. G. (2000). "Nature of the thaumasite sulfate attack mechanism in field concrete." *Cement and Concrete Research*, 30(4), 529-533.

Irassar, E. F. (2009). "Sulfate attack on cementitious materials containing limestone filler — A review." *Cement and Concrete Research*, 39(3), 241-254.

Irassar, E. F., Bonavetti, V. L., and González, M. (2003). "Microstructural study of sulfate attack on ordinary and limestone Portland cements at ambient temperature." *Cement and Concrete Research*, 33(1), 31-41.

Irassar, E. F., Bonavetti, V. L., Trezza, M. A. and González, M. A. (2005). "Thaumasite formation in limestone filler cements exposed to sodium sulphate solution at 20°C" *Cement and Concrete Composites*, 27(1), 77-84.

Irassar, E.F. (2002). "Sulphate attack and sulphate resistant cements", in: S.N. Ghosh (Ed.), Advances in Cement Technology: Chemistry, Manufacture and Testing, Thec Book Int., India, 595–629.

Irassar, E.F., Maio, A. D., and Batic, O.R. (1996). "Sulfate attack on concrete with mineral admixtures." *Cem. Concr. Res*., 26(1), 113-123.

Jallad, K. N., Santhanam, M., and Cohen, M. D. (2003). "Stability and reactivity of thaumasite at different pH levels." *Cement and Concrete Research*, 33(3), 433-437.

Ji, T. (2005). "Preliminary study on the water permeability and microstructure of concrete incorporating nano-SiO2." *Cement and Concrete Research*, 35(10), 1943-1947.

Jo, B.W., Kim, C.H., Tae, G.H., and Park, J.B. (2007). "Characteristics of cement mortar with nano-SiO2 particles." *Construct Build Mater*, 21(6), 1351-1355.

Kurtis, K. E., and Monteiro, P. (1999). “Analysis of Durability of Advanced Cementitious Materials for Rigid Pavement Construction in California: Pavement Research Center.” *Institute of Transportation Studies*, University of California at Berkeley.

Lange, F., Mortel, N., Rudert, V. (1997). “Dense packing of cement pastes and resulting consequences on mortar properties.” *Cem. Concr. Res.*, 27, 1481–1488.

Lee, S. T., Hooton, R. D., Jung, H., Park, D., and Choi, C. S. (2008). “Effect of limestone filler on the deterioration of mortars and pastes exposed to sulfate solutions at ambient temperature.” *Cement and Concrete Research*, 38(1), 68-76.

Lee, S. T., Moon, H. Y., and Swamy, R. N. (2005). “Sulfate attack and role of silica fume in resisting strength loss.” *Cement and Concrete Composites*, 27(1), 65-76.

Lee, S., Lee, D., Kim, D., Jung, H., Park, K., Kim, S., and Lee, C. (2008). “Occurrence of Thaumasite in Lining Concrete of Old-Tunnel Structure.” *Geotechnical Engineering for Disaster Mitigation and Rehabilitation*: Springer, Berlin Heidelberg, In H. Liu, A. Deng and J. Chu (Eds.), 860-865.

Li, H., Xiao, H.g., Yuan, J., and Ou, J. (2004). “Microstructure of cement mortar with nanoparticles.” *Compos B Eng*, 35(2), 185–189.

Li, Z., Wang, H., He, S., Lu, Y., and Wang, M. (2006). “Investigations on the preparation and mechanical properties of the nano-alumina reinforced cement composite.” *Mater Lett*, 60(3), 356–359.

Liu, Z., Schutter, G. D., Deng, D., and Yu, Z. (2012). "Salt Weathering" Distress on Concrete by Sulfates?, *Advances in Crystallization Processes*, Dr. Yitzhak Mastai (Ed.), InTech.

Long, G., Xie, Y., Deng, D., and Li, X. (2011). “Deterioration of concrete in railway tunnel suffering from sulfate attack.” *Journal of Central South University of Technology*, 18(3), 881-888.

Ma, B., Gao, X., Byars, E. A., and Zhou, Q. (2006). “Thaumasite formation in a tunnel of Bapanxia Dam in Western China.” *Cement and Concrete Research*, 36(4), 716-722.

Ma, B., Wang, Y., and Fu, H. (2014). "The effect of limestone type and nanosilica on the durability of limestone cement mortars." *Magazine of Concrete Research*, 66(15), 761-769.

Marchand, J., Odler, I., and Skalny, J.P. (2004). "Sulfate Attack on Concrete" *Taylor and Francis*.

Matthews, J. D. (1994). "Performance of limestone filler cement concrete. Euro Cements: Impact of ENV 197." 113-147.

Mcmillan, F.R., Stantion, T.E., Tyler, I.L., and Hansen., W.C. (1949). "Long-Time Study of Cement Performance in Concrete." *Portland Cement Association*, chapter 5. Concrete exposed of sulfate solis.

Mehta, P. (1992). "Sulfate attack on concrete--a critical review." *Mater. Sci. Concr.*, IIIpp., 105.

Mehta, P. K. (2000). "Sulfate attack on concrete: separating myths from reality." *Concrete International*, 22(8), 171-175.

Mehta, P. K., and Monteiro, J. M. (2013). "Concrete Microstructure Properties and Materials." Publisher: McGraw-Hill Professional; 4th ed., 672p.

Menéndez, E., Matschei, T., and Glasser, F. P. (2013). "Sulfate Attack of Concrete." Performance of Cement-Based Materials in Aggressive Aqueous Environments. Springer Netherlands, 7-74.

Mittermayr, F., Baldermann, A., Kurta, C., Rinder, T., Klammer, D., Leis, A. *et al.* (2013). "Evaporation - a key mechanism for the thaumasite form of sulfate attack." *Cement and Concrete Research*, 49, 55-64.

Montgomery, D. (2013). "Design and Analysis of Experiments." Publisher: John Wiley and Sons, 8th ed., New York, USA, 752p.

Moslemi, A. M., Khosravi, A., Izadinia, M., and Heydari, M. (2014). "Application of Nano Silica in Concrete for Enhanced Resistance against Sulfate Attack." *Advanced Materials Research*, 829, 874-878.

Nazari, A. and S. Riahi (2011). "The effects of ZnO2 nanoparticles on properties of concrete using ground granulated blast furnace Slag as binder." *Materials Research*, 14, 299-306.

Nazari, A., Riahi, S., Riahi, S., Shamekhi, S. F., and Khademno, A. (2010). Influence of Al2O3 nanoparticles on the compressive strength and workability of blended concrete. *Journal of American Science*, 6(5), 6-9.

Nehdi, M. L. and Bassuoni, M. T. (2008). "Durability of self-consolidating concrete to combined effects of sulfate attack and frost action." *Materials and Structures*, RILEM, 41(10), 1657-79.

Neville, A. (2004). "The confused world of sulfate attack on concrete." *Cement and Concrete Research*, 34(8), 1275-1296.

Nobst, P., and Stark, J. (2003). "Investigations on the influence of cement type on thaumasite formation." *Cement and Concrete Composites*, 25(8), 899-906.

Oltulu, Meral, and Remzi Şahin. (2011). "Single and combined effects of nano-SiO2, nano-Al2O3 and nano-Fe2O3 powders on compressive strength and capillary permeability of cement mortar containing silica fume." *Materials Science and Engineering-A-Structural Materials*, 528.22: 7012.

Price, G. C, and Peterson, R. (1968). "Experience with concrete in sulphate environments in Western Canada." *Performance of Concrete*, 93-112.

Ramezanianpour, A. M., and Hooton, R. D. (2012). "Sulfate resistance of Portland-limestone cements in combination with supplementary cementitious materials." *Materials and Structures*, 1-13.

Rasmussen, S. E., Jorgensen, J.E., and Lundtoft, B. (1996). "Structures and Phase Transitions of Na2SO4." *Journal of Applied Crystallography*, 29(1), 42-47.

Rodriguez-Navarro, C., and Doehne, E. (1999). "Salt weathering: influence of evaporation rate, supersaturation and crystallization pattern." *Earth Surface Processes and Landforms*, 24(3), 191-209.

Rodriguez-Navarro, C., Doehne, E., and Sebastian, E. (2000). “How does sodium sulfate crystallize? Implications for the decay and testing of building materials.” *Cement and concrete research*, 30(10), 1527-1534.

Rogers, C., Thomas, M., and Lohse, H. (1997). “Thaumasite from Manitoba and Ontario, Canada.” Paper presented at the *proceedings of the international conference on Cement Microscopy*.

Rollings, R., Rollings, M., Poole, T., Wong, G., and Gutierrez, G. (2006). “Investigation of Heaving at Holloman Air Force Base, New Mexico.” *Journal of Performance of Constructed Facilities*, 20(1), 54-63.

Romer, M., Holzer, L., and Pfiffner, M. (2003). “Swiss tunnel structures: concrete damage by formation of thaumasite.” *Cement and Concrete Composites*, 25(8), 1111-1117.

Safiuddin, M., Gonzalez, M., Cao, J., Tighe, S. L., Safiuddin, M., Gonzalez, M. *et al.* (2014). "State-of-the-art report on use of nano-materials in concrete." *International Journal of Pavement Engineering* 1-10.

Sahmaran, M., Erdem, T. K., and Yaman, I. O. (2007). “Sulfate resistance of plain and blended cements exposed to wetting–drying and heating–cooling environments.” *Construction and Building Materials*, 21(8), 1771-1778.

Said, A.M., Zeidan, M.S., Bassuoni, M.T., and Tian, Y. (2012). “Properties of concrete incorporating nano-silica.” *Construction and Building Materials*, 36, 838-844.

Sanchez, F. and Sobolev, K. (2010). “Nanotechnology in Concrete – a Review.” *Construction and Building Materials*, 24(11), 2060-2071.

Santhanam, M., Cohen, M. D., and Olek, J. (2003). “Effects of gypsum formation on the performance of cement mortars during external sulfate attack.” *Cement and Concrete Research*, 33(3), 325-332.

Scherer, G. W. (2004a). “Stress from crystallization of salt.” *Cement and Concrete Research*, 34(9), 1613-1624.

Scherer, G. W. (2004b). “Factors affecting crystallization pressure,” In K. S. a. J. Skalny (Ed.), International RILEM Workshop on Internal Sulfate Attack and Delayed Ettringite Formation, *RILEM Publications SARL*, Paris, pp. 139-54.

Schmidt, T. (2007). “Sulfate attack and the role of internal carbonate on the formation of thaumasite.” PhD thesis, EPFL, Lausanne, Switzerland.

Schmidt, T., Lothenbach, B., Romer, M., Scrivener, K., Rentsch, D., and Figi, R. (2008). “A thermodynamic and experimental study of the conditions of thaumasite formation.” *Cement and Concrete Research*, 38(3), 337-349.

Shekari A.H., Razzaghi M.S. (2011). “Influence of nanoparticles on durability and mechanical properties of high performance concrete.” *Procedia Eng*, 14, 3036–3041.

Sims, I., and Huntley, S. A. (2004). “The thaumasite sulfate attack-breaking the rules.” *Cement and Concrete Composites*, 26(7), 837-844.

Skalny, J., Marchand, J., and Odler, I. (2002). “Sulfate Attack on Concrete.” *Spon Press*, UK, 217p.

Skaropoulou, A., Kakali, G., and Tsivilis, S. (2012). “Thaumasite sulfate attack in limestone cement concrete: The effect of cement composition, sand type and exposure temperature.” *Construction and Building Materials*, 36(0), 527-533.

Slater, D., Floyd, M., and Wimpenny, D. E. (2003). “A summary of the Highways Agency Thaumasite Investigation in Gloucestershire: the scope of work and main findings.” *Cement and Concrete Composites*, 25(8), 1067-1076.

Smith, B.J. (1994). “Weathering processes and forms.” In: A.D. Abrahams and A.J. Parsons (Eds.), Geomorphology of Desert Environments, Routledge Chapman and Hall, London, 39-63.

Sonebi, M., Bassuoni, M., Kwasny, J., and Amanuddin, A. (2014). "Effect of Nanosilica on Rheology, Fresh Properties, and Strength of Cement-Based Grouts." *J. Mater. Civ. Eng.*

Stark, D. C. (2002). “Performance of Concrete in Sulfate Environments.” *Portland Cement Association*, Skokie, Illinois, USA, 28p.

Taylor, H. F. W. (1997). “Cement Chemistry.” Second Edition: Inst of Civil Engineers Pub.

Thomas, M. D. A., Rogers, C. A., and Bleszynski, R. F. (2003). “Occurrences of thaumasite in laboratory and field concrete.” *Cement and Concrete Composites*, 25(8), 1045-1050.

Tian, B., and Cohen, M. D. (2000). “Does gypsum formation during sulfate attack on concrete lead to expansion?” *Cement and Concrete Research*, 30(1), 117-123.

Torres, S. M., Lynsdale, C. J., Swamy, R. N., and Sharp, J. H. (2006). “Microstructure of 5-year-old mortars containing limestone filler damaged by thaumasite.” *Cement and Concrete Research*, 36(2), 384-394.

Tosun-Felekoğlu, K. (2012). “The effect of C3A content on sulfate durability of Portland limestone cement mortars.” *Construction and Building Materials*, 36, 437-47.

Tsivilis, S., Kakali, G., Skaropoulou, A., Sharp, J. H., and Swamy, R. N. (2003). “Use of mineral admixtures to prevent thaumasite formation in limestone cement mortar.” Cement and Concrete Composites, 25(8), 969-976.

Tsivilis, S., Sotiriadis, K., and Skaropoulou, A. (2007). “Thaumasite sulfate attack (TSA) in limestone cement pastes.” *Journal of the European Ceramic Society*, 27(2), 1711-1714.

Yamada, K., Ichikawa, M., Honma, K., Hirao, H., and Mori, D. (2006). “Possibility of thaumasite formation in marine environments.” *ACI Spec. Publ.*, 234, 507-520.

Zeidan, M. S. (2013). “Performance of concrete incorporating colloidal nano-silica.” PhD thesis, University of Nevada, Las Vegas.

Zhang, Q., Wang, J., and Cheng, S. (2002). “Study on the CPE/Nano SiO2 blends.” *J. Funct. Polym.* 15(3), 271–275.

Zhang, Z., Olek, J., and Diamond, S. (2002). "Studies on delayed ettringite formation in early-age, heat-cured mortars: I. Expansion measurements, changes in dynamic modulus of elasticity, and weight gains." *Cement and Concrete Research*, 32(11), 1729-1736.

Zhou, Q., Hill, J., Byars, E. A., Cripps, J. C., Lynsdale, C. J., and Sharp, J. H. (2006). “The role of pH in thaumasite sulfate attack.” *Cement and concrete research*, 36(1), 160-170.

Appendix A: Physical Salt Attack

Table A.1: ANOVA test results

Source			F	P-Value	F_{cr}	Effect*
	Mixture type	NS dosages (%)				
Fly ash with NS	F	0	6.752	0.029	5.14	Significant
	FS3	3				
	FS6	6				
W/C	0.4 and 0.5		71.367	0.000	5.99	Significant
Interaction	Mixtures and W/C		4.423	0.066	5.14	Insignificant
	Mixture type	NA dosages (%)				
Fly ash with NA	F	0	3.307	0.108	5.14	Insignificant
	FA3	3				
	FA6	6				
W/C	0.4 and 0.5		110.203	0.000	5.99	Significant
Interaction	Mixtures and W/C		0.361	0.711	5.14	Insignificant
	Mixture type	Fly ash dosages (%)				
GU and F	GU	0	5.717	0.075	7.71	Insignificant
	F	30				
W/C	0.4 and 0.5		21.749	0.010	7.71	Significant
Interaction	Mixtures and W/C		3.595	0.131	7.71	Insignificant
	Mixture type	NS dosages (%)				
GU and GUS3	GU	0	0.018	0.899	7.71	Insignificant
	GUS3	3				
W/C	0.4 and 0.5		11.748	0.027	7.71	Significant
Interaction	Mixtures and W/C		0.846	0.410	7.71	Insignificant
	Mixture type	NS dosages (%)	NA dosages (%)			
Fly ash with nano particles	F	0	0	7.418	0.005	3.48	Significant
	FS3	3	-			
	FS6	6	-			
	FA3	-	3			
	FA6	-	6			
W/C	0.4 and 0.5			143.708	0.000	4.97	Significant
Interaction	Mixtures and W/C			2.711	0.092	3.48	Insignificant
	Mixture type	Fly ash dosages (%)	NS dosages (%)			
NS	GUS3	0	3	4.618	0.037	4.07	Significant
	F	30	0			
	FS3	30	3			
	FS6	30	6			
W/C	0.4 and 0.5			74.572	0.000	5.32	Significant
Interaction	Mixtures and W/C			2.338	0.150	4.07	Insignificant

** If P-Value < 0.05 and F > F_{cr}; the mass loss result is statistically significant or else insignificant.*

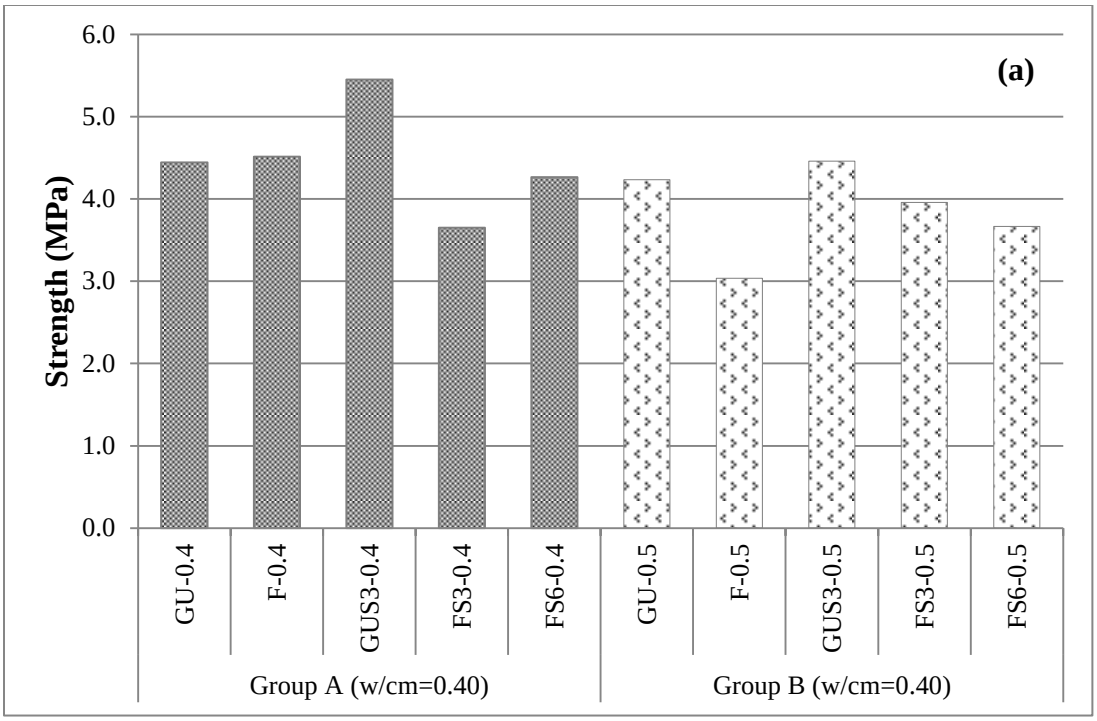

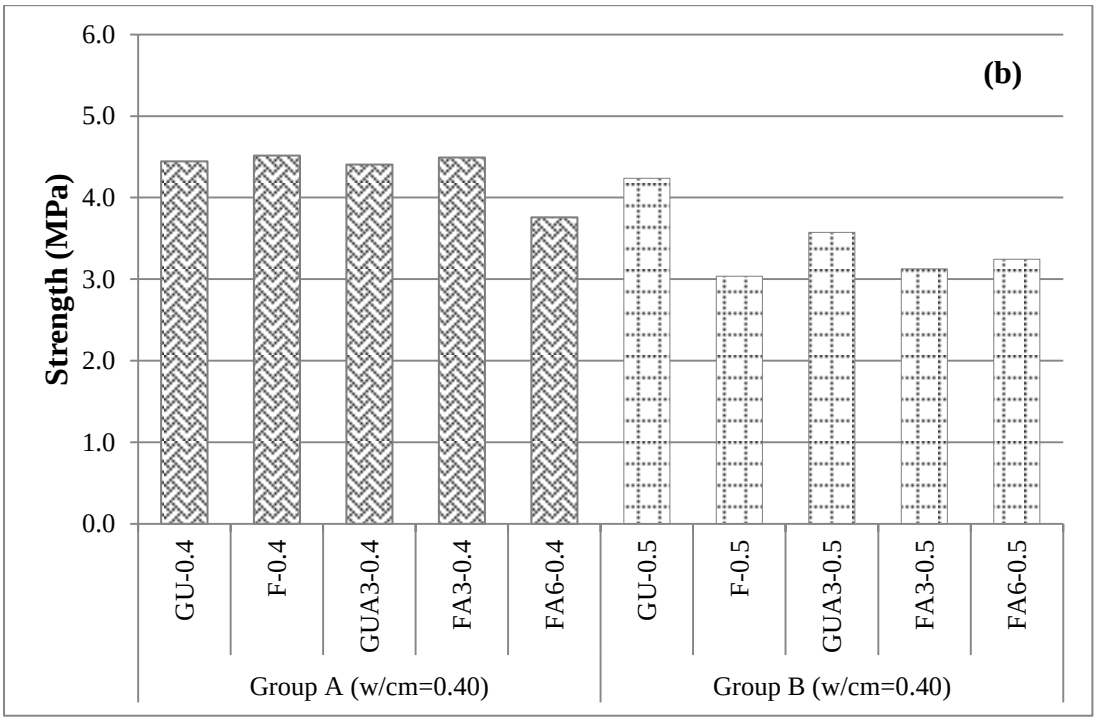

Figure A.1: Splitting tensile strength of concrete cylinders at 28 days: (a) NS and (b) NA.

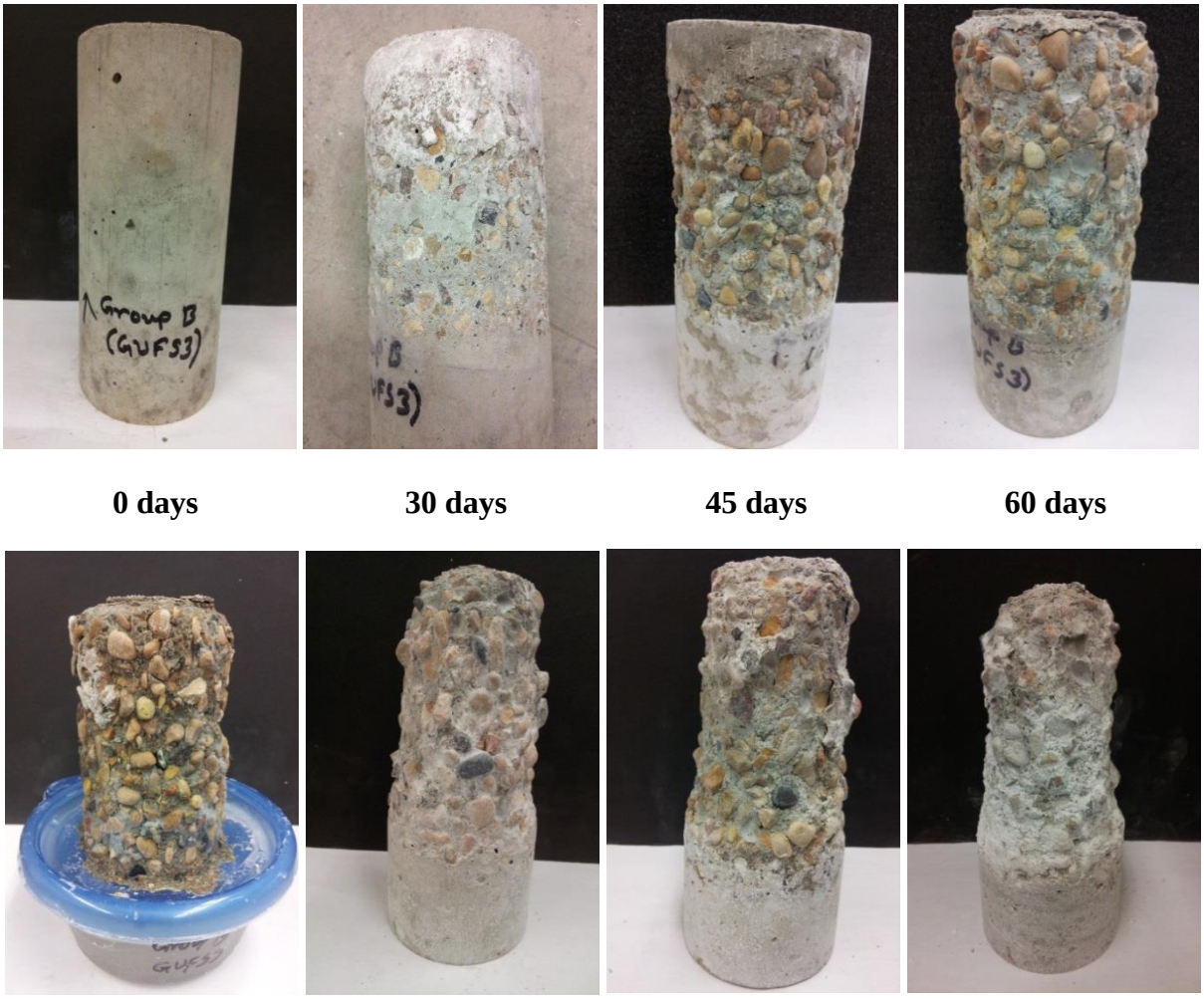

Figure A.2: Progressive degradation of s FS3-0.5 specimen (75×150 mm) at different time interval of exposure.

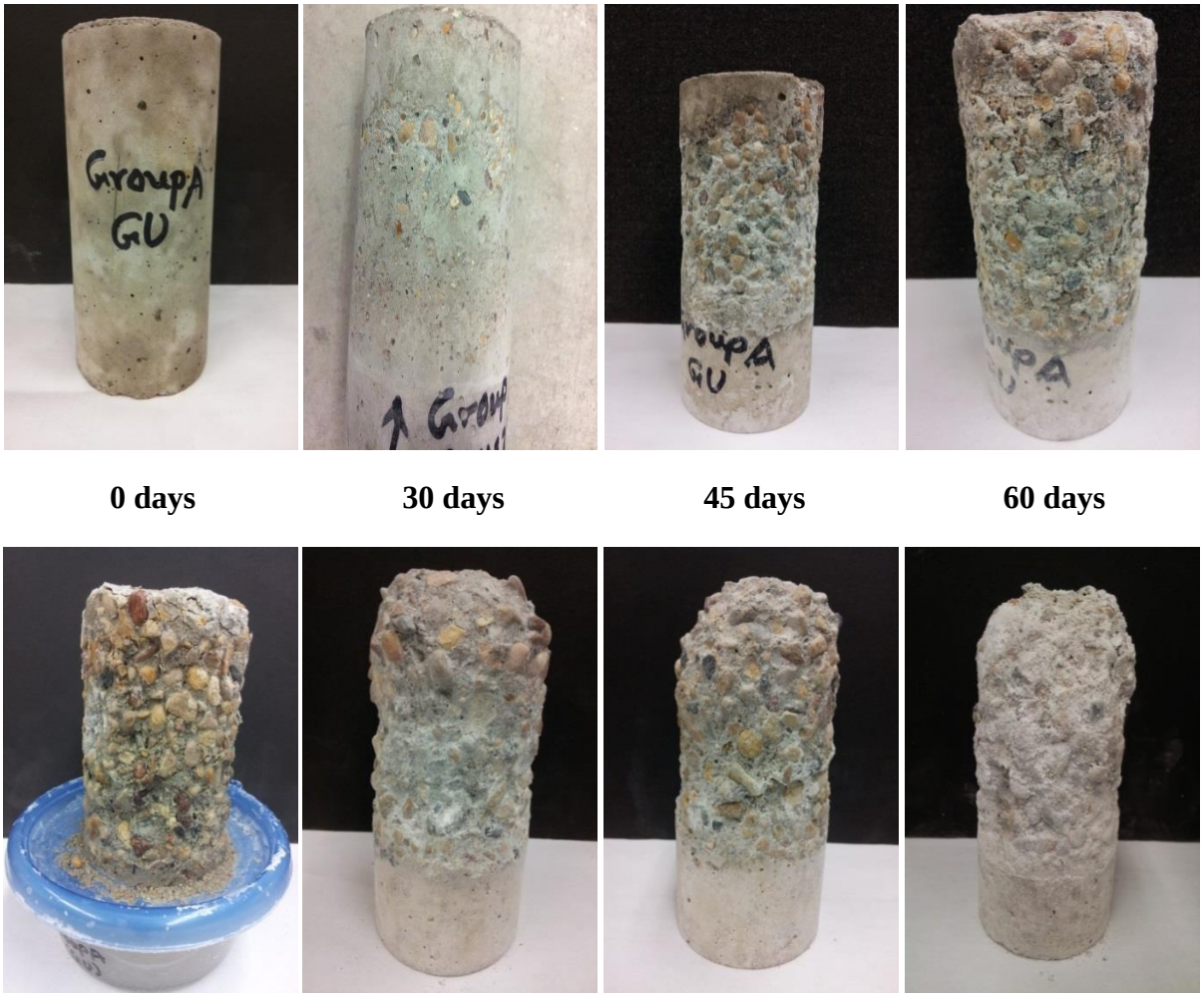

Figure A.3: Progressive degradation of a GU-0.4 specimen (75×150 mm) at different time interval of exposure.

Relative Dynamic Modulus of Elasticity (RE_d**)**

According to ASTM C597, the UPV test was performed on the concrete specimens exposed to PSA environment. For sixteen mixtures, the initial reading of dynamic modulus of elasticity (DME) was measured at the end of curing and before the exposure (at 28 days). Throughout the study, the DME was determined in every 15 days for all the mixtures starting from one month of exposure. Irrespective of the group (w/cm of 0.4 and 0.5) and mixture design, almost all the specimens showed increase of DME after one month of exposure as shown in Figure A.4 and A.5. The variation of RE_d appears from figures can be attributed to the different level of salt growth during the exposure. Although some of specimens were lost significant amount of mass nonetheless there was no sudden drop or increase of RE_d. This might be an indication that the core of the concrete cylinders was intact and sound even though the surface was suffering because of salt crystallization distress. However, constant rapid drop of RE_d was observed as presented in figures starting from 90 days up to the end of the test for all the specimens prepared from both w/cm of 0.4 and 0.5. This is an indication that rapid growth of salt crystallization created enormous pressure inside the capillary pores. Hence, concrete lost its integrity which led to the development of micro-cracks inside the matrix. A relationship of cumulative mass loss and RE_d at 120 days was developed but the mixtures with w/cm of 0.4 and 0.5 were not satisfactorily correlated with each other at high coefficient of determination. Therefore, it can be concluded that the RE_d test is not applicable for short term exposure to evaluate the mechanisms of PSA on concrete.

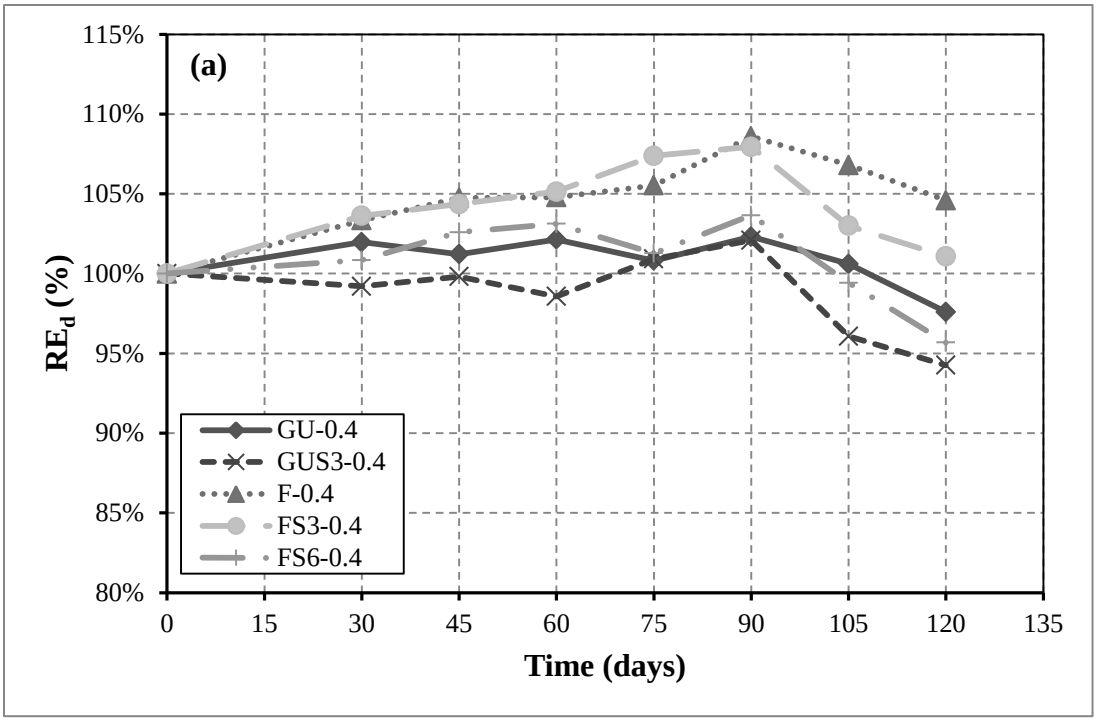

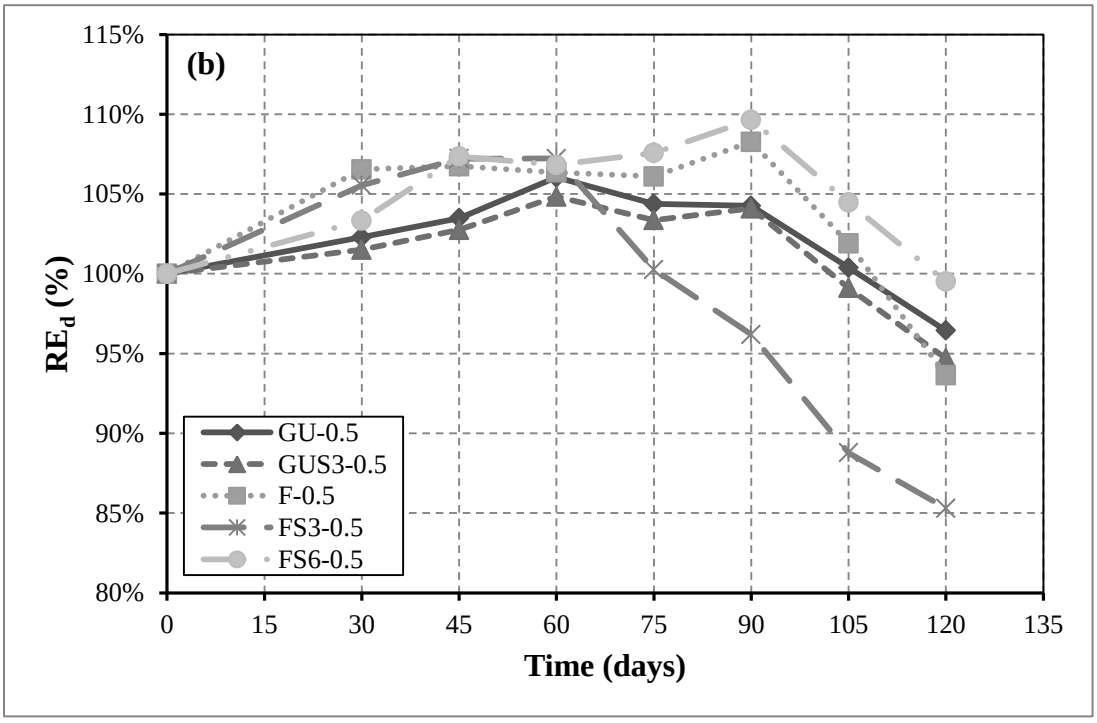

Figure A.4: RE_d of concrete for mixtures with NS: (a) w/cm = 0.40 and (b) w/cm = 0.50.

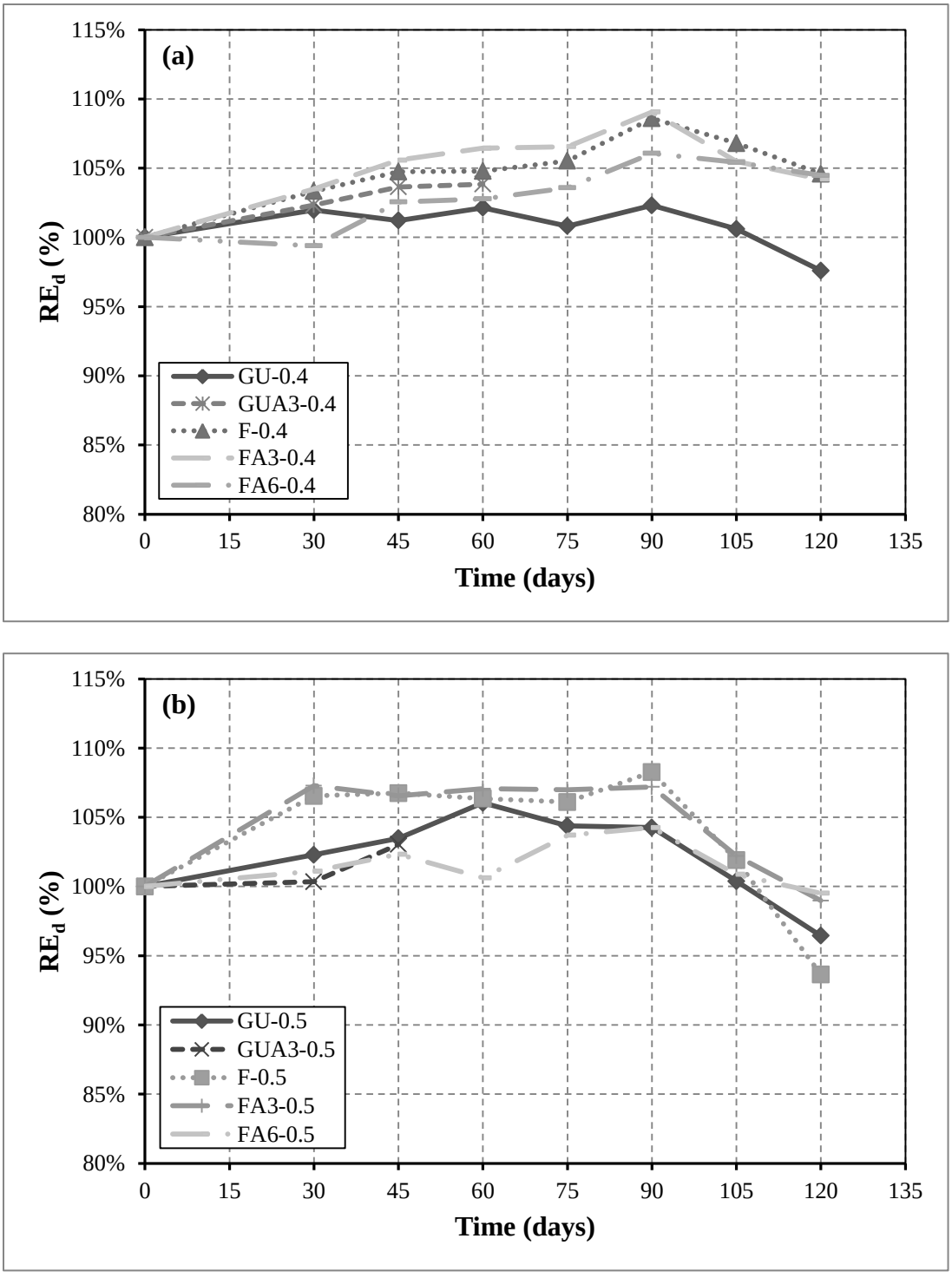

Figure A.5: RE_d of concrete for mixtures with NA: (a) w/cm = 0.40 and (b) w/cm = 0.50.

Absorption

The rate of absorption of concrete mixtures between 1-8 days was determined and plotted in graphs according to ASTM C1585 as shown in Figure A.6 and A.7. The initial sorptivity was calculated from the graphs as the slope of all the points from 1 min to 6 hours and the secondary sorptivity was determined as the slope of the best fit line in between 1 to 8 days of test. The initial and secondary rate of absorptions was listed in table A.2. According to the standard, the correlation coefficients must be equal to or higher than 0.98 to consider the initial and secondary rate of absorptions. However, only the initial rate of absorptions met that coefficients of correlation limit. The initial absorption rates followed certain trend according to the mixture design and addition of nanoparticles. The results complied with the RCPT test results at 28 days; for instance, incorporation of NS in mixtures significantly reduced both chloride penetration depth and initial rate of absorption. The initial rate of absorption was increased as the increase of w/cm (0.4 to 0.5) that indicates the increase of porosity in the cementitious matrix. On the contrary, the secondary rate of absorptions was almost identical for all the mixtures except a few with NA.

The total absorption for the mixtures prepared with w/cm of 0.4 and 0.5 was in the range of 6-7 mm and 7-8 mm, respectively with higher rates of absorption (up to 2 days) for the mixtures with w/cm of 0.5. This conforms to the results of visual assessment and mass loss as the mixtures prepared with w/cm of 0.5 showed more deterioration compared to corresponding mixtures with w/cm of 0.4 due to the higher rate of drying/evaporation and solution uptake.

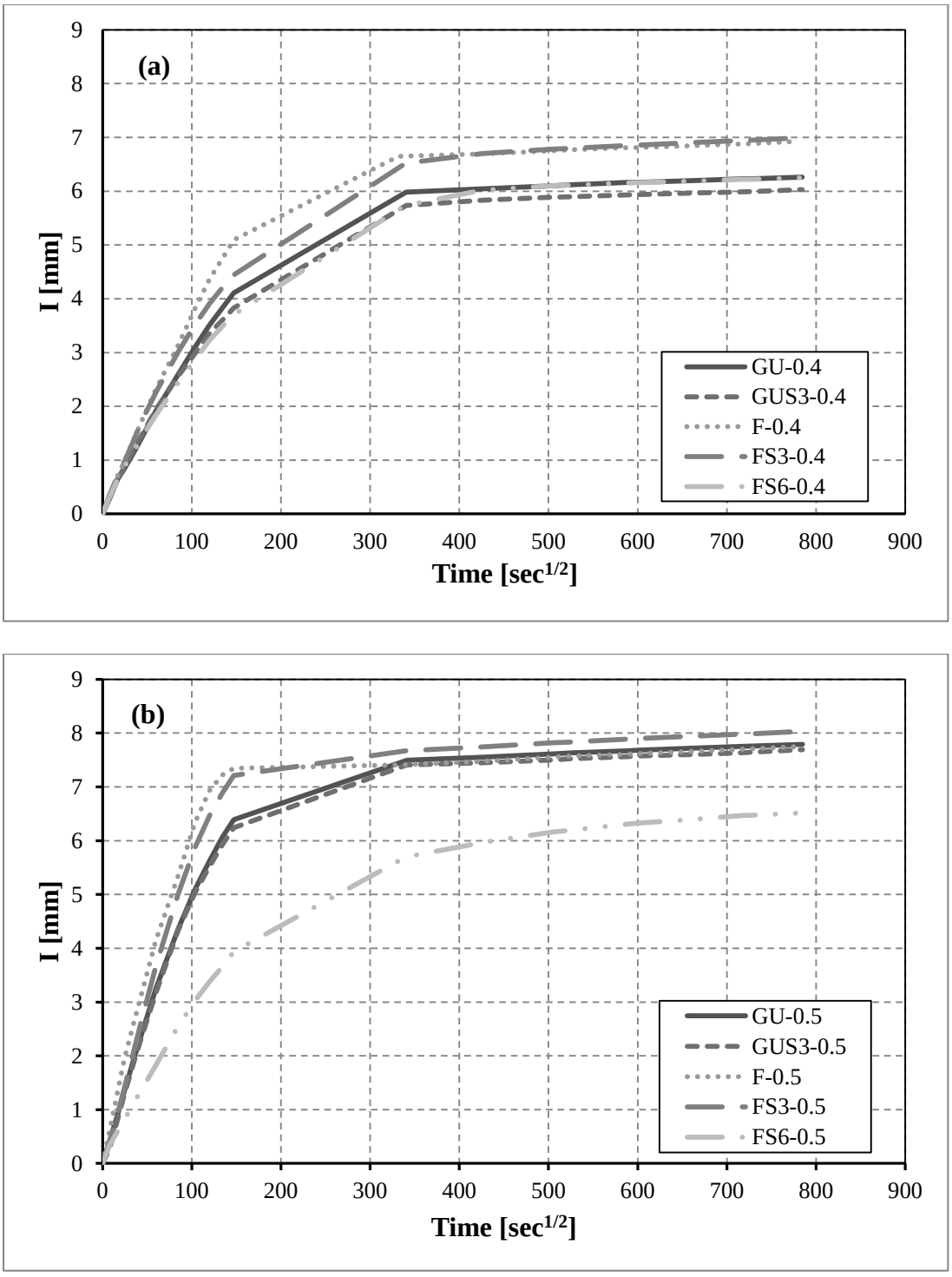

Figure A.6: Rate of absorption of water for mixtures with NS: (a) w/cm = 0.40 and (b) w/cm = 0.50.

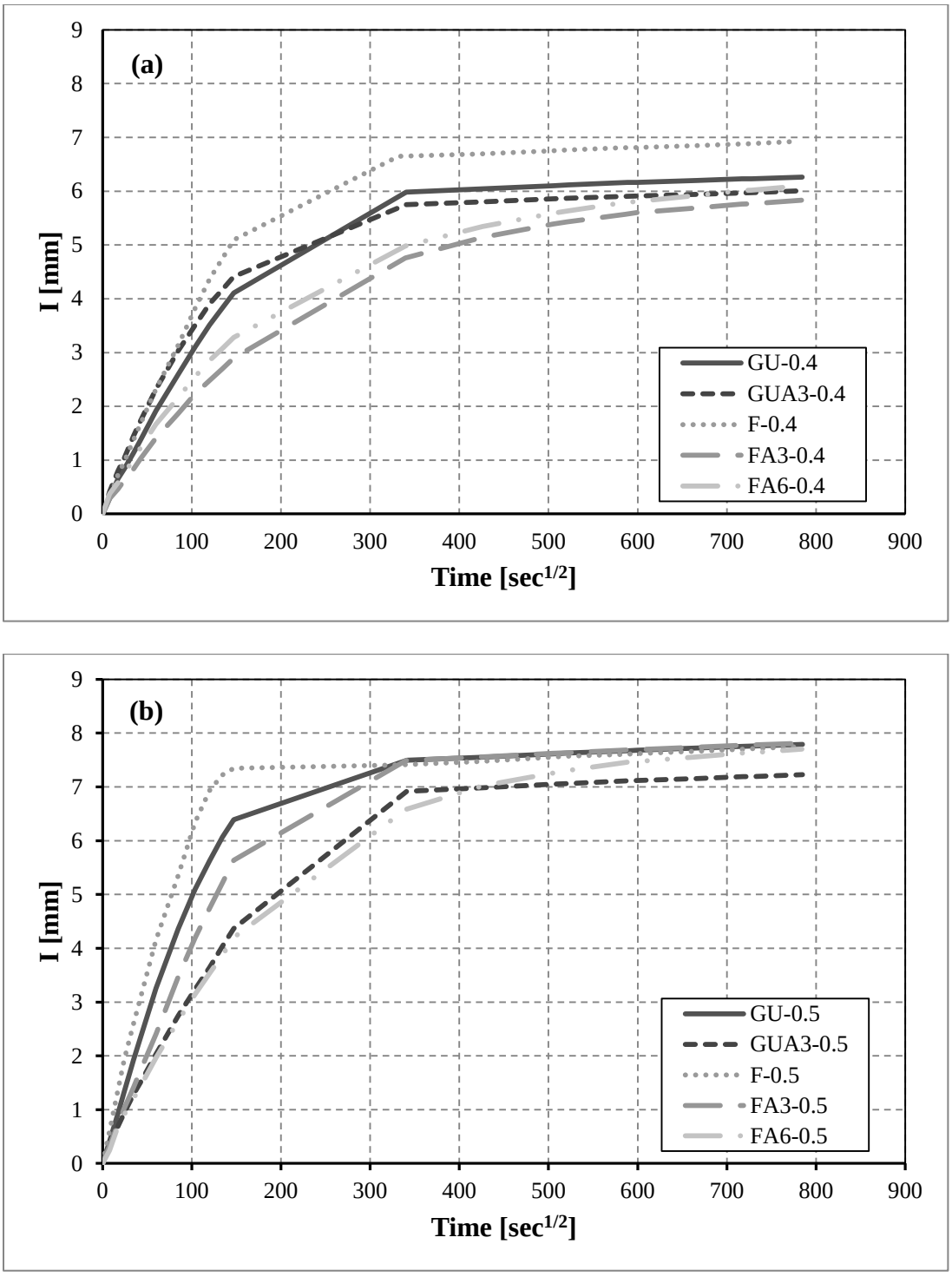

Figure A.7: Rate of absorption of water for mixtures with NA: (a) w/cm = 0.40 and (b) w/cm = 0.50.

Table A.2: Rate of water absorption test results at 28 days

Mixture Types	Initial rate of absorption (mm/√s)	Correlation coefficient (R^2)	Secondary rate of absorption (mm/√sec)	Correlation coefficient (R^2)
w/cm = 0.4				
GU-0.4	0.0279	0.9969	0.0006	0.9913
F-0.4	0.0349	0.9977	0.0006	0.9968
GUS3-0.4	0.0258	0.991	0.0006	0.9668
GUA3-0.4	0.0297	0.9871	0.0006	0.9939
FS3-0.4	0.0304	0.99	0.001	0.9478
FS6-0.4	0.0249	0.9921	0.001	0.8144
FA3-0.4	0.0195	0.9947	0.0023	0.9284
FA6-0.4	0.0218	0.9918	0.0024	0.9538
w/cm = 0.5				
GU-0.5	0.0443	0.9894	0.0007	0.9971
F-0.5	0.0513	0.9752	0.0008	0.9959
GUS3-0.5	0.0439	0.987	0.0006	0.9972
GUA3-0.5	0.029	0.9966	0.0007	0.9924
FS3-0.5	0.0511	0.9876	0.0008	0.9965
FS6-0.5	0.0267	0.9958	0.0018	0.9432
FA3-0.5	0.0387	0.9989	0.0007	0.9951
FA6-0.5	0.0282	0.9957	0.0023	0.9125

At a w/cm of 0.4, the results show that the total absorption of the mixture incorporating 30% fly ash without nanoparticles (F-0.4) was marginally higher than that of other mixtures. However, this mixture had lower mass loss at the end of PSA exposure (120 days after 28 days of curing). This can be ascribed to the slow pozzolanic activity of fly ash which typically leads to a coarser pore structure at 28 days (age of absorption test). However, the incorporation of NA reduced the rate of absorption (Figure A.7a) for mixtures with single and blended binders likely due its physical filler effect on refining the pore structure. This trend was also notable in Figure A.7b during the initial absorption period, but diminished in the secondary absorption period. The total absorption and visual distress results had some agreement as the NA addition at different

dosages reduced the total absorption and visual distress, especially for mixtures prepared with blended binders and w/cm of 0.4. For all mixtures with w/cm of 0.5, the trends of total absorption at 28 days and visual rating after 60 days of exposure were comparable, irrespective of the binder type and NA addition. However, it appears that there is no clear trend between the total absorption values and mass loss results at the end of the accelerated test. The addition of NS at 3% with fly ash was insignificant in terms of total absorption corresponding to the other mixtures. At higher dosage of NS, however, the total absorption was reduced due to the filler effect of nanoparticles that produced disconnected pore system inside the cementitious matrix which led to higher distress and mass loss.

The exposure cycle of PSA can be split into multiple processes as mentioned in Chapter 2. Water penetrates into concrete by capillary absorption (wicking), and it is subsequently drawn out from the evaporation front by water vapor diffusion. Repetitive wetting and drying also promotes salt crystallization and growth, in addition to the continual hydration of the matrix, particularly in the case of blended binders with fly ash. All these processes induce synergistic effects that progressively alter the pore structure of the matrix. Although in the ASTM C1585 test method water enters into concrete by capillary absorption, but it does not evaporate in the same way as in PSA exposure because of the vapor barrier on top and sides of concrete discs. Also, there is no replication of the aforementioned processes and their synergistic effects on the pore structure. While there was some agreement between the visual assessment and absorption, no definite trend was obtained between the mass loss at the end of exposure and total absorption at 28 days. Therefore, further studies are needed to assess the relationship between the characteristics of pore structure (e.g. pore size distribution, total porosity and pore connectivity) and mass loss results, which was shown in Chapter 4.

Appendix B: Conventional Sulfate Attack

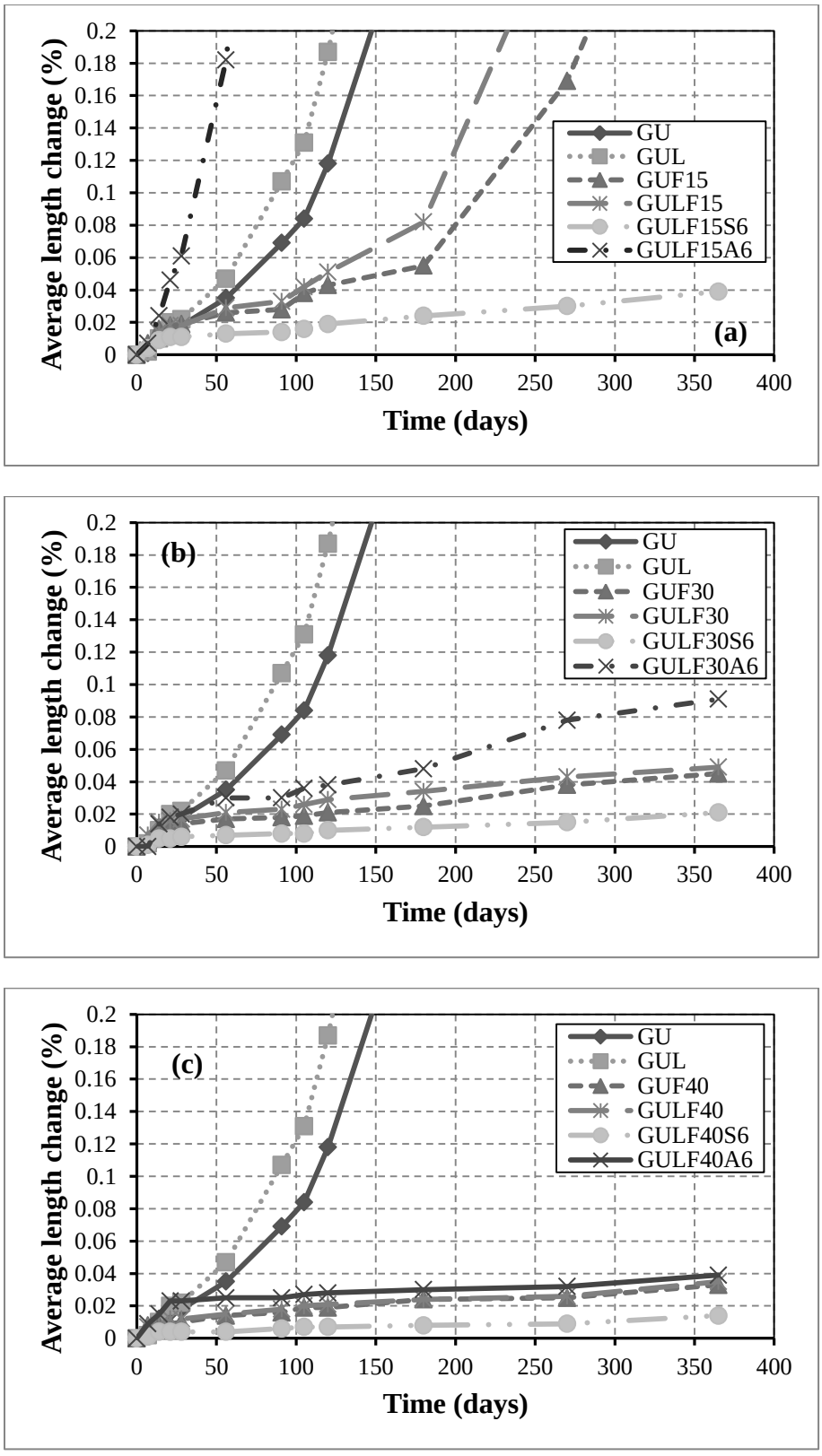

Figure B.1: Expansion of mortar prisms exposed to sodium sulfate solution at 23°C: (a) group A, (b) group B, and (c) group C mixtures.

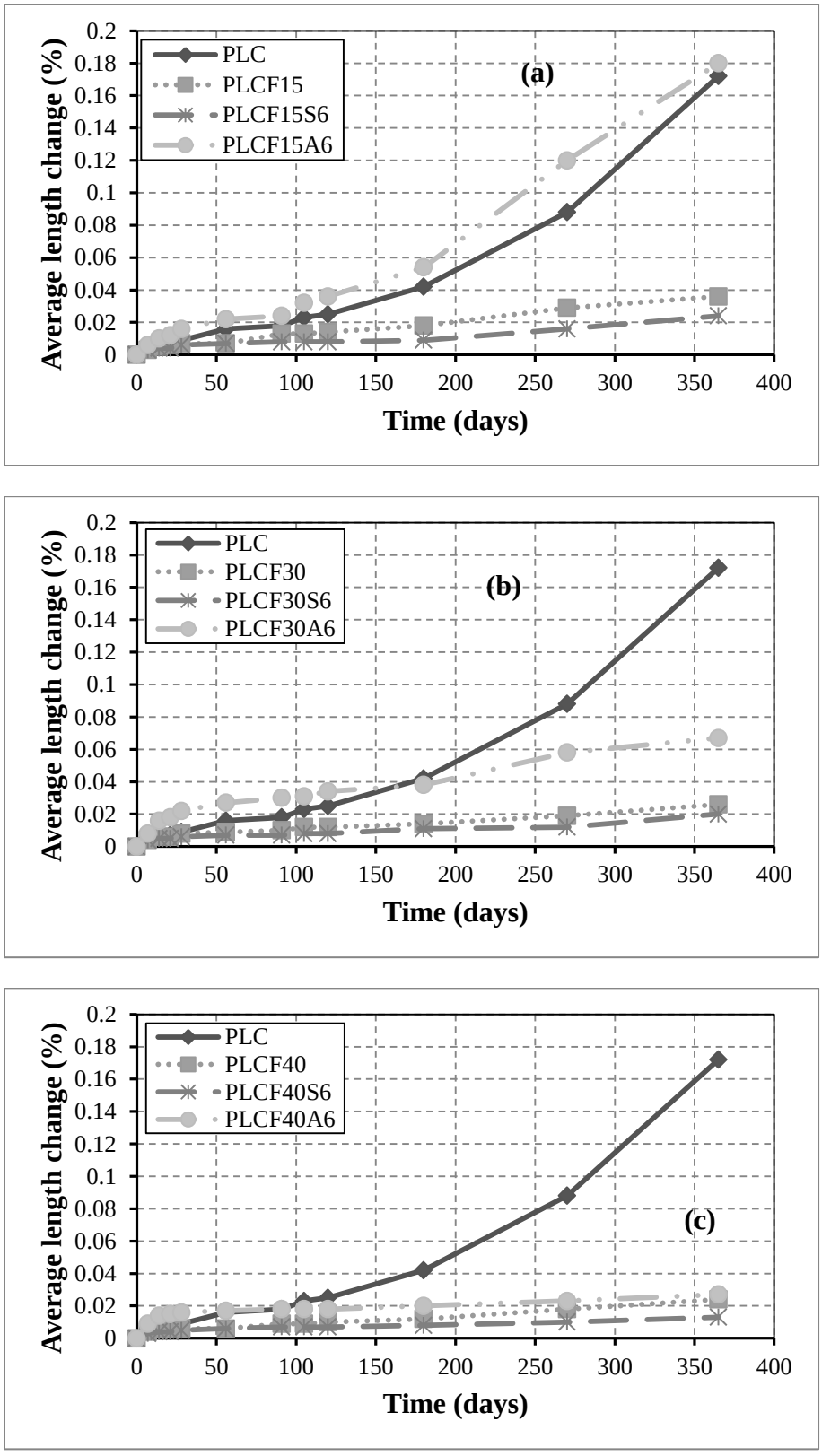

Figure B.2: Expansion of mortar prisms exposed to sodium sulfate solution at 23°C: (a) group D, (b) group E, and (c) group F mixtures.

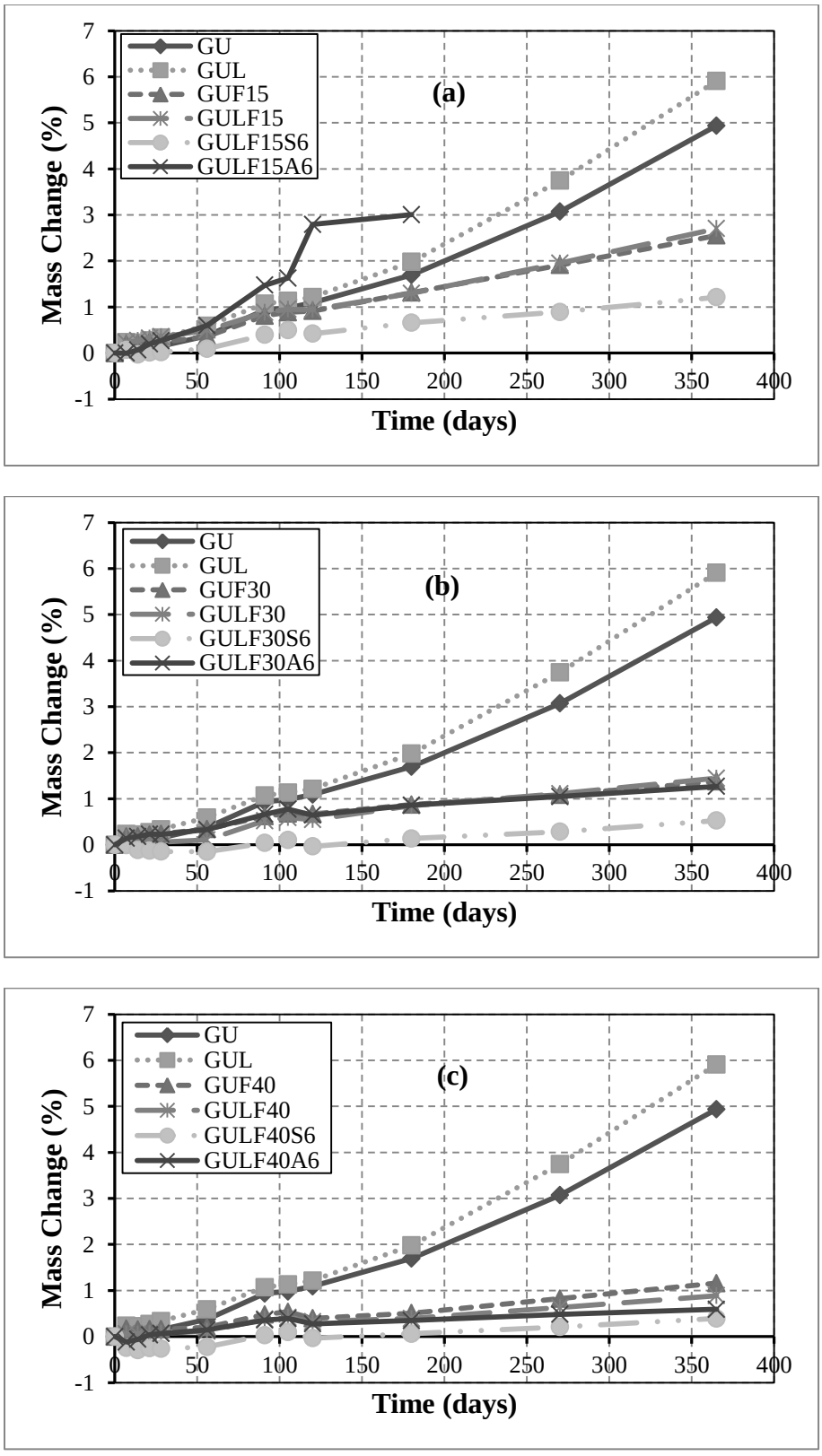

Figure B.3: Change of mass of GU/GUL specimens vs. the time of exposure: (a) group A (b) group B and (b) group C.

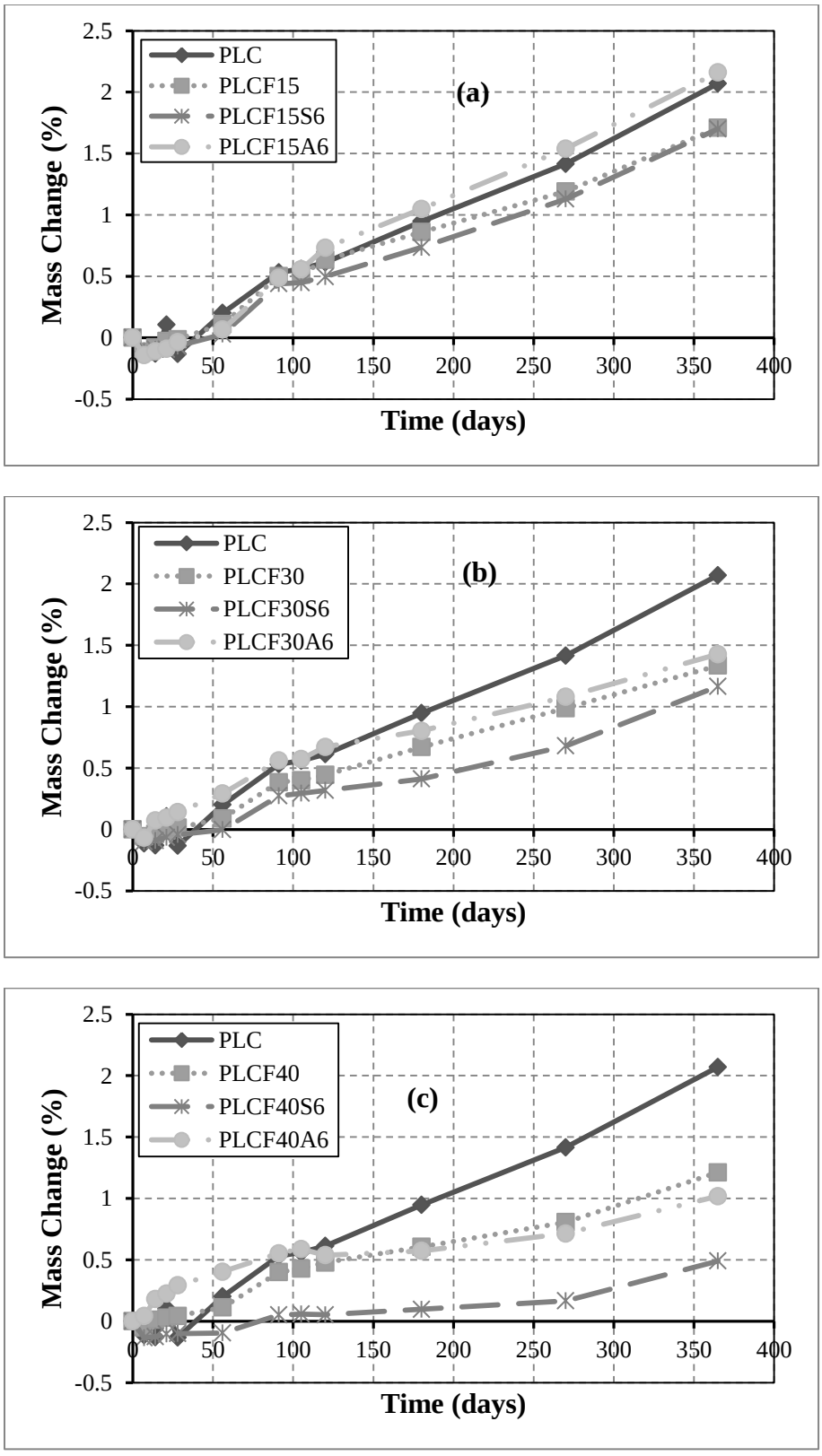

Figure B.4: Change of mass of some PLC specimens vs. the time of exposure: (a) group A (b) group B and (b) group C.

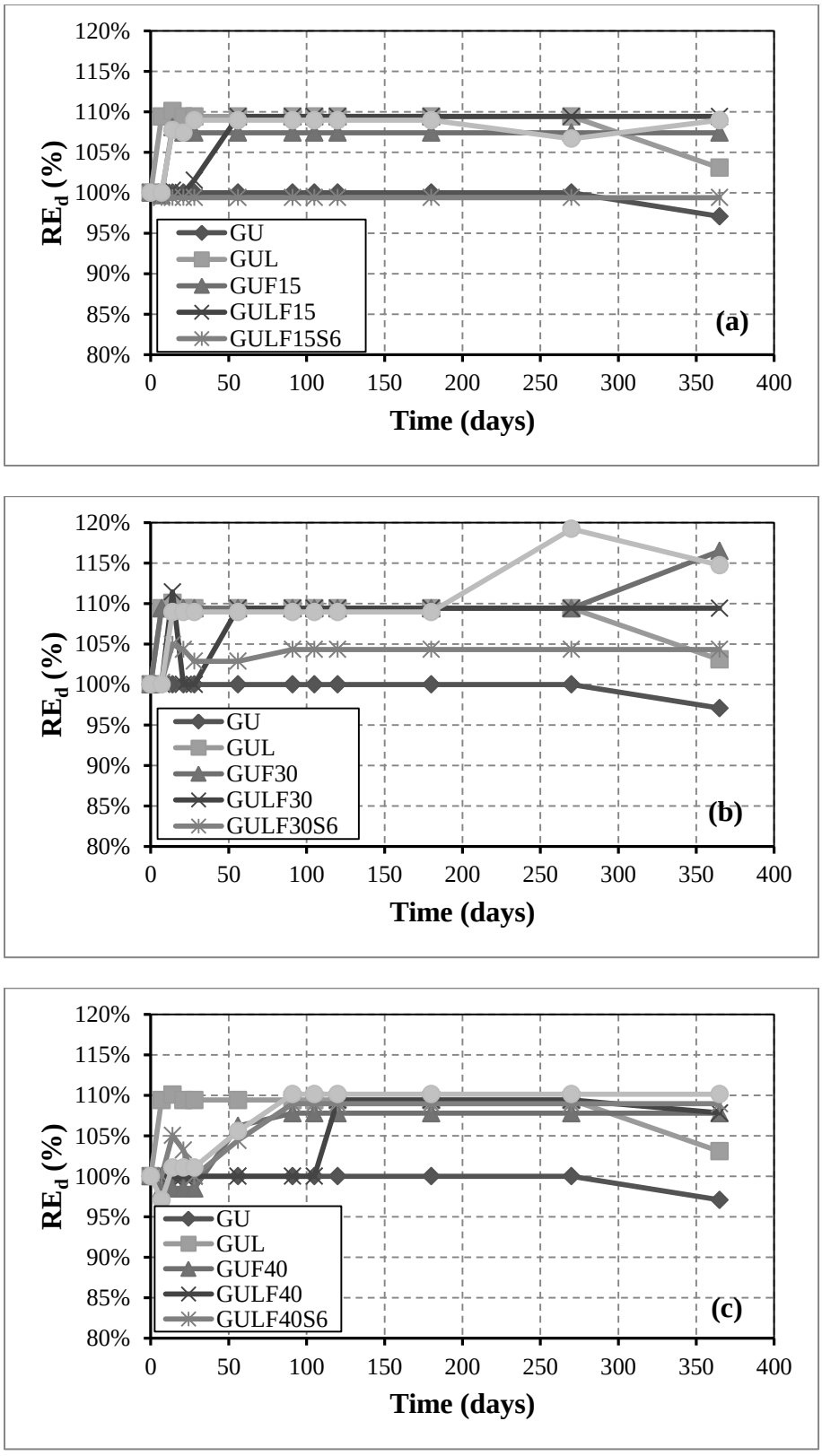

Figure B.5: Relative dynamic modulus of elasticity of GU/GUL mortar cubes vs. the time of exposure: (a) group A (b) group B and (b) group C.

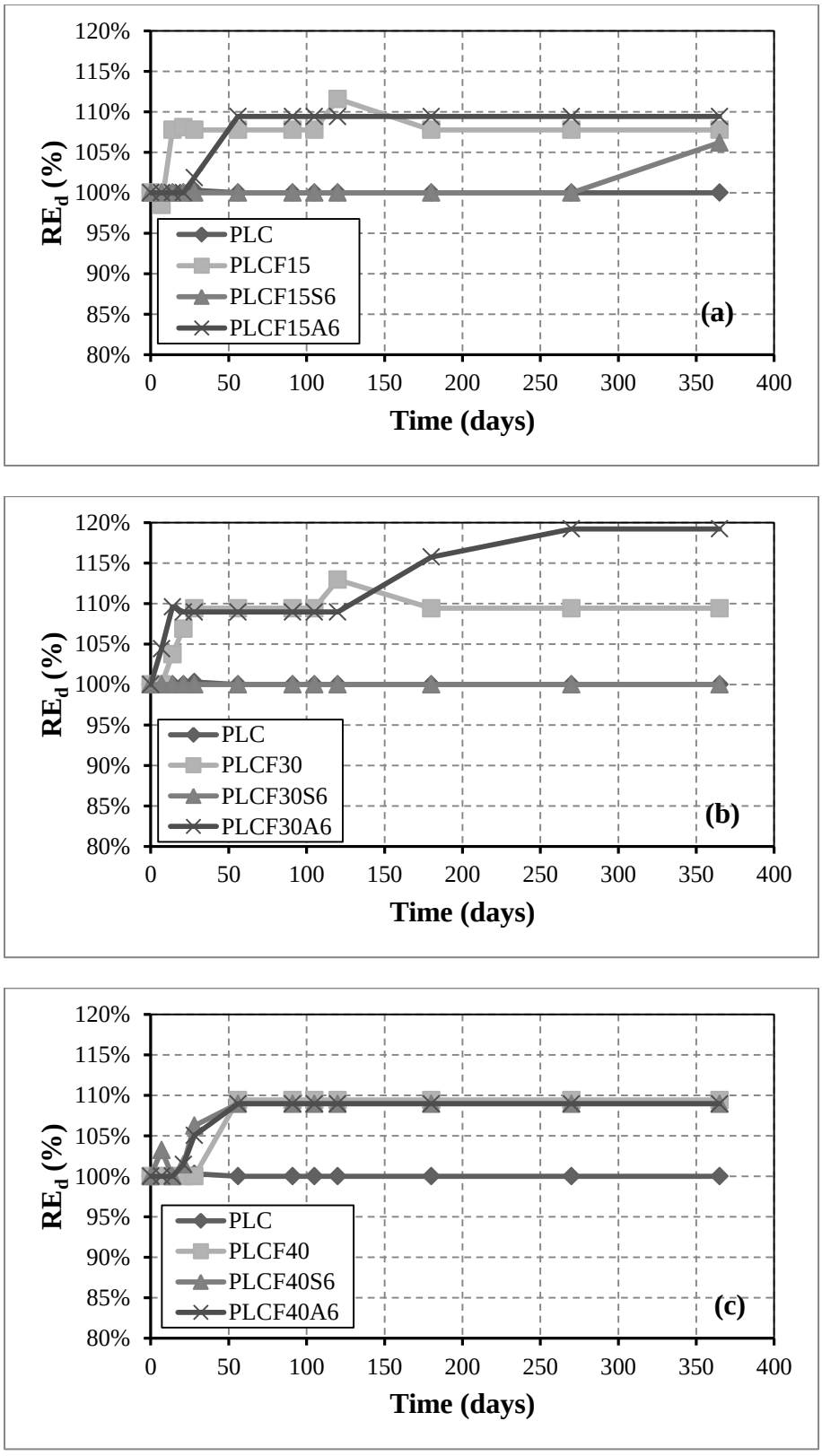

Figure B.6: Relative dynamic modulus of elasticity of PLC mortar cubes vs. the time of exposure: (a) group A (b) group B and (b) group C.

Appendix C: Thaumasite Sulfate Attack

Table C.1: Filed case studies on TSA of concrete

Source	Location	Type of structure	Nature of Deterioration	Possible causes of TSA
Crammond and Halliwell (1995)	UK	Concrete piles	Profusion of thaumasite in 300 mm concrete piles.	Oolitic limestone gravel aggregate and sulfate-bearing groundwater.
Rogers *et al.* (1997) and Thomas *et al.* (2003)	Winnipeg, Manitoba, Canada	Water supply aqueduct	Sinuous cracks along the length of the aqueduct and the width of cracks varied from 20 to 120 μm.	Adjacent ground water, sulfate in concrete, limestone aggregate, and subsoil containing high sulfate content.
Bickley (1999)	Arctic , Canada	RC column foundations and slabs-on-grade	Severe deterioration within two years of construction.	Freeze-thaw action (or low temperature), carbonate aggregates and high sulfate concentration in soil.
Clark (2002)	UK	Internal rendered walls	TSA occurred at or near the joint of underlying brickwork and on the back of renders.	Contamination of render walls with gypsum plaster and dampness.
Clark (2002)	Bristol, UK	Deterioration in floor slabs	Expansion, softening, cracking and uplift of the concrete slab.	Carbonate aggregate and demolition rubble (source of the sulfate).
Clark (2002)	South Wales, UK	Harbour wall steps	Cracking and spalling.	Sulfates from seawater.
Clark (2002)	South Wales, UK	Drainage adit	Softening, expansion and discolouration.	Use of bituminous limestone as coarse and fine aggregates and groundwater was the source of sulfates.
Slater *et al.* (2003)	Gloucestershire, UK	Road overbridges, underbridges, footbridges, underpass, pipe bridges and box culverts.	White pulpy appearance, expansion and local patches of softening or blistering at mid-height.	Pyrite and indirect sulfide in the Lower Lias Clay, sufficient water-soluble sulfate in groundwater, limestone as coarse and fine aggregate.
Freyburg and Berninger (2003)	Germany	Train-tunnel	Wet mush and scaling of surface.	Portland limestone cement, gypsum- and anhydrite-containing stone beneath the tunnel, groundwater contained magnesium, and limestone aggregate.

Source	Location	Type of structure	Nature of Deterioration	Possible causes of TSA
Freyburg and Berninger (2003)	Germany	Concrete basin of a saltwater swimming bath	No measurable strength at the bottom of the pool.	Partial biogenic limestone as aggregate, sulfate-containing ground water and the saltwater contained sodium- and magnesium sulfate.
Hagelia *et al.* (2003)	Ekeberg, Oslo, Norway	Highway tunnel	Friable, permeable and brittle concrete.	Alum Shale (contains pyrite) and aggressive ground water.
Romer *et al.* (2003)	Switzerland	Tunnels	Efflorescence, layers of secondary minerals, surface scaling, crystallization of salt, and availability of flowable water.	Low temperatures and availability of carbonate, potassium, sodium, magnesium, sulfate and chloride in groundwater.
Ma *et al.* (2006)	Lanzhou City, China	Hydraulic power plant	Expansion, cracking and softening, and loss of strength.	Lower temperature and higher humidity inside the tunnel, groundwater containing sulfates ions, and carbonated concrete.
Rollings *et al.* (2006)	Holloman, New Mexico	Air force base	Heaving exceeded 75 mm, staircase entries were displaced or cracked, and sealants between building and paved areas were loose due to movements.	Availability of water, permeable recycled concrete, possible soil contamination as a secondary source of alumina.
Lee *et al.* (2008)	Soowon, South Korea	Railway tunnel	Severely polluted, partially mushy, spalling and cracking.	Surrounding soil and groundwater contained magnesium and calcium sulfate ions.
Long *et al.* (2011)	Chuxiong city of Yunnan Province, China	Railway tunnel	White salt crystals, swelling and flaking.	Surroundings contained sulfate ions and yearly temperature less than 15˚C.
Mittermayr *et al.* (2013)	Austria	Railroad and highway tunnel	White mushy concrete and soft efflorescence.	Surrounding anhydrite and gypsum horizons and massive lime- and dolostone units.

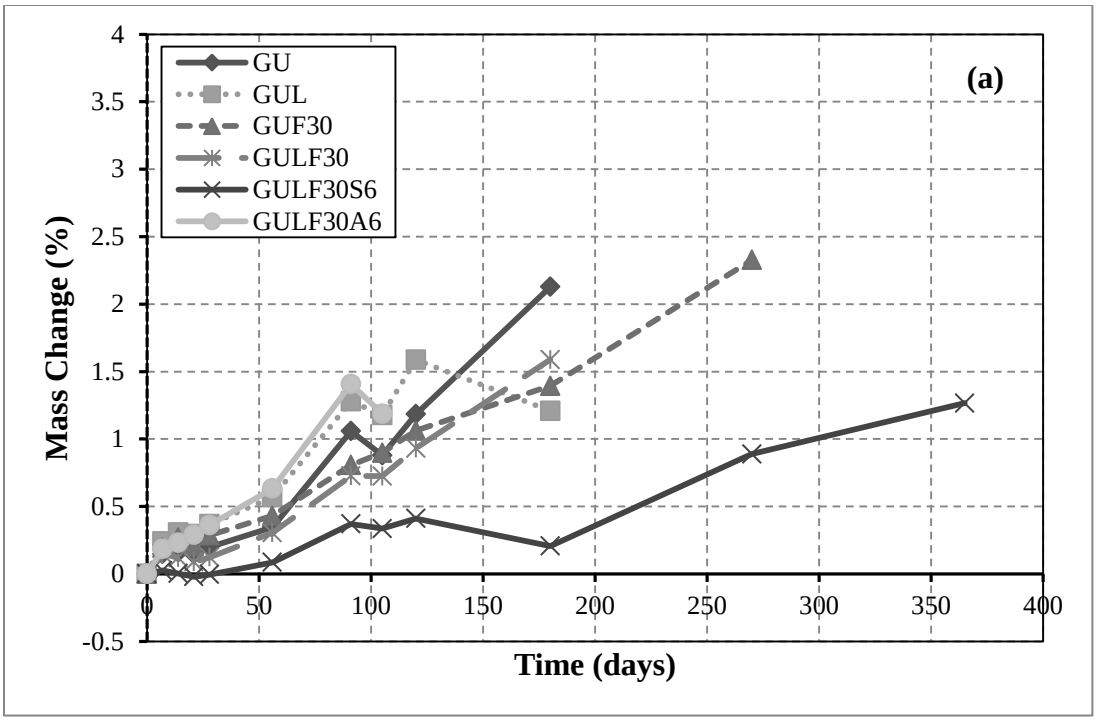

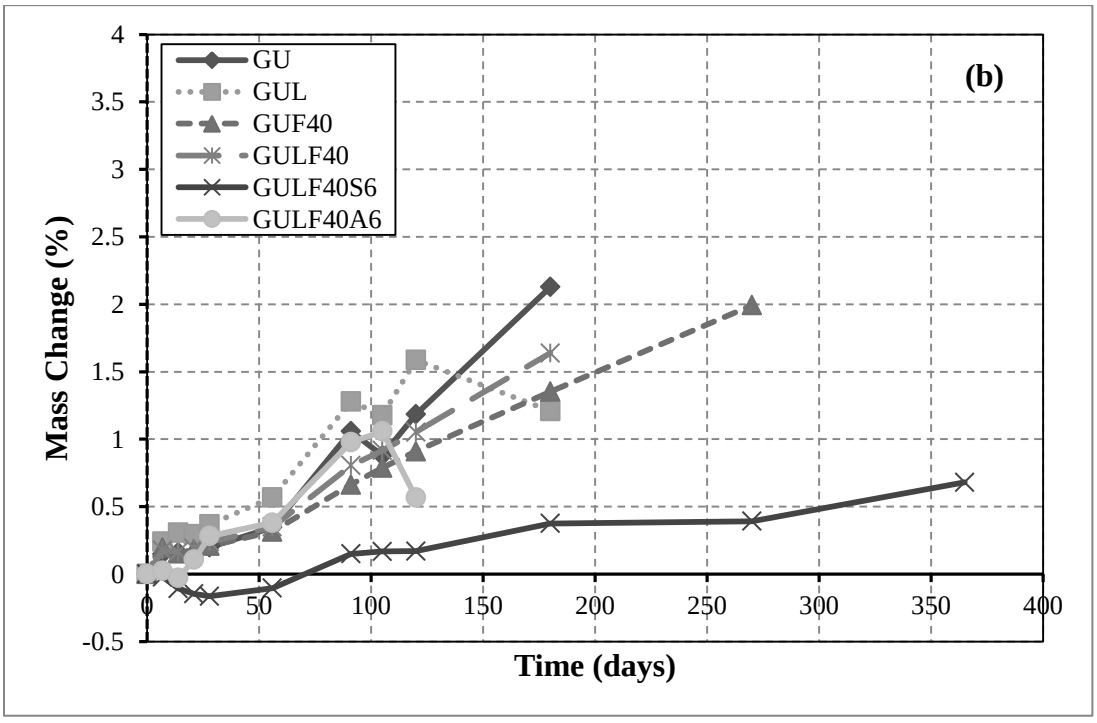

Figure C.1: Change of mass of GU/GUL specimens vs. the time of exposure: (a) group B and (b) group C.

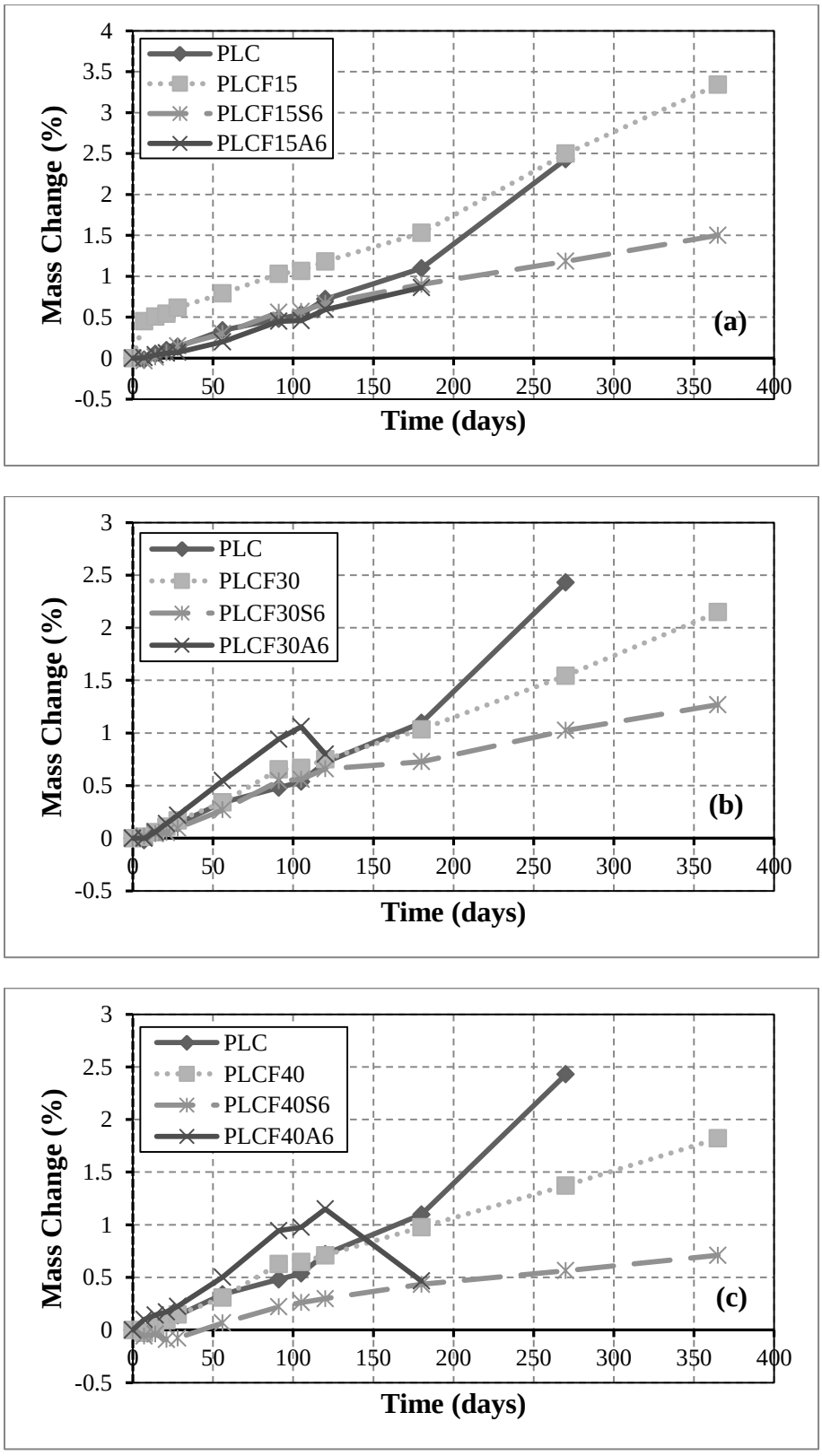

Figure C.2: Change of mass of PLC specimens vs. the time of exposure: (a) group A (b) group B and (b) group C.

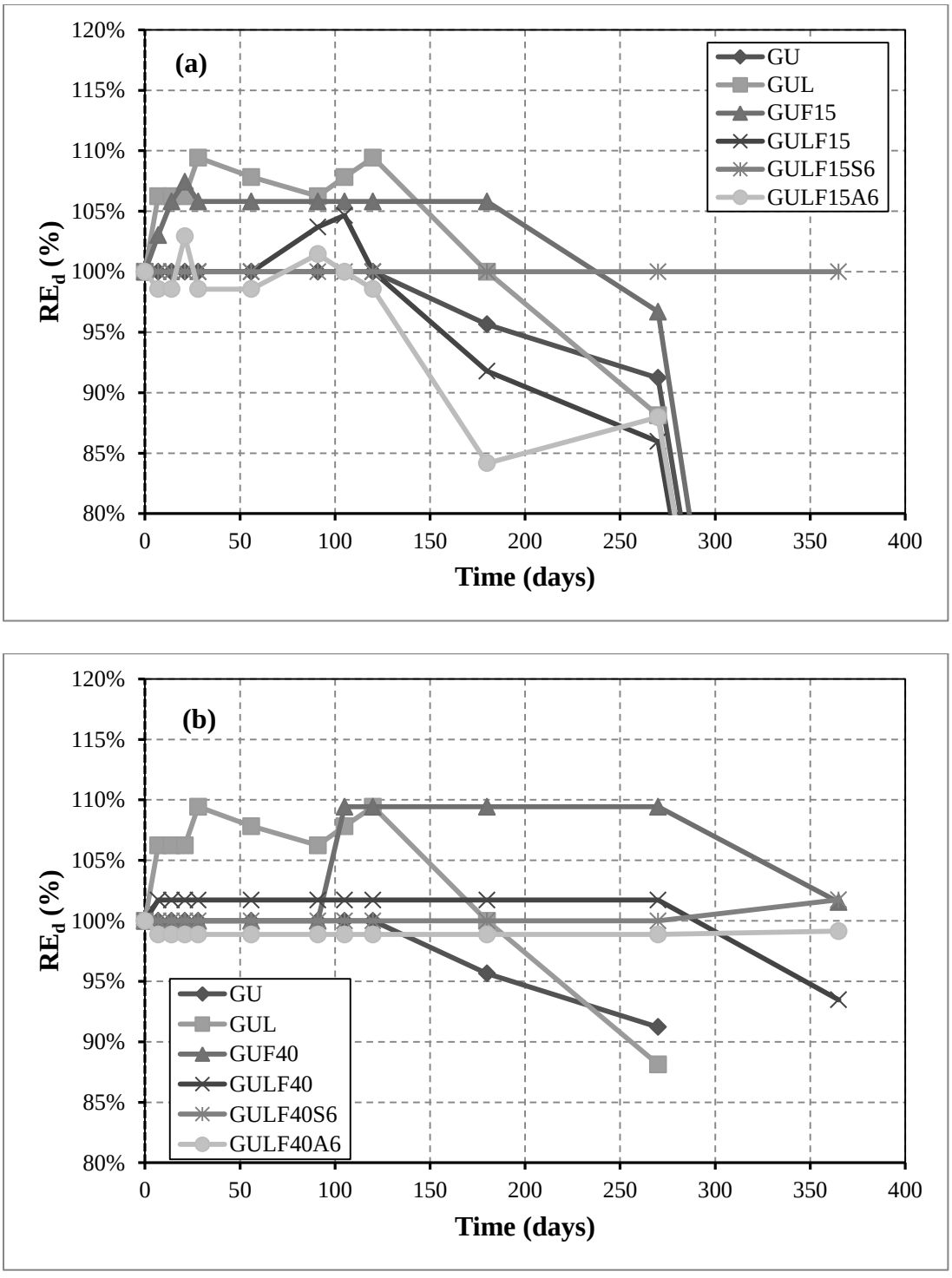

Figure C.3: Relative dynamic modulus of elasticity of GU/GUL mortar cubes vs. the time of exposure: (a) group A and (b) group C.

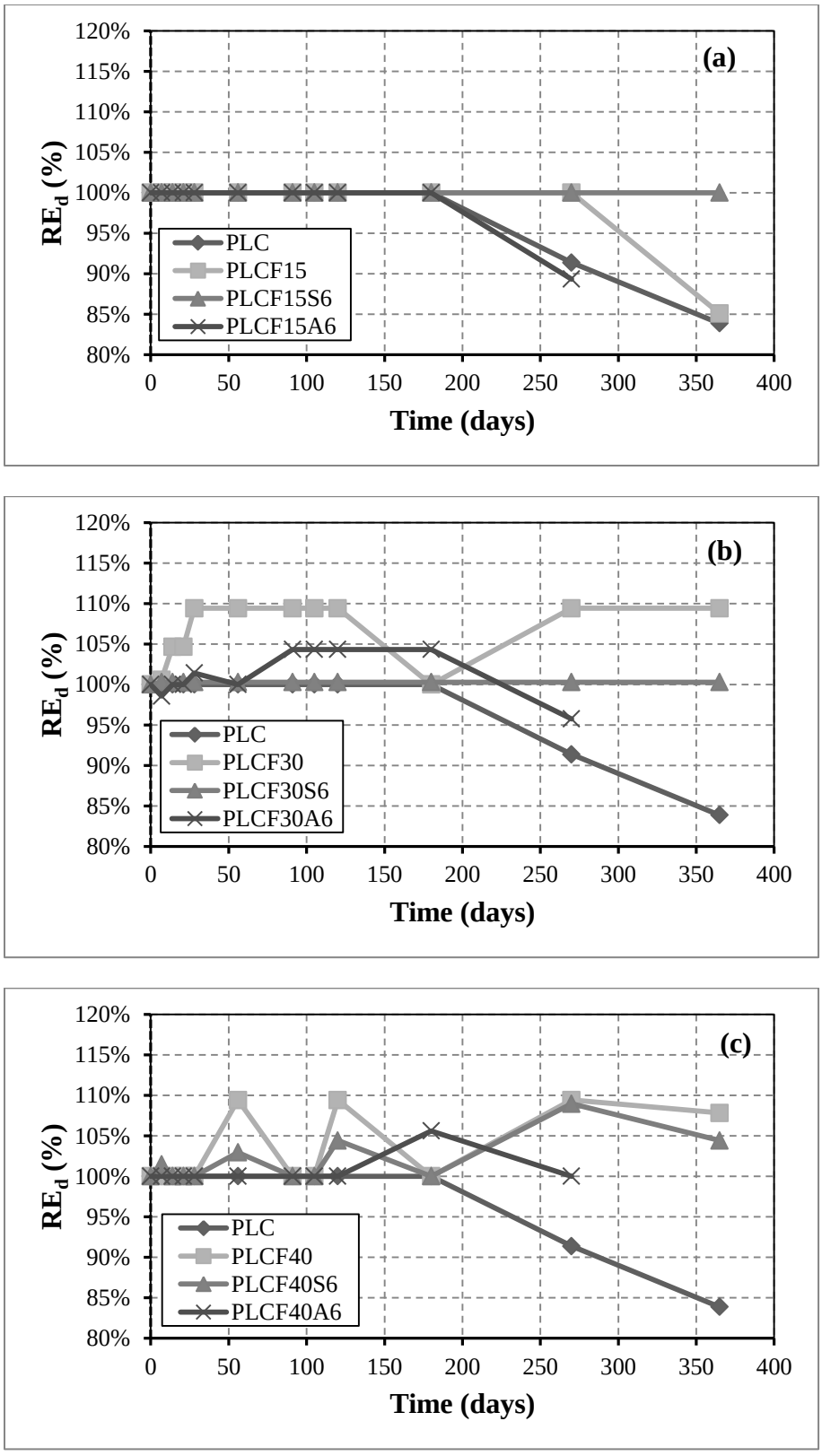

Figure C.4: Relative dynamic modulus of elasticity of PLC mortar cubes vs. the time of exposure: (a) group A and (b) group C.